

The influence of G-quadruplex structures

on meiosis

Dissertation

zur

Erlangung des Doktorgrades (Dr. rer. nat.)

der

Mathematisch-Naturwissenschaftlichen Fakultät

der

Rheinischen Friedrich-Wilhelms-Universität Bonn

vorgelegt von

Eike Schwindt

aus

Saarbrücken

Bonn, November 2019

Angefertigt mit Genehmigung der Mathematisch-Naturwissenschaftlichen Fakultät der
Rheinischen

Friedrich-Wilhelms-Universität Bonn

1. Gutachter: Prof. Dr. Katrin Paeschke

2. Gutachter: Prof. Dr. Oliver Gruss

Tag der Promotion: 12.02.2020

Erscheinungsjahr: 2021

Table of contents

1	Summary	1
2	Introduction.....	2
	G-quadruplexes: Discovery, Structure, Relevance	2
	<i>In vivo</i> functions of G-quadruplex structures	6
	G-quadruplex structures and cancer	9
2.1	G-quadruplex ligands	9
2.2	Meiosis.....	10
2.3	Meiosis in <i>S. cerevisiae</i>	11
2.4	Early meiosis and G ₁ /S transition in <i>S. cerevisiae</i>	11
2.5	Meiosis and G4 structures	14
2.6	Aim of the thesis.....	14
2.7	Methods.....	15
2.8	DNA extraction.....	15
2.9	Extraction of plasmid DNA	15
3	Plasmid cloning	15
3.1	Transformation of chemically competent <i>E. coli</i> cells	16
3.2	Cre/loxP-System.....	16
3.3	Sporulation.....	17
3.4	Determination of cell phase by flow cytometry	17
3.5	BG4/D1 overexpression and purification	18
3.6	Determination of Protein-DNA binding affinity via micro scale thermophoresis	
3.7	(MST)	19
3.8	BG4 chromatin immunoprecipitation (ChIP) and high-throughput sequencing	20
3.9	Basic bioinformatics analysis of ChIP-seq data	22
3.10	G4 Affinity purification.....	22
3.11	Yeast transformation.....	24
3.12	PCR.....	25

	Agarose gel electrophoresis.....	26
	Quantitative RT-PCR	26
	G4 folding and confirmation by circular dichroism (CD) spectra.....	27
3.15	Yeast TCA Whole Cell Extracts (Protein extraction)	27
3.16	SDS-PAGE	28
3.17	Coomassie staining of SDS-PAGE.....	29
3.18	Western analysis	29
3.19		
3.20	<i>Southern</i> analysis	30
3.21	Strains, media, growth	32
3.22		
4	Results.....	35
3.23	Stabilization of G4s impairs spore formation.....	35
4.1	Phen-DC ₃ treatment leads to G ₁ arrest in meiotic cells	37
4.2	Ime1 overexpression does not rescue G ₁ arrest	40
4.3	No elevated DNA damage response was recorded due to Phen-DC ₃ treatment	45
4.4	Phen-DC ₃ treatment leads to an altered proteome in sporulating cells.	48
4.5	Genome-wide mapping of G4 structures during vegetative growth and during	
4.6	sporulation in <i>S. cerevisiae</i>	50
4.7	Proteins bind specifically to G4 structures	55
5.1	Telomeric insertion stimulates meiotic DSBs	58
5.2	Discussion	60
5.3	Effect of G4s on meiotic DSB formation	60
5.4	Proteins acting during meiosis at G4s	63
5.5	Early effects of G4 formation on meiosis.....	65
5.6		
5.7	Ime1, the master regulator of meiosis is crucial for the G ₁ /S-phase transition	65
	DNA damage accumulation can stop G ₁ /S transition during meiosis	66
	Changes in transcriptional level of essential meiotic genes	68
	Genome-wide mapping of G4 structures in chromatin of <i>S. cerevisiae</i>	69
6	Appendix.....	98
7	Acknowledgments.....	137

1 Summary

Several lines of evidence emphasize the potential function of G-quadruplex (G4) structures during DNA replication, transcription and recombination. Although there are experimental evidences that G4s play a role during meiosis, the question if G4 structures influence meiosis has not been addressed yet. Meiosis is a specialized cell division of eukaryotic germ cells. It consists of a single DNA replication followed by two cell divisions, which results in four gametes with a haploid chromosome set. By this, parental cells can pass on its genetic material from generation to generation without leading to aneuploidy.

In this thesis I aimed to identify and characterize the impact of G4 structure formation during meiosis in *Saccharomyces cerevisiae*. I mapped genome-wide the occurrence of G4 structure during vegetative growth and meiosis by G4-chromatin immunoprecipitation (ChIP)-seq and I identified 115 robust G4 binding proteins, which act during meiosis. Additionally, I analyzed the proteome of cells during meiosis and cells that were treated with the G4-stabilizing chemical compound Phen-DC₃. Several proteins were specific for each data set down- or upregulated, respectively. This argues for an altered protein expression upon G4 stabilization.

Further, stabilization of G4 structures by adding Phen-DC₃ to meiotic yeast cells *in vivo* led to cell cycle arrest between G₁ and premeiotic S-phase. In subsequent experiments I shed light on the cause of this arrest upon G4 stabilization. In the past it was shown that G4s often act as obstacles and consequently, resulting in genome instability. Therefore, I tested if G4 stabilization leads to genome instability during meiosis and consequently to an activation of the G₁/S-checkpoint and G₁ arrest. Interestingly, deletion of the checkpoint proteins Mec1 and Tel1 did not rescue the observed phenotype, demonstrating a G4 stabilization caused G₁ arrest, which is independent of checkpoint activation.

It was demonstrated that preferred meiotic double-strand break (DSB) sites, termed as hot spots overlap with regions, which are prone to fold into G4 structures. Meiotic DSBs are essential for the proper segregation of the homologue chromosomes during meiosis I. The overlap between meiotic DSB hot spots and G4 motifs led to the hypothesis that G4s are involved in meiotic DSB formation. For this reason, I evaluated the meiotic DSB frequency at meiotic DSB hot spot *HIS4* in dependency of G4 motifs. During this thesis I discovered that meiotic DSBs are induced independently of G4 motifs at *HIS4*, which indicates that G4s do not play a direct role in DSB formation during meiosis.

2 Introduction

G-quadruplexes: Discovery, Structure, Relevance

Nucleic acids of eukaryotes can form a variety of secondary structures. Besides canonical secondary structures such as B-DNA or RNA hairpins, guanine quadruplexes are of rising interest and new insights indicate that G-quadruplexes (G4) have an important role in diverse biological processes. In the following chapter I will give a brief introduction about G4s and why they are an important field in plenty different aspects. The observation that guanine repeats self-associate into four-stranded secondary structures *in vitro* date back to the early 1960s¹. Almost 30 years later in the late 1980s Dipankar Sen and Walter Gilbert discovered that synthesized single-stranded DNA encoding guanine-rich IgG switch region forms four-stranded DNA structures *in vitro*, if monovalent cations are present². These four-stranded secondary structures which form in DNA^{2,3} as well as in RNA⁴ consist of two or more planar stacked “G-quartets”¹⁻³. Each G-quartet is composed of four guanines which are held together by Hoogsteen hydrogen bonds between the four carbonyl groups of the guanines, forming a so called G4 structure (Figure 1)^{2,5}. G4s are under physiological conditions very stable structures and exhibit resistance against degradation by nucleases^{6,7}.

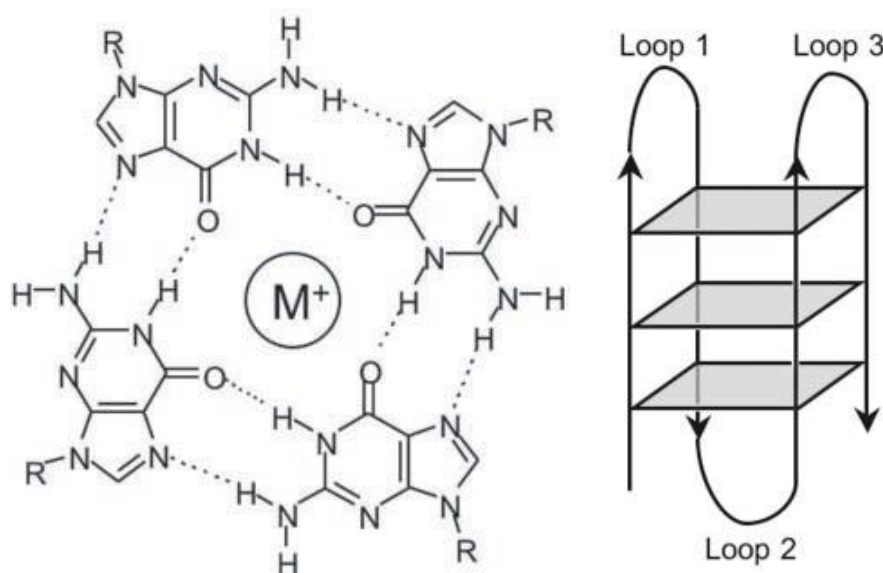


Figure 1: Left, schematic picture of a G-quartet with a stabilizing monovalent cation within the core. Right, schematic picture of a unimolecular G4, consisting of three G-quartets⁸.

Unimolecular G4s exhibit a sequence motif (G4 motif), generally described as G₃+N₁₋₇G₃+N₁₋₇G₃+N₁₋₇G₃ (G: guanine, N: any base)^{8,9}. This commonly used G4 motif exhibit at least four runs of separated guanines, so called G-tracts, which consists of three guanines^{2,3}.

On basis of this G4 motif, computational studies identified over 300 000 putative G4s in the human genome and 668 G4 motifs in the genome of *Saccharomyces cerevisiae*^{10,11}. More recently, an *in vitro* G4-seq approach even revealed more than 700 000 potential G4 structures in the human genome and 103 in the genome of yeast^{12,13}.

Recent studies are partially moving away from the canonical G₃₊ N₁₋₇ G₃₊ N₁₋₇ G₃₊ N₁₋₇ G₃₊ G4 motifs. G4 motifs can form stable G4 structures under physiological conditions even when exceeding the postulated loop length of N₁₋₇¹⁴⁻¹⁶. Also, G-tracts with only two guanines are feasible but result in less stable G4 structures¹⁷. In line with findings that loops, which exceed seven nucleotides can form stable G4s, it was demonstrated that G4 motifs with a central loop up to 30 nucleotides form relatively stable G4 structures¹⁴. Still, increasing loop length correlates with decreasing stability of G4 structures^{14,18,19}. Moreover, the loop composition plays a role in stability. Guédin et al.²⁰ presented that an adenine on the first position of loops containing two, three or four nucleotides has a negative effect on the stability of G4 structures. No such effect was observed if the adenine is present at another position of the loop. Thus, it seems that purines within loops are generally disadvantageous for the stability of G4 structures compared to pyrimidines. However, cytosines are underrepresented in loop regions. The suggested reason is that the possible Watson Crick hydrogen bonds between cytosines and guanines would compete with Hoogsteen hydrogen base pairing between the guanines of a G-quartet¹⁸.

Different factors contribute to G4 stabilization such as the interactions between delocalized π -electrons of guanines among stabilized G-quartets. Furthermore, G4s are stabilized by monovalent cations with stabilization strength in following order: K⁺ > Na⁺ > NH₄⁺ > Li⁺²¹⁻²⁵. Without cations G4s cannot form due to negative electrostatic repulsion of the eight carbonyl O6 atoms of the adjacent G-quartets^{26,27}. One of the key factors for the stability of G4s *in vivo* is the physiological concentration of potassium and sodium (~140 mM K⁺ and ~10 mM Na⁺)²⁸. In particular, potassium-associated G4 structures were shown to be more stable when compared with its sodium bound counterparts. Even though, sodium cations are smaller and can move within the G4 core, whereas potassium-stabilized G4 structures exhibits a slightly higher stability due to the higher dehydration energy of sodium^{3,27,29,30}. Furthermore, G4 folding experiments showed significantly higher folding efficiency of ssDNA in presence of K⁺ than Na⁺³¹. Additionally, due to the preference of potassium over sodium it was shown that K⁺ can replace Na⁺ in G4 structures^{31,32}.

Generally, G4 structures are highly polymorph. Even with interrupted G-tracts G4s can adopt stable structures by forming bulges between two adjacent guanines within a G-tract (Figure 2)³³.

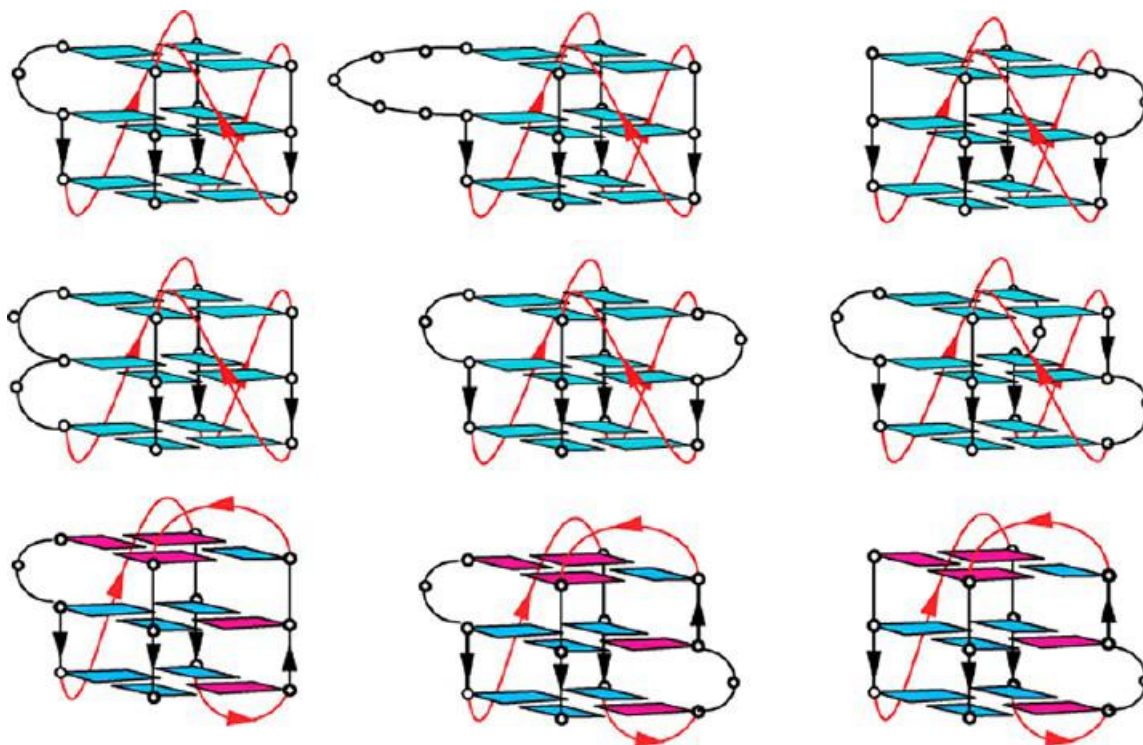


Figure 2: Schematic picture of unimolecular G4s with various bulge formations³³.

Further, circular dichroism (CD) spectra and UV-melting experiments suggested that bulges do not interfere with G4 topology. They can adopt the same confirmations as G4 structures without bulges³³. G4 structures with bulges consisting of cytosine, thymine or uracil exhibit a comparable stability with similar CD spectra and melting temperature. Only adenine shows a slightly lower T_m compared to the other bases. This is according to previous presented studies in which G4s with adenine loops showed lower melting temperatures³⁴. Complementary, an increasing bulge size is inversely proportional to the G4 stability. This is in agreement with previous studies that demonstrated a decreasing stability of G4 structures with longer loop sizes^{14,18,19}. Also, if G-tracts are interrupted by more than one bulge the stability of the G4 structure is significantly decreased³³. X-ray crystallography and nuclear magnetic resonance (NMR) revealed the large topology variety of G4s^{35,36}. They can consist of a single nucleic acid strand, so called intramolecular or unimolecular G4s, or of multiple nucleic acid strands, termed as intermolecular G4s³⁷. Furthermore, G4 structures can be classified in parallel³⁸, antiparallel³⁹ and hybrid configurations (Figure 3)^{32,40-42}. An intramolecular G4 can form 26 different thermo- and steric stable loop configurations *in vitro*, which shows the potential variety of G4 structures⁴³. Generally, G4 structures exhibit a very high structural complexity. Their confirmation is dependent on a variety of factors like primary sequence³⁴, loop configuration⁴³,

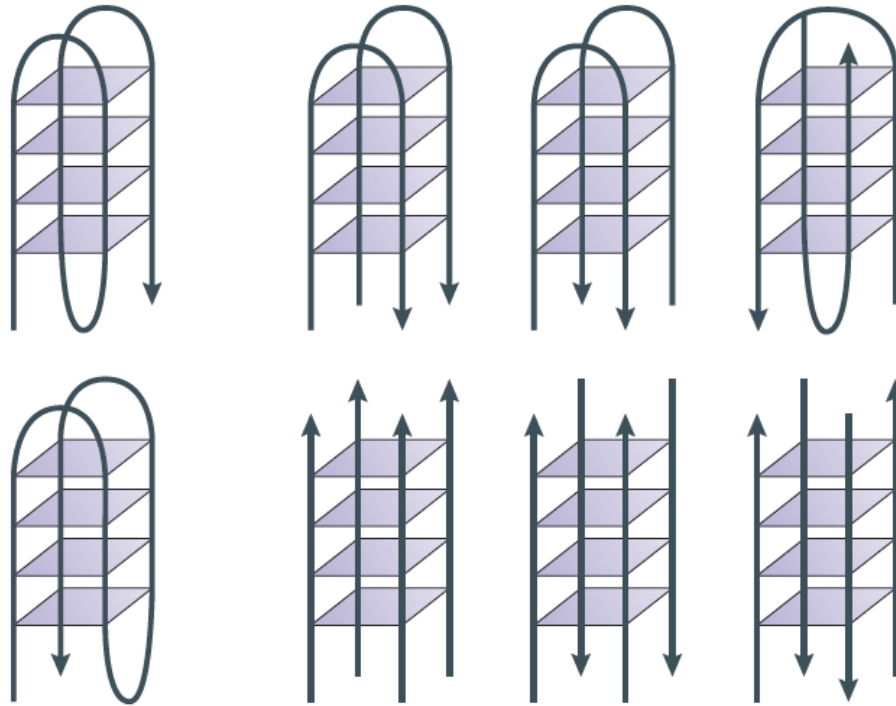


Figure 3: Schematic pictures of different G4 topologies. Left, intramolecular G4s. Right, intermolecular G4s²⁴⁶.

symmetry of their guanines⁴⁴, flanking region^{45,46}, cell crowding^{47,48}, stabilizing cations⁴⁹ and ligands^{38,39}. The G4 confirmation depends also on G4 forming and stabilizing proteins *in vivo*^{50–53}. It is not possible to predict the confirmation of a G4 *in vivo* on basis of its G4 motif alone. Nevertheless, there are some indications for determinants if looked at it isolated. For instance, the *S. cerevisiae* telomere protein Rap1 not only binds to G4s, it additionally promotes the formation of parallel G4s^{50,51}. Computational simulations combined with experimental data lead to the prediction that very short T1 (thymine) loops can only form parallel G4s due to steric constrains^{16,18}. Tippana et al.¹⁶ showed that even one very short loop leads to a parallel conformation where it makes no difference which of the three loops (first, middle or last) within a G4 consists of one nucleotide. In harmony, if the G4 exhibit a 199 motif (first loop one, middle and last loop nine nucleotides) it is forming a stable parallel G4. If two or more nucleotides are present in all loop regions the G4 can adopt both, parallel and antiparallel structures. In the two nucleotides loops the parallel formation is favored but with increasing loop length the conformation shifts towards an antiparallel conformation^{16,45,54}. It is suggested that these results are transferable to all residues because the loop length is the primary reason for steric constrains. Taking together, longer loops preferentially adopt the antiparallel structure whereas the parallel formation is favored for short loops^{16,54,55}.

***In vivo* functions of G-quadruplex structures**

2.2 For a long time, it was believed that G-quadruplexes are *in vitro* artefacts due to their high stability and consequently, the supposed high energy that would be crucial to resolve and form G4 structures *in vivo*. Even today direct approaches to show G4s *in vivo* or in living cells are challenging but there are multiple studies that show the importance of G4 structures for biological processes.

Computational analysis provided first hints for the biological relevance of G4s¹⁰. These studies revealed that G4 motifs are not randomly distributed in the genome. They are overrepresented and conserved at certain DNA regions from prokaryotes to eukaryotes^{10,11,56-58}. This conservation is the highest among mammalian species⁵⁹. G4s are significantly enriched and conserved at promoters, replication origins, transcription factor binding sites, at the border of introns and exons, at immunoglobulin gene class switch recombination sites, rDNA, telomeres and at mitotic and meiotic double-strand break (DSB) sites^{10,11,56,60}. The evolutionary constraints are also assumed to be an indication that G4s have a cellular function¹⁰.

Within the chromatin, consisting of DNA packaged to nucleosomes by associated proteins, G4s are more prone to form at nucleosome depleted regions and in a state when the DNA is temporarily single-stranded⁶¹. Partially single-stranded DNA occurs generally at the lagging strand during DNA replication, during transcription, DNA repair or at the long single-stranded overhang at Telomere ends⁶². Even though, upcoming evidences indicating that G4s are also accessible and energetically capable within a double-stranded genomic environment⁶³.

The first evidences for the *in vivo* occurrence and function of G4s were obtained in telomeres. Telomeres are DNA-protein complexes at the end of chromosomes and consist of tandem repeats which exhibit in most organism G4 motifs. For instance in human, telomeres consist of up to 10 000 base pairs (bp) of the tandem repeat TTAGGG⁶⁴ and in *S. cerevisiae* of the less homogenous 300 ± 75 bp tandem repeat C₁₋₃A/TG₁₋₃⁶⁵. Telomeres are essential to protect chromosomes against degradation by endonucleases, end-to-end fusion and being recognized as DBSs⁶⁶. The first direct evidence that G4 structures form *in vivo* arose from studies in *Stylonychia lemnae*. Here, G4 structures were visualized by two single-strand antibody fragments specific against the telomeric G4s of *S. lemnae*⁶⁷, which were generated *in vitro* by ribosome display. Additionally, it was also demonstrated that G4 structures are regulated throughout the cell cycle by two telomere binding proteins. They become specifically resolved during telomere replication and elongation⁶⁸⁻⁷⁰.

In human first evidence of G4 formation at telomeres were observed when G4 stabilizing ligands like BRACO19 led to telomere shortening by blocking the enzyme telomerase, which

otherwise elongates the telomeric sequence⁷¹⁻⁷⁴. Without telomerase activity, telomeres are shortened by 50-200 nucleotides in every round of replication as seen in most somatic cells⁷⁵ until a critical length, which leads to pausing of cell division and induction of apoptosis⁷⁶. In 2016, the existence of parallel G4 structures at telomeres was confirmed by Liu et al.⁷⁷. By using the single chain variable fragment antibody D1, which binds specifically to parallel G4 structures, they identified G4s at human telomeres. Beyond telomeres, other studies were able to visualize human DNA-G4s and RNA-G4s *in vivo* with the single-stranded antibody BG4^{78,79}.

Many of the so far found G4-binding proteins are linked to telomeres, such as TEBP α and TEBP β in ciliates^{52,53}, Rap1⁵⁰ and Est1⁸⁰ in *S. cerevisiae* and the protection of telomeres protein 1 (POT1)⁸¹ and TRF2⁸² in human. TEBP, Rap1 and Est1 were shown to promote G4 formation whereas POT1 unfolds G4s *in vitro*.

How proteins specifically interact with G4 structures is not fully understood. It was suggested that an arginine- (R), glycine- (G) rich motif, the so called RGG motif, is essential and sufficient for G4 structure recognition as well as binding. RGG motifs are present in RNA binding proteins with an affinity towards G4s^{83,84}. The RGG motif consists of RGG repeats with interspersed spacers of different, mainly aromatic, amino acids. Studies with peptides that exhibit similar lengths and RGG repeats revealed that the arrangement of the repeats and the amino acid composition of the spacers are more important than the number of RGG repeats for G4 structure binding. Recently, a G4-binding protein was identified based on the prediction of its RGG motif⁸⁴.

Due to their high thermostability and slow folding kinetics G4s need to be regulated precisely⁸⁵. They must be unwound for instance during replication and must be formed when needed during transcriptional regulation.

Many helicases were identified to unfold G4 structures with a high potency *in vitro*⁸⁶⁻⁹³. The human helicase FANCD1 is such an example whose deficiency is directly linked to a disease due to the loss of G4 unwinding activity⁹³. Patients with *Fanconi anaemia* exhibit FANCD1 mutations, which cause the loss of helicase activity. This in turn results in genomic deletions in G-rich regions with the potential to form G4 structures, which leads to genome instability and loss of genes. The human WRN and BLM helicases and the yeast Sgs1 and Pif1 helicases are involved in telomere maintenance and are potent unwinders of G4s *in vitro*⁹⁰⁻⁹². Among other functions Pif1 is a particular potent G4 unwinder even compared to other G4 unwinding helicases⁹⁴. Pif1 is a highly conserved helicase from bacteria to human. It was the first helicase with an indicated role in G4 maintenance *in vivo*⁹⁵. Its deficiency in yeast leads to mutations of G4 motifs and replication fork slow-down and stalling in the proximity of G4 motifs.

Furthermore, the mutated G4 motifs, which lost the ability to form G4s are not bound any longer by Pif1 and no further replication fork stalling is detected⁹⁵. Additionally, expression of human PIF1 in *S. cerevisiae pif1Δ* cells leads to a full rescue of the Pif1-deficient phenotype⁹⁴.

A further strong evidence for the regulatory function of G4s *in vivo* was presented in the human pathogen bacteria *Neisseria gonorrhoeae* where G4s are associated with recombination events⁹⁶. *Neisseria* possesses a G4 motif in its antigenic switch region, where via a recombinational mechanism the antigenic variation is achieved. This G4 motif forms a parallel G4 *in vitro* and if the G4 motif is modified that it cannot form a G4 structure the antigen variation is impaired, too. Contrary, modifications of the loop region had no effect, neither on G4 folding nor on the antigenic variation. Moreover, treating cells with a parallel G4 stabilizing ligand n-methyl mesoporphyrin IX (NMM) affects the antigenic switch⁹⁶.

Two hypotheses have come forward for the role of G4s during transcription. Depending on the DNA strand the G4 structure would form on it could either repress or promote transcription. A G4 structure on the template strand is supposed to block the transcription machinery whereas on the non-template strand the G4 structure could assist transcription by keeping the template strand in a single-stranded conformation. Furthermore, G4 structures could act as a loading platform for transcriptional enhancer or repressor⁹⁷. The assumption that G4 structures are involved in the regulation of transcription is also supported by computational analyses showing that over 40% of human genes have G4 motifs in close proximity to their promoters⁹⁸. Especially the overrepresentation at promoter sites of highly transcribed genes such as oncogenes is noteworthy⁹⁹.

G-quadruplex structures and cancer

Recent studies have shown an overrepresentation of G4s in promoter regions of oncogenes. Therefore, G4s became recently a popular therapeutic anti-cancer drug target^{100,101}. The first and most investigated oncogene with a putative G4 in its promoter is the human c-MYC^{102–104}.
2.3 c-MYC expression is associated with cell proliferation and is overexpressed in 80% of cancer types^{105–110}. A mutation in the c-MYC G4 motif that causes loss of G4 structure formation affects the transcription of c-MYC¹⁰².

As mentioned above, G4s also form at telomeres. In the majority of somatic cells telomerase is not expressed, whereas expression of telomerase is a hallmark of many cancer cells. 85-90% of all cancer types have active telomerase, resulting in immortalized cells^{111,112}. This makes telomeres and telomerase therapeutic targets for anti-cancer drug research^{74,113}. Clinical approaches targeting inhibition of the telomerase-facilitated elongation of telomeres by G4-stabilizing ligands led to proliferation stop and apoptosis of cancerogenic cells⁷³.

The effort of finding G4-related anti-cancer drugs resulted in numerous G4 stabilizing ligands over the last two decades^{114–118}.

2.4 **G-quadruplex ligands**

In addition to cations, chemical compounds, termed G4 ligands are capable of stabilizing G4 structures. There are numerous different G4 stabilizing ligands currently on the market^{119–124}. However, in yeast to this date only two of these are entering yeast cells (NMM and Phen-DC₃). NMM was one of the first ligands known to bind G4s^{119,120}. NMM is postulated to bind with high specificity to parallel G4 formations¹²⁵. Moreover, it was demonstrated that the unwinding of NMM-stabilized G4s by RecQ and BLM helicase is impaired^{126,127}.

Another G4 ligand with a high specificity and affinity is Phen-DC₃ (Figure 4). Phen-DC₃ is thermostable and is live cell permeable^{121,122,128}. It was shown that Phen-DC₃ blocks the unwinding of G4s by yeast Pif1 due to its stabilization effect, which leads to mutations of G4 motifs¹²⁹. Moreover, Phen-DC₃ induces an antiparallel conformation of telomeric G4 structures in fission yeast¹³⁰. The binding of Phen-DC₃ to G4 structures is facilitated via the similar shape and size of Phen-DC₃ and G-quartets that enables Phen-DC₃ to stack on the external G-quartet of a G4 structure. This stabilization is realized by the π -electron overlap between the aromatic compounds¹²⁸.

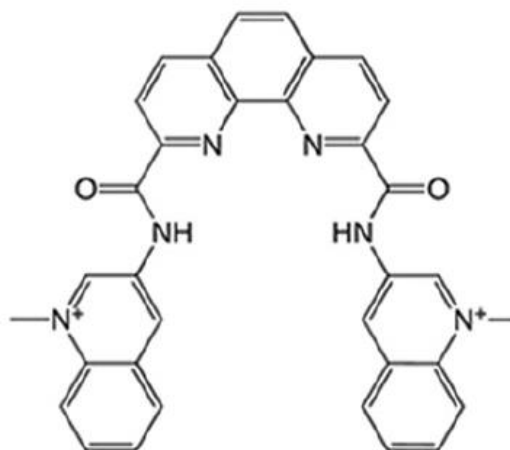


Figure 4: Structural formula of G4 stabilizing ligand Phen-DC₃¹²².

Telomestatin, BRACO19 and TMPYP4 are G4 ligands that were shown to be potent repressors of various cancer cell lines. BRACO19 and Telomestatin exhibit a high selectivity for G4s and an affinity in nanomolar range^{122,123}. Telomestatin possesses some disadvantages though, such as low chemical stability, bad water-solubility and difficult synthesis conditions¹³¹.

For the clinical use of G4 ligands in anti-cancer therapy scientists have to overcome some issues in the future. The specificity of G4 ligands need to be optimized. A variety of G4 ligands have been developed with an aromatic ring system to ensure the π - π stacking with the external G-quartet of G4 structures. The problem is that the majority of G4s exhibit a terminal G-quartet which makes the specificity for certain G4 structures difficult¹¹⁷. Furthermore, the concentration of G4 ligands need to be significantly below the general cytotoxic level^{46,72,118,132}. Nevertheless, a new milestone for the clinical use of G4 ligands was reached recently. Two ligands, CX-5461 and CX-3543, were approved for clinical trials as anti-cancer drugs¹²⁴. CX-5461 and CX-3543 act specifically on BRCA and non-homologous end joining (NHEJ)-deficient cancer types, which lost the capacity to repair DNA damage induced by stabilized G4 structures, leading to genome instability¹²⁴.

Meiosis

Meiosis is a specialized cell division of eukaryotic cells¹³³. It consists of a single DNA replication followed by two cell divisions, which results in four gametes with a haploid chromosome set. In contrast, the mitotic cell cycle contains a single round of DNA replication followed by one cell division, resulting in an unchanged, diploid chromosome set.

Meiosis in *S. cerevisiae*

2.6 Meiosis is a complex process resulting in an altered expression of approximately 1600 genes in *S. cerevisiae*¹³⁴. 250 out of these 1600 genes are meiosis-specific. Depending on nutrient conditions, haploid yeast cells arrest in G₁-phase or enter the mitotic cell cycle. Diploid cells on the other hand have an additional choice besides vegetative growth and G₁ arrest, if nitrogen and fermentable carbon sources are missing, cells will enter meiosis, also called sporulation in yeast¹³⁵.

The meiotic cell cycle is separated in meiosis I and meiosis II. During early meiosis I, after premeiotic S-phase, the formation of meiotic DSBs by Spo11 takes place^{136,137}. Thereafter, homologous recombination leads to connections between the homologue chromosomes¹³⁸. These connections are essential for the proper segregation of the homologs during meiosis I^{139,140}. A beneficial side effect of meiotic recombination is the increased genetic variance that arises from a partially genomic exchange between two homologous chromosomes after processing the DSBs¹⁴¹.

2.7 **Early meiosis and G₁/S transition in *S. cerevisiae*.**

Meiosis starts with the decision of the G₁ cell to enter meiosis. This goes in hand with expression of the master regulator Ime1 (inducer of meiosis I). Ime1 is a transcription factor, which supports the expression of the early meiotic genes¹⁴². Ime1 levels are low in diploid cells during vegetative growth and its expression level rises in response to various extrinsic and intrinsic signals due to starvation^{143,144}. The complex regulation of Ime1 is reflected by its exceptionally large promoter and various proteins, which bind to the promoter region and affect its expression. The promoter is with around 2100 bp the largest promoter in *S. cerevisiae*¹⁴³. Ime1 expression is repressed via diverse pathways in response to environmental glucose and nitrogen levels and by the a1 and α2 gene product. In contrast, its expression is induced by the a1-α2 repressor complex, nitrogen starvation and by the presence of a non-fermentable carbon source such as acetate^{143,145}.

In the following, I will list the proteins and other factors, which affect Ime1 expression and thus influences its function and consequently cell entry into meiosis. The Ime1 regulating nitrogen signal is mediated via various signals, amongst them the G₁ cyclins and the TOR (*target of rapamycin*) pathway.

The G₁ cyclins Cln1, Cln2 and Cln3, which are essential for mitotic S-phase¹⁴⁶, are major factors affecting Ime1 expression. Together with the cyclin-dependent kinase (CDK) Cdc28,

G₁ cyclins promote G₁/S transition in mitotic cell but block the meiotic G₁/S transition by repressing Ime1 transcriptionally and post translationally^{147,148}. Overexpression of Cln3 can push cells into the mitotic cell cycle even under otherwise sporulation-favoring conditions¹⁴⁸. Cln3 has a role in sensing nitrogen starvation due to responsive downregulation. Additionally, Cln3 regulates Ime1 post translational. Ectopic expression of Ime1 in acetate-based nitrogen-rich media is not sufficient for inducing sporulation. As a transcription factor, it is essential that Ime1 localizes to the nucleus to activate the expression of early meiotic genes. This localization is inhibited if G₁ cyclins are present. In G₁ cyclins deficient cells Ime1 accumulates in the nucleus, resulting in meiotic activation^{145,148–150}.

The nuclear localization is additionally controlled by the TOR pathway. As a result of nitrogen starvation or addition of rapamycin the TOR pathway is down regulated, leading to nuclear accumulation and an increased half life time of Ime1¹⁵¹.

Apart from nitrogen, the availability of a carbon source (e.g. glucose) influences Ime1 expression on multiple levels. Upon carbon depletion, Ime1 expression is enhanced by Msn2/Msn4 and repressed by Sok2 and Yhp1 when a sugar source is present^{143,152,153}. Upon carbon starvation Msn2 gets activated, which in turn activates the RAS-cAPK pathway. This leads to localization of Msn2 in the nucleus where it binds to the Ime1 promoter and facilitates its expression. Under non-stress conditions (carbon source is present) or in the presence of high cAPK concentrations Ime1 expression is inhibited and Msn2 is located to the cytoplasm¹⁴³. In contrast, Yhp1 binds directly to Ime1 promoter and represses its expression under high glucose conditions but its level drops due to transfer of cells from carbon rich to acetate-based media. However, Yhp1 deletion leads to no physiological phenotype, indicating towards an alternative mechanism helping cells to cope up with Yhp1 deficiency¹⁵².

Ime1 is regulated by Rme1 (regulator of meiosis) which binds to the Ime1 promoter and thereby represses its transcription¹⁵⁴. Diploid cells express both genes corresponding to the mating type, the Mata a1 and the Mata α 2 gene. Both gene products together form a diploid-specific repressor¹⁴⁵. This repressor inhibits Rme1 that is active in haploid cells. Hence, Rme1 does not repress Ime1 in diploid cells. The repression in haploid cells is accomplished by the Rme1-transcribed lncRNA IRT1¹⁵⁵. IRT1 represses Ime1 expression by preventing the binding of transcriptional enhancers to the Ime1 promoter¹⁵⁵. This repression is mediated via the recruitment of Set2 methyltransferase and Set3 deacetylase complex by IRT1 to establish a repressive chromatin environment¹⁵⁵. Taken together, Ime1 is regulated by multiple factors and deletion of a single one does not necessarily result in a strong effect on Ime1 transcription^{143,144,152}.

After Ime1 is activated, Ime1 binds to the meiosis repressing protein Ume6¹⁵⁶⁻¹⁵⁸ to initiate meiosis. Upon binding vegetative growth is stopped and the expression of meiotic-specific genes starts. It is suggested that by binding of Ime1 the interaction of Ume6 to a repressive histone deacetylase complex is disrupted¹⁵⁹. Additionally, it was shown that the interaction between Ime1 and Ume6 is prevented by glucose and is stimulated under nitrogen starvation¹⁵⁷. As a response to nitrogen starvation Ume6 and Ime1 are phosphorylated by Mck1 and Rim11^{160,161}. The phosphorylation of both, Ume6 and Ime1, is necessary for active transcription-factor-complex Ime1-Ume6, which results in expression of early meiotic genes¹⁶⁰⁻¹⁶³. Early meiotic genes regulated by Ime1 include genes for G₁/S transition, inclusive Ime2, a serine-threonine protein kinase¹⁶⁴.

Ime2 eliminates the repression of S-phase promoting factor (SFB), consisting of Cdc28 and B type cyclins (mainly Clb5 and Clb6) by decreasing the level of the Cdc28 inhibitor Sic1¹⁶⁵. Afterwards, Cdc28-Clb5/6 complex initiates premeiotic DNA replication. Mitotic and meiotic replication share the same replication origins¹⁶⁶. Nevertheless, there are some distinguishable differences between the S-phase and G₁/S transition of mitotic and meiotic cells. For instance, the meiotic S-phase is noticeable longer in organisms studied so far¹⁶⁷. In *S. cerevisiae* the transition takes ~60 minutes for premeiotic S-phase compared to 17 minutes for mitotic S-phase¹⁶⁸.

In vegetative cells the G₁ cyclins have an essential role during the G₁/S transition. Especially Cln3 has a major function in Clb5/6 and Cln1/2 expression. The Cdc28-Cln3 complex promotes the expression of its targets by phosphorylation of the transcription factor complexes Swi4-Swi6 (SBF) and Mbp2-Swi6 (MBF)^{169,170}. This enables the transition to the mitotic cell cycle and activates the transcription of around 200 genes including CLN1/2 and CLB5/6. Hence, the SBF and MBF complexes are key components in the mitotic cell cycle activation and as a consequent repressor of meiosis¹⁶⁹⁻¹⁷².

In meiotic cells Ime1 promotes the expression of Clb5 and Clb6. Clb5 and Clb6 are involved in mitotic S-phase but their function can be complemented by functionally redundant Clb1-4, which is on the other hand not sufficient for premeiotic S-phase. Clb5/Clb6 mutants fail to undergo premeiotic S-phase^{165,173}. Moreover, Cln1 and Cln2 trigger the degradation of Cdc28 inhibitor Sic1, which in turn Ime2 substitutes in meiotic cells¹⁶⁵.

In summary, mutations of CLN1-3, SBF or MBF blocks mitotic S-phase leading to G₁ arrest but promote meiosis. In contrast, mutations in genes essential for meiotic G₁/S transition like Ime1, Ime2 or Clb5/6 blocks the functional premeiotic S-phase but have no effect on the completion of mitotic S-phase^{146,165,174}.

Meiosis and G4 structures

2.8 There are some indications for a role of G4s during meiosis. Computational analysis in yeast and humans revealed that G4 motifs overlap with meiotic DSB hot spots¹⁰. Meiotic DSB hot spots are preferred sites for meiotic recombination. Additionally, an involvement of G4s during meiosis is supported by the fact that several proteins, which act during meiosis bind to G4s or promote G4 formation *in vitro*, for instance Mre11, Hop1 and Kem1¹⁷⁵⁻¹⁷⁷.

Mre11, as a part of the MRX (Mre11-Rad50-Xrs2) complex, is a major component of DSB processing in mitotic cells, as well as for Spo11 induced DSBs during meiosis^{137,178}. Kem1 is an exonuclease which is also suggested to be involved in meiosis, because Kem1 deficient cells arrest during meiotic prophase¹⁷⁶ and the meiosis specific protein Hop1 is a part of the synaptonemal complex, which mediates the pairing between homologue chromosomes^{177,179}.

Aim of the thesis

2.9 The overall aim of the thesis is to investigate the influence of G4 structures on meiosis.

G4 structures will be examined during vegetative growth and sporulation genome-wide by G4-ChIP-seq. Using an affinity-based purification strategy coupled with mass spectroscopy G4 binding proteins that act during meiosis will be identified. In the latter the relevance and impact of G4 structure stabilization on meiosis will be analyzed by a combination of molecular and genetic analyses. Utilizing Phen-DC₃ sporulation progress will be analyzed via FACS analysis. The expression of genes crucial for sporulation will also be probed after G4 stabilization in *S. cerevisiae*. Also, the effect of G4 stabilization on genome stability will be monitored via different markers for genome instability.

G4s are suggested to be involved in meiotic DSB formation. To test this hypothesis meiotic DSBs will be visualized via Southern blot and their formation examined in dependency of different G4 motifs.

3 Methods

DNA extraction

For yeast DNA extraction the MasterPure™ Yeast DNA Purification Kit (epicenter Cat. Nos. MPY80010 and MPY80200) was used. As starting material 1.5 ml saturated yeast culture or
3.1 around 25 ml of a Yeast culture with an OD₆₀₀ 0.5 was used. The following steps were performed as written in the protocol. DNA concentration was determined by NanoDrop 2000c UV-Vis spectrophotometer from Thermo Scientific.

Extraction of plasmid DNA

3.2 Plasmid DNA was extracted from bacterial cells using FavorPrep Plasmid DNA Extraction Mini Kit (Favorgen), following manufacturer's instructions.

Plasmid cloning

3.3 DNA fragments obtained from PCR or purchased from Sigma-Aldrich and desired plasmids were digested regarding to suitable restriction sites according to supplier's recommendations and buffer conditions. Following inactivation of restriction enzymes were performed according to supplier's instructions. To avoid re-ligation of linearized plasmids, the terminal 5' phosphate groups were removed by Shrimp Alkaline Phosphatase (SAP, NEB). For this, 1 µl of SAP was added directly to inactivated digested sample and incubated for 1 h at 37°C, followed by purification via PCR Purification Kit (Qiagen) according to supplier's instructions or gel electrophoresis (3.15) for cut out fragments ≥ 50 bp. Then, ligation of digested DNA fragments and dephosphorylated DNA plasmids were achieved in a 10 µl reaction by T4 DNA ligase (NEB) in a molar ratio of 5:1. Total mass of DNA in the ligation reaction was 200 ng and incubation took place overnight at room temperature. Afterwards, the obtained plasmids were transformed in competent *E. coli* cells. Its correctness was confirmed later via scPCR (3.14).

Transformation of chemically competent *E. coli* cells

Desired vectors were transformed in chemically competent *E. coli* by heat shock method.

3.4 ~100 ng of plasmid was mixed with 50 µl competent cells. After 30 mins incubation on ice, the cells were heat shocked for 45 sec at 42°C, followed by 5 min cooling on ice. 500 µl of pre-warmed (37°C) SOC medium was added to the sample and recovery was performed for at least 1 hour at 37°C for. After recovery the cells were spun down, resuspended in 150 µl ddH₂O and plated on desired antibiotic LB plates.

Cre/loxP-System

3.5 In order to insert a yeast telomeric sequence and variations of it at locus *HIS4* the Cre/loxP-System was used.

First the desired oligonucleotides were designed with an additional EcoRV (NEB) restriction site at each end and purchased from Sigma-Aldrich (Appendix Table 4). Then, the oligonucleotides and plasmid pUG6, possessing two loxP sites and KanMX as selective marker, were digested with EcoRV (NEB) and cloned as described in 3.3. Correctness of cloning was confirmed via scPCR (3.14). After successful cloning the plasmid was partially amplified via PCR (3.14) using primer, according to desired PCR fragment, containing the favored oligonucleotide, 2 loxP sites and KanMX as marker. Additionally, to complementary sequence according to plasmid pUG6 the primer possessed a second complementary part according to desired *HIS4* locus due to desired integration (Appendix Table 4). The PCR fragment was transformed into the yeast genome as described in (3.13) and the cells were plated on selective plates against KanMX containing G418 (200 µg/ml). After 2 days at 30°C the colonies were examined via scPCR for positive integration of PCR fragment using primer.

Thereafter, the positive colonies were used for a further transformation of plasmid pSH65. pSH65 possesses a gene for the enzyme Cre-recombinase under a galactose inducible GAL1 promoter together with a bleomycin selective marker. Cre-recombinase cuts specific a DNA region between two loxP sites out. In this case, the selective marker KanMX between two loxP sites at locus *HIS4*, leaving the desired oligonucleotide and the loxP sites behind at *HIS4*. To achieve this, the positive cells for *HIS4* integration were used for a transformation according to (3.13) with plasmid pSH65. After transformation cells needed a recovery in YPD for at least 1 hour at 30°C before plated on selective plates, containing Zeocin™ (300 µg/ml), a member of the bleomycin/phleomycin family of antibiotics isolated from *Streptomyces*. After 2 days at

30°C appeared colonies were transferred to liquid YPD media containing 2% raffinose as carbohydrate source instead of 2% glucose and were grown at 30°C and 200 rpm overnight. Next day, cells were transferred to media containing 2% of glucose as sugar and incubated for 6 hours at 30°C and 200 rpm in order to induce Cre-recombinase expression. After that, cells were transformed to YPD media containing 2% glucose and grown overnight, thereby inhibiting Cre expression. On the following day cells were plated on non-selective YPD plates containing 2% galactose and grown for 2 days at 30°C. Finally, appearing colonies were replica plated on selective KanMX plates due to screen for lost KanMX cassette.

Sporulation

3.6 200 µl of saturated overnight culture was added to 50 ml ddH₂O, washed once and then resuspended in 2 ml Sporulation medium. After 72 hours at 25°C and 200 rpm the yeast cell formed four spores (Tetrads). If needed the spores were separated afterwards via tetrad dissection. For tetrad dissection 200 µl of sporulation culture were pelleted and resuspended in 20 µl Zymolyase (0.5 mg/ml), followed by 15 min incubation at 30°C. Thereafter the single spores were separated on an YPD plate using a tetrad dissection microscope (SPOREPLAY+). For approaches with defined time points of sporulation yeast cells were cultured in pre-sporulation medium before transferring to Sporulation medium. Therefore, pre-sporulation-medium was inoculated with an overnight culture, for instance 100 ml pre-sporulation medium with 75 µl overnight culture, and grew at 30°C and 200 rpm till an OD₆₀₀ 1.2-1.3, which took around 20 hours. Afterwards the culture was washed twice in 50 ml ddH₂O and transferred to double volume sporulation medium and shook at 25°C and 200 rpm till desired time point was
3.7 reached.

Determination of cell phase by flow cytometry

Yeast cell cultures with an OD₆₀₀ 0.5 were used. Between 5 and 7 ml of culture were fixed with 1 ml EDTA (0.5 M)/NaN₃ (0.3% w/v) solution. Cells can be stored for several days at 4°C. 1 ml of suspension was pelleted and washed twice in 1 ml 50 mM sodium citrate. Afterwards resuspended in 1 ml in 70% ethanol and placed at -20°C for at least 15 min till up to 2 weeks. Further, cells were resuspended in 500 µl 50 mM sodium citrate plus 10 µl RNase A (10mg/ml, Invitrogen). RNA digestion was performed at 37°C for 1 hour followed by 2 hours proteinase K (Invitrogen) digestion at 50°C. Therefore, the cells were resuspended in 500 µl 50 mM sodium citrate plus 10 µl proteinase K (20mg/ml). After this, cells were treated with 2 µl

SYTOX Green (Invitrogen) and shortly before using fluorescence-activated cell scanning (FACS), the cells were separated via Biorupter, 3 cycles 30 sec on/off high intensity.

Following settings were used for the FACS sorter, FSC 400 V, SSC 445 V, FITC 465 V.

BG4/D1 overexpression and purification

3.8 *E. coli* B121 strain containing pSang10 plasmid including BG4/D1 was inoculated in 3 ml 2xTY medium plus 1% Glucose, 50 µg/ml Kanamycin and grew overnight at 37°C and 200 rpm. Next day 2-liter 2xTY medium plus 50 µg/ml Kanamycin was inoculated with 2.5 ml overnight culture. Cells grew till an OD₆₀₀ 0.5-0.8 and following expression initiation via 0.5 mM IPTG. Protein was expressed overnight at 25°C and 200 rpm. On the following day cells were pelleted at 4000 g for 30 minutes at 4°C. Pellet was resuspended in 160 ml ice cold TES buffer and stirred for 10 minutes on ice. Followed lysis was achieved by adding ice cold TES buffer diluted 1:5 and stirring for 15 min on ice. Then, cell fragments were pelleted by 16000 g at 4°C for 30 min and supernatant 0.45 µm filtered. The lysate was later incubated with 6 ml slurry Ni NTA beads rotating for one hour at 4°C. Beads were washed before use with 50 ml washing buffer. The following purification was achieved via a Nickel affinity column. The saturated beads were washed with 1-liter ice cold washing buffer and eluted with 5 ml elution buffer. Buffer exchange and concentration of antibody was achieved using Amicon® Ultra-15 Centrifugal Filter Unit (Merck).

10x PBS buffer	95 mM Na ₂ HPO ₄ ·7H ₂ O 1.46 M NaCl 26 mM KCl 14 mM KH ₂ PO ₄
inner cell salt buffer (50 mL)	25 mM HEPES (pH 7.6) 110 mM KCl 10.5 mM NaCl 1 mM MgCl ₂ (filter and store at 4°C)
PBS with high imidazole (50 mL)	PBS pH8 + 2.5 M Imidazole (no need to adjust pH here)

wash buffer (1 L)	PBS pH8.0 100 mM NaCl (20 mL at 5 M) 10 mM Imidazole (4mL at 2.5 M)
elution buffer (100 mL)	PBS pH8 250 mM Imidazole (10mL at 2.5M)
TES (250 mL)	50 mM Tris pH8 (12.5mL at 1M) 20% sucrose (50g) 1mM EDTA (500µL at 0.5M)
TES 1:5 (250 mL)	1:5 TES diluted with MilliQ water Protease Inhibitor (1 tablet (EDTA free) for 50mL) Benzonase (20 µl) 2 mM MgSO ₄ (250µL at 2M)

3.9 **Determination of Protein-DNA binding affinity via micro scale thermophoresis (MST)**

To determine the specific binding of antibody BG4 to G4s a binding affinity assay via MST (Monolith NT.115, NanoTemper) was performed. As positive control a G4 motif, 5'-TGAGGGTGGGTAGGGTGGGTAA-3' and as a negative control an oligonucleotide without G4 motif, 5'-GCGCGAGCTCGCGTAGATGCGAATGTGAG-3 were used. The oligonucleotides were 5' Cyanine labeled and prior to MST folded (3.17). The MST instrument detects the motion of fluorescent molecules, in this case the 5' Cyanine labeled oligonucleotides, along a temperature gradient, an effect termed "thermophoresis". The motion of molecules is dependent on the molecular hydration shell, charge or size. Because at least one of these parameters change with every binding event, a wide range of biomolecules can be measured. Next, BG4 was transferred into MST optimized buffer (50 mM Tris-HCl, 150 mM NaCl, 10 mM MgCl₂, 0,05 % Tween-20). A dilution series 1:1 (10 µl volume) from 1 to 16 of BG4 was performed starting with a concentration of 5 µM. This goes on till tube 16 and a resulting end concentration of 1.25 nM. Afterwards the labeled oligonucleotides were added in a constant concentration of 10 nM to a final volume of 20 µl. After resuspending and 5 min incubation at room temperature, the samples were transferred to provided MST capillaries (MO-K022) and

thermophoresis measured using Monolith NT.115. Following settings were used, excitation power 100% and MST power 20, 40 and 80%.

BG4 chromatin immunoprecipitation (ChIP) and high-throughput sequencing

The BG4 ChIP seq was performed according to the protocol of Robert Hänsel-Hertsch et al.¹⁸⁰ with a few changes due to suitability to yeast cells. 50 ml YPD medium was inoculated with an overnight culture to OD₆₀₀ 0.1. After the culture reached an OD₆₀₀ 0.5 the cells were crosslinked with 1% formaldehyde for 5 min at 25°C and 200 rpm. After, 125 mM glycine was added and the cells were shaking for additional 5 min at 25°C and 200 rpm. Later, the cells were pelleted by centrifuging for 5 min at full speed and at 4°C. Then, washed once with 30 ml ice cold HBS and once with 20 ml ice cold ChIP lysis buffer. Next, cells were resuspended in 200 µl ChIP lysis buffer plus 2 µl protease inhibitor cocktail (PIC) (Sigma P8215) and snap frozen in liquid nitrogen. The cells can be stored at -80°C. Further, the samples were thawed and glass beads were added in order to lyse the cells via fast prep, 6.0 m/s MP 45 sec. Afterwards the lysate was transferred to a new tube and centrifuged full speed 30 min at 4°C. The pellet was resuspended in 130 µl ChIP lysis plus PIC diluted 1/100. Thereafter, the cells were sheared by covaris e220, following settings were used: 140 W, 5% duty, 200 cycles/burst 25 min (Appendix Figure 1a). The sonicated lysate was then centrifuged for 20 min full speed at 4°C and the fragmented chromatin containing supernatant was transferred to a fresh tube. At this step the chromatin can be stored at -80°C for 3 months. To check chromatin quality and fragmentation 10 µl of the sample was added to 70 µl TE buffer (pH 7.5) and 1 µl RNase A (10 mg/ml) followed by 20 min incubation at 37°C. Further, proteins were digested by adding 1 µl proteinase K (20 mg/ml, Invitrogen) for 2 hours at 65°C. DNA was purified using the MinElute kit (Qiagen), following the provided protocol and eluted in 20 µl of ddH₂O. The fragmented DNA was thereafter loaded on a 2% agarose gel and separated by size to assess the quality of the DNA and its fragmentation. The distribution should be between 100-500 bp for optimal BG4 ChIP performance. Total chromatin concentration was determined via Qubit (Invitrogen), according to the manufacturer's instructions.

1 µg of chromatin per sample was used to perform BG4 ChIP. The sample was filled up with ChIP lysis buffer supplemented with 1% BSA to a total volume of 50 µl / 100 µl. RNA digestion was performed by adding 1 µl RNase A (10 mg/ml, Invitrogen) followed by 20 min incubation at 37°C and 1400 rpm. For each sample, 10 µl were put on ice, it was used as an input later on. After RNase digestion 500 ng of BG4 was added to the chromatin sample, following 1 hour incubation at 16°C while head over tail rotating. Meanwhile 65 µl of anti-FLAG beads were

washed three times with 650 µl ChIP lysis buffer supplemented with 1%BSA. For the washing of the beads a magnetic rack was used. Afterwards, the washed beads were added to the chromatin/BG4 sample (total volume: 100 µl) and the sample was rotated an additional hour at 16°C. The supernatant was discarded afterwards and the beads were washed three times with 200 µl ice cold wash buffer. For the washing steps the beads were inverted several times. Then, two wash steps were performed at 37°C, 200 µl wash buffer was added and the beads were rotated for 10 head over tail. Then, the wash buffer was completely removed and 75 µl TE buffer (pH 8.0) plus 1 µl Proteinase K (20mg/ml) was added, the same goes for the saved input. The samples and the input were incubated for 1 hour at 37°C and another 2 hours at 65°C. Eventually, the supernatant and the inputs were transferred to a fresh tube and the DNA was purified using Ampure XP beads. The purification was performed as described in the manual and DNA was eluted in 25 µl provided EB buffer. To determine if the DNA amount was sufficient 5 µl sample were quantified using Qubit. G4 enrichment over background was tested using Primer (Appendix Table 4) in a Quantitative PCR. Library preparation was performed with NEBNext Ultra II DNA library kit for Illumina (NEB) as described in manufacturer's instructions and send for next generation sequencing to core facility, NGS Core Facility, Life & Brain Center, 53127 Bonn.

TE buffer (1x)	10 mM Tris-Cl (pH 8) 1 mM EDTA
HBS (500 mL)	50 mM HEPES (pH 7.6) 140 mM NaCl
ChIP lysis buffer (500 ml)	50 mM HEPES (pH 7.6) 140 mM NaCl 1 mM EDTA (pH 8.0) 2.5 mM Deoxycholic acid 1% IGEPAL CA-630
ChIP-seq wash buffer	100 mM KCl 10 mM Tris pH 7.4 0.1% Tween 20

Basic bioinformatics analysis of ChIP-seq data

3.11 The HiSeq 2500 V4 supplied 25 million reads for each sample. The reads were paired end and 50 bp in length. The bioinformatical analysis was performed as described in the protocol of Hänsel-Hertsch et al.¹⁸⁰ using the open source Galaxy (www.usegalaxy.org) platform. In brief, the sequencing quality was first evaluated by the quality-control tool FastQC (bioinformatics.babraham.ac.uk/projects/fastqc). Followed by adaptor removing via Cutadapt¹⁸¹ and alignment of trimmed sequences with BWA-MEM^{182,183}. Sequences with an alignment quality of < 10 were discarded. Next, soft-clip local imperfect alignments using the CleanSam tool (broadinstitute.github.io/picard). Finally, PCR duplicates were removed by MarkDuplicates in the Picard tool (broadinstitute.github.io/picard) using the default parameters. Peak calling and genome browser track generation were performed using MACS v2.0^{184,185}. Input DNA served as control.

G4 Affinity purification

3.12 7 nmol of pre-folded G4 motif and mutated G4 motif (Figure 12a) were biotinylated by incubation with 0.1 mM biotin-14-dATP (Invitrogen), 1x terminal deoxynucleotidyl transferase reaction buffer and 15 units terminal deoxynucleotidyl transferase (TdT) for 4 hours. In order to remove unincorporated biotin, the DNA was precipitated by adding 100 mM NaCl and 2.5 volumes 100% ethanol and following incubation for 30 min at 4°C. Afterwards the DNA was pelleted via centrifuging at full speed for 30 min at 4°C and washed with 1 ml 70% ethanol followed by an additional pelleting. All ethanol left overs were removed and the DNA was dissolved in 150 µl ddH₂O. Moreover, due to desalt the DNA, the water was exchanged, using a YM-30 column (Microcon).

Yeast lysate for the affinity purification was obtained from 400 ml sporulation culture with an OD₆₀₀ ~0.6 for each biotinylated Oligonucleotide and time point. For the affinity purification lysate from time points 3 and 7 hours after transferring to sporulation medium were used. The cells were pelleted at 4000g for 20 min at 4°C. Afterwards washed once with 200 ml ice cold ddH₂O and once with 200 ml ice cold lysis buffer. Further, the pellet was resuspended in 6.4 ml lysis buffer (1:100 v/v protease inhibitor cocktail (PIC) (Sigma P8215) added) and separated on 16 tubes a 400 µl before snap frozen in liquid nitrogen. Following lysis was achieved using glass beads and Fastprep (6.0 m/s MP 45 sec). Subsequently the lysates were transferred to fresh falcon and combined. To each sample, originally derived from 400 ml culture, 480 µl avidin (5mg/ml) (Calbiochem) was added and incubated for 30 min at 4°C rotating head over

tail. In the meantime, 1600 μ l Dynabeads M-280 (Invitrogen) were washed three times with 4 ml BS/THES buffer and added to lysate for 60 min at 4°C pre-incubation. 2 μ l lysate was kept as input control. During the incubation additional 1.5 ml Dynabeads were washed three times with 4 ml 2xBW buffer. After that, the beads were resuspended in 1.5 ml 2xBW buffer, mixed with 1.5 ml biotinylated oligonucleotides and incubated for 60 min at room temperature, rotating head over tail. After incubation the biotinylated DNA bound beads were washed three times with 3 ml TE buffer followed by blocking with 2xBW buffer supplemented with 0.1% BSA for 15 min at 4°C, rotating head over tail. Furthermore, the beads were washed two times with 4 ml BS/THES buffer (1:100 v/v protease inhibitor cocktail (PIC) (Sigma P8215) added) and one time with 4ml BS/THES buffer plus 5 μ g random DNA oligonucleotides. Then, the beads were resuspended in 1.5 ml BS/THES buffer and incubated with before pre-incubated lysate, additionally 50 mM KAc and thousand-fold excess DNA, compared to beads bound DNA, was added. The sample was rotated for 12 hours head over tail at 4°C. The beads were washed twice with 4 ml BS/THES buffer supplemented with 5 μ g DNA containing unfolded G4 motif and washed five additional times with 4 ml BS/THES. To elute the proteins, the beads were incubated with 600 μ l elution buffer for 4 min at room temperature, rotating head over tail. The elutions were dialyzed and concentrated using speedvac. Proteins were identified via Mass spectroscopy.

Lysis buffer	0.1 M HEPES pH 7.5
	0.01 M potassium acetate
	10% glycerin
	0.5% Nonidet P-40
	1 mM EDTA pH 8.0
	1 mM DTT
2xBW buffer	10 mM Tris-HCl pH7.5
	1 mM EDTA pH 8.0
	2 M NaCl

BS / THES buffer	22 mM Tris-HCL pH 7.5
	10 mM HEPES pH 7.5
	8,9% saccharose
	62 mM NaCl
	5 mM calcium chloride
	50 mM KCl
	1 mM EDTA pH 8.0
	12% glycerin
	1 mM DTT

Yeast transformation

3.13 An overnight culture was used to inoculate 50 ml of YPD media to an OD₆₀₀ 0.1. After the culture reached OD₆₀₀ 0.5 – 0.7 the cells were spun down via centrifuging, 5 min at 1500 rcf. Then washed once in 50 ml ddH₂O and once in 15 ml SORB buffer. Thereafter the cells were resuspended in 360 µl SORB buffer plus 40 µl salmon sperm and separated on eight aliquots à 50 µl. The salmon sperm was before denaturated for 5 min at 95°C and stored on ice. The competent cells can be stored at -80°C. The transformation was carried out by adding 5 µl of desired integrative oligo, PCR product, digested integrative plasmid or favored plasmid to 50 µl competent yeast cells. 300 µl PEG buffer was added and the mixture was vortexed vigorously. Thereafter the cells were incubated for 30 min at 30°C and 500 rpm on a thermomixer. Afterwards 40 µl DMSO was added and heat shock was initiated. The heat shock was at 42°C for 15 min. Further, cells were spun down for 30 sec at full speed, eventually resuspended in 150 µl ddH₂O and plated on selective plates. For KanMX, hygromycin and nourseothricin a (3 h for Kan, 5-6 h for hyg and nat) recovery in YPD is necessary. Then, plates were incubated for 2 days at 30°C. Obtained colonies were tested on correctness by scPCR.

SORB buffer (500 mL)	100 mM LiAc
	10 mM Tri-HCl pH 8.0
	1 mM EDTA pH 8.0
	1 M Sorbitol

PEG buffer (50 mL)

100 mM LiAc

10 mM Tri-HCl pH 8.0

1 mM EDTA pH 8.0

40% (w/v) PEG 3350/400

PCR

DNA fragments of interest were amplified by PCR using polymerase and Primer listed xxx. In 3.14 the following tables are the reagents and program used for a standard PCR. Annealing temperature for each reaction depends upon T_m of used primer.

DNA template	100-300 ng
Polymerase buffer (10x)	5 µl
Forward primer (10 mM)	1 µl
Reverse primer (10 mM)	1 µl
dNTPs (2.5 mM each)	1 µl
Polymerase	1 U
ddH ₂ O	Fill up till 50 µl

Program	Temp.(°C)	Time
Initial denaturation	95	5 min
Denaturation	95	30 sec
Annealing	50-60	30 sec
Elongation	72	1 min/kb
Final elongation	72	5 min

In order to identify the integrity of a transformation scPCRs were performed. For this, a part of the putative positive colony was added to the PCR reaction instead of template DNA. Furthermore, the initial denaturation was prolonged to 10 min due to break the cells open in order to release the inner DNA.

Agarose gel electrophoresis

3.15 To separate DNA fragment various sizes 0.8%-2% (w/v) Agarose gels and 1x TAE buffer were used. To visualize the DNA fragments ethidium bromide (0.5 ug/ml) was added to the solubilized agarose. The agarose was solubilized in 1xTAE by heating up in a microwave and poured in a suitable gel frame. 6x DNA loading buffer was added to the DNA samples in a final concentration of 1x before loading. The loaded samples were separated at 80-120 V for 30 – 120 minutes. Subsequently, if needed bands were cut out and DNA was extracted via Gel Extraction Kit (Qiagen).

50x TAE buffer	50 mM EDTA pH 8.0
	2 M Tris base
	1 M acetic acid
DNA loading buffer (6x)	30% glycerol
	0.25% bromophenol blue

Quantitative RT-PCR

3.16

Expression level of genes were determined via qRT-PCR. Total RNA was isolated using Maxwell RSC simplyRNA blood kit and Maxwell RSC Instrument (Promega). Manufacturer's instructions were followed as described with minor changes for lysis. Instead of lysis via Lyticase, lysis was achieved by using glass beads and Fastprep. Following settings were used for Fastprep, 6.0 m/s MP 45 sec. 1µg of total RNA was applied to reverse transcription using Super script III (Invitrogen). Manufacturer's instructions were performed, using Oligo(dT)₂₀ primer to transcribe mRNA. Expression of mRNAs was quantified by qRT-PCR CFX96 Real Time System (Bio-Rad), using Act1 as reference gene. For each reaction 10µl SYBR Green mix (Bio-Rad), 0.4 mM of each primer and 5 ng cDNA were used. Finally, the sample was filled up to a total volume of 20 µl with ddH₂O. Each reaction was performed in triplicates as followed:

PCR-program (40 cycles)

Initial denaturation:	95°C	5 min
Denaturation:	95°C	10 sec
Annealing:	52°C	10 sec
Elongation:	72°C	20 sec
Melting curve:	95°C	5 sec
	65°C	1 min
	97°C	continuously 0.11°C/s

G4 folding and confirmation by circular dichroism (CD) spectra

3.17 Oligos presenting a G4 motif were ordered at Sigma and diluted to final concentration of 100 mM in ddH₂O. Afterwards, in order to perform G4 folding, a wanted concentration of Oligos was diluted in 10 mM Tris-Cl (pH 7.5) and 150 mM KCl or 1M NaCl. The sample was heated for 5 minutes at 95°C, followed by slow cool down over night by switching of the heater. Folded G4s can be stored at -20°C for 2 months. For confirmation of correct folding 15-20 µg of folded DNA were diluted in a total volume of 200 µl ddH₂O and Circular dichroism (CD) was performed using Jasco J-810 spectropolarimeter (Jasco).

3.18

Yeast TCA Whole Cell Extracts (Protein extraction)

Cells were grown to OD₆₀₀ ~ 0.5 collected by centrifugation (10 ml culture) and the supernatant discarded. Pellet were resuspended in 1 ml 20% Trichloroacetic acid (TCA) and transferred to an FastPrep suitable tube. Cells were pelleted and resuspended in 200 µl 20% TCA. Glass beads were added to meniscus and cells lysated using FastPrep, 6.0 m/s 1 min. Afterwards, 400 µl 5% TCA was added and holes were poked in the top and bottom of the tube. The tube was placed on a fresh Eppendorf tube and centrifuged 1 min 500g. Tube, which contained the glass beads was discarded and samples centrifuged with 3000 g, 10min, 4°C. Supernatant was discarded and 100 µl 1x laemmli buffer and 50 µl 1 M Tris Base added to the pellet. Samples were mixed by vortexing and boiled at 95°C for 5 min. Then centrifuged for 10 min at 3000 g and 4°C. Supernatant was transferred to a fresh tube and stored at -20°C till further usage via SDS-PAGE.

Stacking gel composition:

H ₂ O (ml)	2.975
0.5 M Tris-HCl, pH 6.8 (ml)	1.25
10 % (w/v) SDS (ml)	0.05
Acrylamide/ Bis-acrylamide (30 % / 0.2 % w/v) (ml)	0.67
10 % (w/v) ammonium persulfate (AP) (ml)	0.05
TEMED (ml)	0.005

SDS running buffer (10x) 0.25 M Tris base, 1.92 M glycine, 1% (w/v) SDS

Coomassie staining of SDS-PAGE

3.20

By SDS-PAGE separated proteins were visualized via Coomassie staining. Therefore SDS-PAGEs were incubated for ~1 hour in Coomassie stain (50% methanol, 10% glacial acetic acid, 40% ddH₂O, Coomassie Blue R-250) followed by destaining in 10% acetic acid, 50% methanol, and 40% H₂O until bands were visual.

3.21

Western analysis

Proteins Prior separated protein of interest was detected by using antibody based Western analysis. According to the length and wide of the gel one Nitrocellulose membrane and four Whatman paper were used for semi wet transfer. The membrane and Whatman papers were wetted in 1x Towbin plus 20% methanol. The Gel, membrane and Whatman papers were stacked in a semi dry chamber in following order, on the top and at the bottom two wet Whatman paper were placed and in line to the current flow the membrane and the gel were placed in order to transfer the proteins from the gel to the membrane. Transfer was accomplished using x cm length multiplied with x cm width and 0.8 mA for 90 mins. After the transfer, the membrane was blocked in TBST + 5% BSA for 1 hour at room temperature. Then, the membrane was transferred to TBST containing 2% BSA and favored antibody in recommended dilution. Antibody incubation was either 1 hour at room temperature or at 4°C overnight. Further, the membrane was washed 3 times in TBST for 15 minutes and subsequently

the secondary antibody was added in a recommended dilution in TBST plus 2% BSA. After 2 hours of incubation at room temperature washing was performed as described above and the membrane was developed using enhanced chemiluminescence system (ECL) (GE healthcare) or previous mixed developing solution (0.2 mM coumaric acid + 1.25 mM Luminol + 0.3% H₂O₂).

Towbin buffer (10x)	0.25 M Tris 1.92 M Glycine 0.1% (w/v) SDS final pH: 8.6
Transfer buffer (1x)	1x towbin buffer 20% methanol
10x TBS buffer	100 mM Tris-HCl pH 7.5 1.5 M NaCl
Tris buffer saline tween (TBST)	250 mM Tris 150 mM NaCl 2 mM KCl 0.05% (v/v) Tween 20 pH 7.4

3.22

Southern analysis

In order to visualize meiotic DSBs at *HIS4* locus, *S. cerevisiae rad50s* mutants were collected after 24 hours in sporulation media (25 ml) and pelleted followed by DNA extraction. The DNA was afterwards digested using BglII (NEB) and purified using PCR Purification Kit (Qiagen). 15µg of digested DNA was subsequently loaded on 0.8% agarose gel and separated for 120 min at 120V. Further the gel was crosslinked using UV crosslinker Bio-Link 254 (Vilber), applying 120 mJ in 254 nm. Afterwards the gel was incubated for 30 min in denaturation solution and 30 min in blotting solution while shaking. In the meantime, one Amersham HybondTM-N⁺ membrane (GE Healthcare), five Whatman paper and a stack of tissues were cut accordingly to the size of the gel. The gel was arranged as followed from bottom to the top, saran wrap, gel, in blotting solution pre-wet membrane, two pre-wet Whatman paper, three Whatman paper and a stack of tissues. All together wrapped in saran wrap, burdened with a 200 ml bottle and steeped overnight. The next day the membrane was crosslinked with 254 nm applying 120 mJ.

Afterwards the membrane was transferred to a hybridization tube and prehybridized in 20 ml pre-warmed Church buffer for 30 min, rotating at 65°C in a hybridization oven. After prehybridization, the church buffer was discarded and 15 ml prewarmed Church buffer was added supplemented with 150 µl prior denaturated salmon sperm and before labeled probe. The labeled probe was made accordingly to manufacturer's instructions (DecaLabel DNA Labeling Kit, Thermo Scientific). As probe template PCR product was used corresponding to primer (Appendix Table 4).

Hybridization was performed overnight at 65°C, rotating in a hybridization oven. On the following day the membrane was washed three times with wash buffer I for 5 min, rotating at 65°C, followed by two was steps with wash buffer II for 10 min, rotating at 65°C. The church buffer with the radioactive probe can be stored at -20°C for later usage. The meiotic DSBs were thereafter detected on a phosphor storage screen, stored at room temperature overnight and visualized using a Phosphoimager (GE healthcare).

Southern analysis using DIG labeled Probe was performed according to manufacturer's instructions (PCR DIG Probe Synthesis Kit, DIG Luminescent Detection Kit for Nucleic Acids, Roche).

20x SSC buffer	300 mM Na ₃ Citrate x 2H ₂ O 3 M NaCl
Denaturation solution	1.5 M NaCl 0.5 M NaOH
Blotting solution	1.5 M NaCl 0.25 M NaOH
Church buffer	1 mM EDTA (pH 8.0) 0.17% Phosphoric acid 0.5 M Na ₂ HPO ₄ x 12H ₂ O 7% SDS
Wash buffer I	1x SSC buffer 0.1% SDS
Wash buffer II	0.1x SSC buffer 0.1% SDS

YPD-, SC-plates	YPD / SC medium 2% (w/v) Agar
Drop Out mix	2.5g Lysine 1.25g Tyrosine 1.25g Methionine 2.5g Arginine 1.25g Serine 1.25g Valine 2.5g Threonine 1.25g Isoleucine 1.25g Phenylalanine 2.5g Cysteine 1.25g Aspartic acid 1.25g Proline
Minus Leucine	2.5g Adenine 1.25g Histidine 2.5g Tryptophan 2.5g Uracil
Minus Uracil	2.5g Adenine 1.25g Histidine 2.5g Tryptophan 2.5g Leucine
Minus Tryptophan	2.5g Adenine 1.25g Histidine 2.5g Leucine 2.5g Uracil
Minus Histidine	2.5g Adenine 2.5g Tryptophan 2.5g Leucine 2.5g Uracil

Minus Adenine	1.25g Histidine 2.5g Leucine 2.5g Uracil 2.5g Tryptophan
Pre-sporulation medium	1% (w/v) Peptone 0.5% (w/v) Yeast extract 1% (w/v) $C_2H_3KO_2$ 0.17% (w/v) Yeast nitrogen base without AS with ammonium sulfate 1% (w/v) $(NH_4)_2SO_4$ 0.5% (w/v) $C_8H_5KO_4$ Adjust pH 5.5 with KOH
Sporulation medium	0.5% (w/v) KOAc 5 mg/ml Adinine 5 mg/ml Histidine 5 mg/ml Leucine 5 mg/ml Tryptophan 5 mg/ml Uracil

4 Results

Several lines of evidence emphasize the potential function of G4 structures during DNA replication, transcription and recombination^{10,11,56,96}. So far, only a few studies questioned, if G4 structures also influence meiosis. Therefore, my PhD studies aimed to identify and characterize the impact of G4 structure formation during sporulation (meiosis) in *S. cerevisiae*. To achieve this, I used different molecular and biochemical strategies.

I examined the effect of G4 stabilization *in vivo* on meiosis by adding Phen-DC₃ to sporulating cells. I mapped the occurrence of G4 structures during vegetative growth and sporulation genome-wide by G4 ChIP-seq. In order to identify proteins that specifically act during meiosis and recognize G4 structures, an affinity purification strategy coupled with mass spectrometry was performed. Finally, to investigate the correlation between G4s and preferred meiotic DSB sites, G4 motifs were inserted in the genome and meiotic DSB formation was mapped.

For these studies, I used *S. cerevisiae* strains of W303 or SK1 background^{187,188}. The SK1 background is especially suitable for time sensitive questions of meiosis due to its fast and synchronic sporulation capacity¹⁸⁷.

4.1 Stabilization of G4s impairs spore formation

Numerous studies demonstrated the capacity of Phen-DC₃ to stabilize G4 structures and its effect on various processes *in vivo*^{121,122,128–130,189,190}. But, so far, no examinations of its stabilizing effect were performed during meiosis.

To investigate if G4 stabilizing by Phen-DC₃ effects sporulation or vegetative growth, different concentrations of Phen-DC₃ (2.5, 5 and 10 μ M) were added to sporulating and vegetative cells. For meiosis an overall marker of fitness is spore formation. In vegetative cells the general fitness is estimated by growth rate (doubling time), by measuring the optical density at 600 nm (OD₆₀₀).

To monitor vegetative growth YPD media was inoculated with an overnight culture to an OD₆₀₀ of 0.2 and different concentrations (2.5, 5 and 10 μ M) of Phen-DC₃ were added. Cells were cultured at 30°C 200 rpm shaking for seven hours. The growth rate of wild type (WT) and Phen-DC₃ samples were determined every hour. No significant changes in vegetative growth were determined up to a concentration of 10 μ M (Figure 5a). Both, treated and untreated had a calculated doubling time of around 95 minutes.

Next, I determined the effect of G4 stabilization on sporulation. Phen-DC₃ was added directly after transition from pre-sporulation media (pre-SPM) to sporulation media (SPM). In order to

enter more efficiently and synchronously into sporulation cells were cultured for approximately 20 hours in pre-SPM till an OD₆₀₀ 1.3. After this, cells were cultured in SPM, which lacks a nitrogen source and a fermentable carbon source in order to induce sporulation. Spore formation was microscopely determined after 72 hours in SPM at 25°C and 200 rpm. Contrary to vegetative cells, if Phen-DC₃ was added to SPM, a reduced spore formation was detected. 2 μM Phen-DC₃ resulted in 30% spores, whereas 5 μM and 10 μM resulted in 4% and 3% respectively compared to around 50% of observed tetrads for cells in SPM without Phen-DC₃ (Figure 5b).

The loss of spore formation can be a result of changes during different meiotic steps. In *S. cerevisiae* a point of meiotic commitment exists that roughly coincides with prophase I briefly after S-phase. Till this point cells require the continued presence of the starvation signal. If nutrient rich medium is provided before this point, cells exit sporulation and return to vegetative growth. In accordance, if cells are supplied with nutrient rich medium after reaching the meiotic commitment point, cells continue with sporulation¹⁹¹⁻¹⁹⁵.

To test if the cells exceeded the point of meiotic commitment, I treated sporulating cells with 10 μM Phen-DC₃ for 10 hours at 25°C and 200 rpm. After this, cells were washed and reinserted in rich yeast media (YPD) plus 10 μM Phen-DC₃. Growth was monitored via optical density (OD₆₀₀). As expected, during meiosis cells did not grow (Figure 5c). However, after transition to YPD, which was supplemented with 10 μM Phen-DC₃ cells started growing again. This demonstrates that cells are arrested prior to the meiotic commitment point and that they retained the ability of vegetative growth. Furthermore, these analyses strengthen the argument that observed changes by Phen-DC₃ are specific for sporulation.

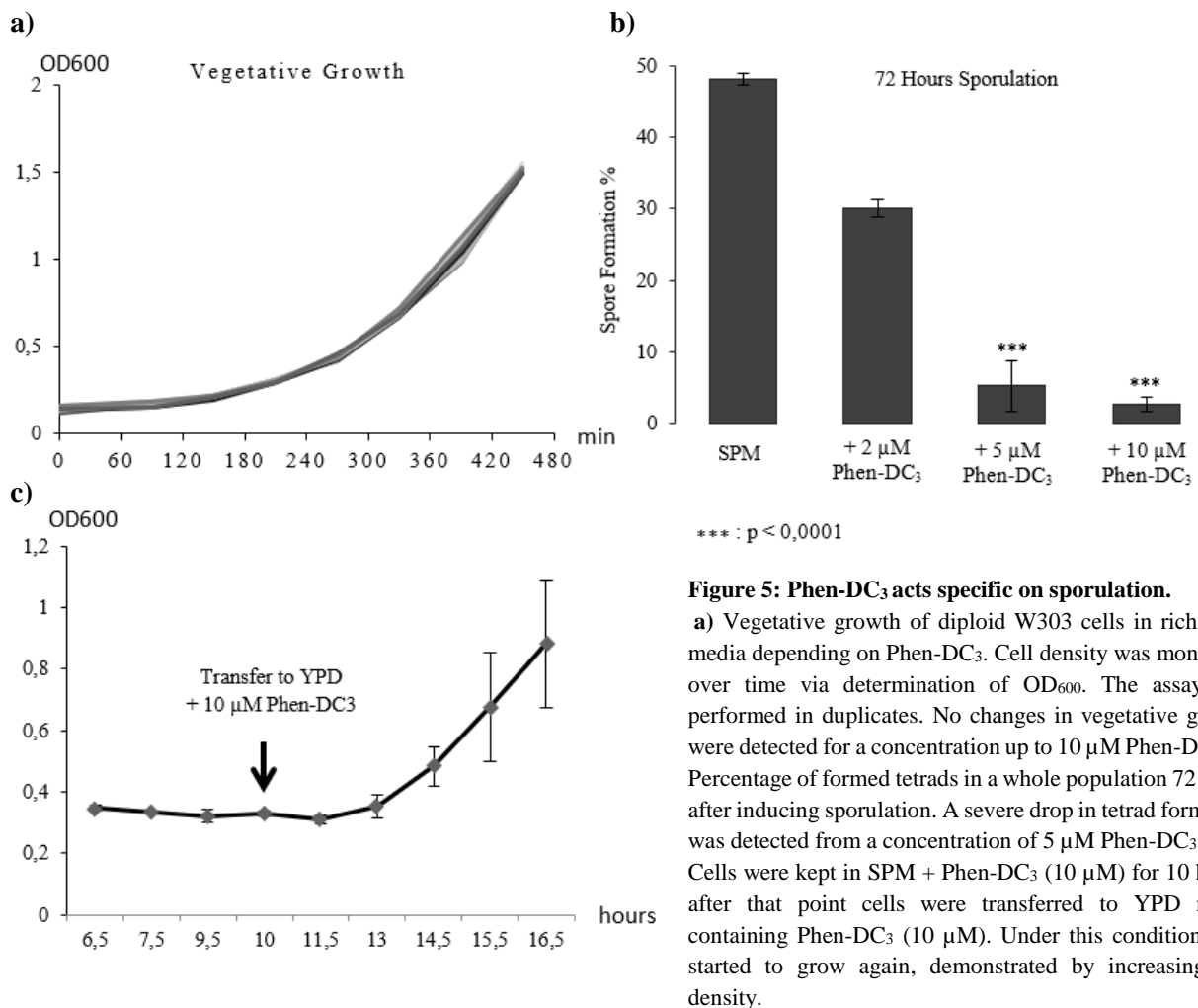


Figure 5: Phen-DC₃ acts specific on sporulation.

a) Vegetative growth of diploid W303 cells in rich YPD media depending on Phen-DC₃. Cell density was monitored over time via determination of OD₆₀₀. The assay was performed in duplicates. No changes in vegetative growth were detected for a concentration up to 10 μM Phen-DC₃. **b)** Percentage of formed tetrads in a whole population 72 hours after inducing sporulation. A severe drop in tetrad formation was detected from a concentration of 5 μM Phen-DC₃ on. **c)** Cells were kept in SPM + Phen-DC₃ (10 μM) for 10 hours, after that point cells were transferred to YPD media containing Phen-DC₃ (10 μM). Under this condition cells started to grow again, demonstrated by increasing cell density.

4.2

Phen-DC₃ treatment leads to G₁ arrest in meiotic cells

Along the genome are regions associated with particular high levels of meiotic DSBs, so called hot spots¹⁹⁶. There is a strong overlap of meiotic hotspots with G4 regions¹⁰ and I propose that lack of spore formation might be due to altered meiotic DSBs.

The meiotic DSB formation and processing takes place after premeiotic S-phase during Prophase I¹⁹⁷. Here, DSBs are formed by Spo11 and processed by the MRX complex¹³⁷. DSB formation during meiosis can be monitored by Southern blot analysis (3.22). To visualize meiotic DSBs an established approach is to use a *rad50s* mutation. These mutants are deficient in DSB repair, due to an unfunctional MRX complex, thus meiotic DSBs accumulate¹⁹⁸.

In this thesis I used a *rad50s* mutant strain termed as FX3 (Appendix Table 5), provided by the University of North Carolina, Department of Biology, Curriculum in Genetics and Molecular Biology (Appendix Table 5)¹⁹⁹.

To map the DSB formation, depending on Phen-DC₃ I examined the hot spot location *YDR186c* – *YDR188w* (chr IV)²⁰⁰. The genomic DNA was extracted from sporulating cells after 24 hours of sporulation according to Fen et al.¹⁹⁹ and subsequently digested by PstI (NEB). A labeled PCR probe was designed accordingly to open reading frame *YDR189w* (Appendix Table 4).

In agreement with literature obvious meiotic DSBs were observed in *rad50s* cells (Figure 6a). After treatment with Phen-DC₃ meiotic DSBs vanished, using 5 or 10 μM Phen-DC₃. This experiment revealed that G4 stabilization prevents meiotic DSB formation.

The meiosis starts with the decision of the G₁ cell to perform meiosis on the basis of multiple factors, including lack of nitrogen, lack of glucose and mating type¹⁴². This leads to an exit from the mitotic cell cycle in G₁ and entry into premeiotic S-phase. To identify the stage in which the G4 stabilization impairs sporulation and prevents DSB formation I performed FACS analysis to determine the cell cycle distribution of Phen-DC₃-treated cells (3.7). For FACS analysis SYTOX Green was used. SYTOX Green is a high affinity nucleic acid stain and allows a quantitative measurement of cell cycle phases: G₁-phase (2n), G₂-phase (4n, double amount of DNA after DNA synthesis during S-phase). Sporulating cells and cells treated with Phen-DC₃ were prepared accordingly to methods 3.6. Phen-DC₃ was immediately added after transfer to SPM in an end concentration of 10 μM. The SK1 background strain was used for FACS analysis because it sporulates faster and more synchronously than other yeast backgrounds and samples were taken every 2 hours. Untreated control cells showed a characteristic distribution of meiotic cells. Cells shift from G₁- to G₂-phase with progressing time in SPM indicated by a shift from 2n to 4n genomic DNA (Figure 6b). After Phen-DC₃ treatment, FACS analysis revealed a cell cycle arrest in G₁-phase (2n) prior to premeiotic S-phase. Even 24 hours after inducing sporulation cells were still in G₁-phase as observed by a high peak at 2n.

To test if the effect of G4 stabilization by Phen-DC₃ is limited on the start of sporulation Phen-DC₃ was added after different time points upon transfer to SPM. 10 μM Phen-DC₃ was added immediately (0 min), after 30 min and every full hour up to 6 hours after transfer to SPM. The effect of Phen-DC₃ on meiosis was measured by quantification of spore formation 72 hours after inducing sporulation via microscope. The cell phase was also determined by FACS 12 hours after transferring to SPM. As observed in Figure 6c and 6d the repressive effect of Phen-DC₃ on spore formation and progression to G₂-phase disappeared with increasing time that cells were in SPM prior to Phen-DC₃ addition. When Phen-DC₃ was added 5 hours or later after inducing sporulation, tetrad formation and progression to G₂-phase were similar to sporulating

cells without Phen-DC₃. This showed that G₄ stabilization must act on the transition from G₁-phase to S-phase and on the decision of the cell to enter meiosis.

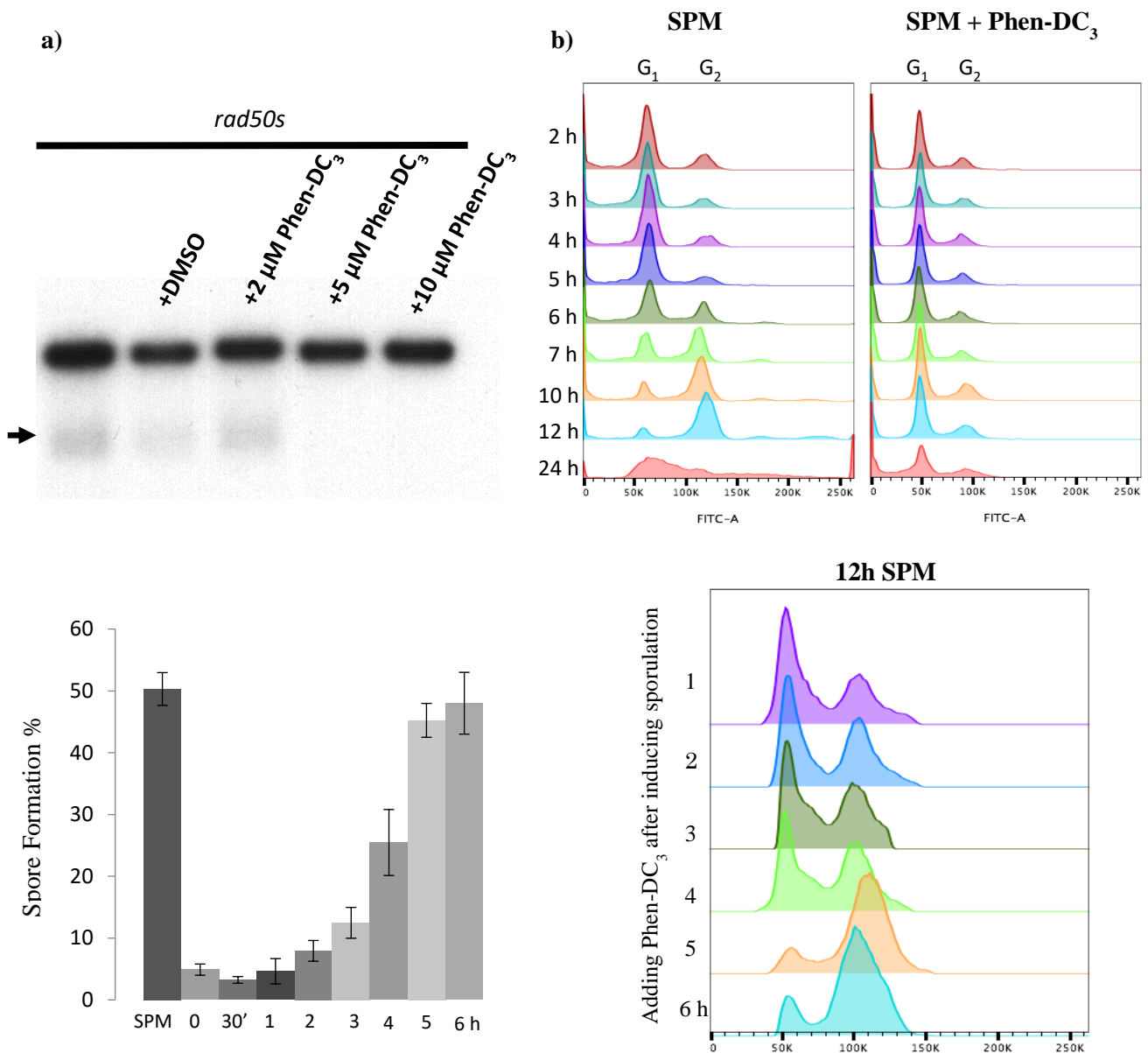


Figure 6: Phen-DC₃ leads to an arrest of cells in G₁-phase after transfer to SPM. **a)** Southern blot analysis of meiotic DSBs in dependency of Phen-DC₃. Sporulation was induced in diploid *rad50s* mutants and stopped after 24 hours. DMSO functions as a control to exclude the possible effect of the solvent on meiotic DSB formation. Lower bands represent meiotic DSBs. No meiotic DSBs were visualized upon a concentration of 5 μM of Phen-DC₃. **b)** Cell phase determination via FACS of sporulation induced SK1 cells with and without Phen-DC₃ (10 μM). For cells in SPM a clear progression from G₁- to G₂-phase was observed after 6h hours of sporulation. In contrast, sporulating cells treated with Phen-DC₃ did arrest in G₁-phase. **c)** 10 μM Phen-DC₃ was added to different time points after inducing sporulation, ranging from 0 (Phen-DC₃ immediately added) to 6 hours. Afterwards, percentage of tetrads were detected after 72 hours in SPM. Tetrad formation was less impaired when Phen-DC₃ was added at later time points after inducing sporulation. **d)** Cell phase determination via FACS 12 hours after inducing sporulation and in dependency of different Phen-DC₃ treatment time points. If Phen-DC₃ was added after one hour of sporulation most cells were still in G₁-phase after 12 hours in SPM. With increasing time in SPM prior to Phen-DC₃ treatment, G₁ arrest diminished. If Phen-DC₃ was added 5 hours or later after sporulation induction the majority of the cells progressed to G₂-phase after 12 hours sporulating time.

Ime1 overexpression does not rescue G₁ arrest

4.3 The decision to enter meiosis in *S. cerevisiae* is connected to a high expression level of the transcription factor Ime1¹⁴². Its expression is low during vegetative growth and rises in response to intrinsic and extrinsic signals such as nitrogen starvation and lack of a fermentable carbon source¹⁴². Upon a transfer to SPM, which lacks a nitrogen and a fermentable carbon source, expression of Ime1 is triggered and subsequently its targets, the early meiotic genes are expressed and subsequently transition to premeiotic S-phase takes place.

The level of *IME1* expression in vegetative and sporulating cells in dependency of Phen-DC₃ treatment was determined by quantitative PCR (3.16.). RNA was extracted and transcribed into cDNA from untreated and treated cells with 10 μM Phen-DC₃ (immediately added after transfer to SPM) 3 and 7 hours after inducing sporulation. As a control RNA was extracted from vegetative cells (OD₆₀₀ 0.5) with and without 10 μM Phen-DC₃. Quantitative PCR was performed in biological triplicates and technical duplicates using specific primers directed against Ime1 (Appendix Table 4). To determine *IME1* expression levels quantitative PCR results were normalized against expression levels of the housekeeping gene *ACT1*. As expected, high *IME1* expression levels were detected in cells 3 and 7 hours after inducing sporulation. Contrary, a 4- and 9-fold reduction of *IME1* expression was measured in cells 3 and 7 hours after inducing sporulation in addition of 10 μM Phen-DC₃ (Figure 7a).

Several points hint that G4s might directly affect the transcription of *IME1* by acting as a regulator within the promoter. i) Ime1 is indispensable for entry in sporulation and previous studies showed that a deletion of Ime1 resulted in a similar G₁ arrest after transfer to SPM as seen for Phen-DC₃^{145,201}. ii) the promoter region of Ime1 has the potential to form G4s according to the QGRS Mapper (<http://bioinformatics.ramapo.edu>). iii) the performed affinity purification against a G4 structure (3.12) identified Msn2 and subunits of the Set3 deacetylase complex (Set3, Snt1 and Hos4) (Appendix Table1). These proteins are directly involved in the regulation of Ime1.

Ime1 is negatively regulated by the lncRNA IRT1¹⁵⁵. IRT1 mediates the mating type control of sporulation. In Mata and Mata α haploids the expression of Ime1 is inhibited by the transcription of the Ime1 promoter antisense lncRNA IRT1. The lncRNA repression requires additionally the Set2 histone methyltransferase and the Set3 histone deacetylase complex. Together they establish a repressive chromatin state at the Ime1 promoter. Because of the identification of 3 subunits of the Set3 deacetylase complex by a G4 pull down, sporulation in dependency of Phen-DC₃ was performed in a *set2 set3* double mutant. By this I wanted to investigate if the observed G₁ arrest is due to a repressive chromatin at the *IME1* promoter by Set3 deacetylase

complex binding to stabilized G4s. If so, deletion of Set2 and Set3 should result in a rescue of Phen-DC₃-caused G₁ arrest. The diploid double mutant *set2 set3* strain was provided by the Amon Lab (Appendix Table 5)¹⁵⁵. Sporulation was induced and 10 μM Phen-DC₃ was added simultaneously. 72 hours later spore formation was determined via light microscopy. The spore efficiency of the double mutant *set2 set3* in SPM substituted with Phen-DC₃ was comparable to wild type cells treated with Phen-DC₃ (< 5%). A deletion of Set2 and Set3 did not lead to a rescue of deficient spore formation by Phen-DC₃. This indicates that missing Ime1 in Phen-DC₃-treated cells is not caused by Set2 and Set3 induced repressive chromatin at the *IME1* promoter.

To further validate, if the observed lack of *IME1* expression after Phen-DC₃ treatment is the cause of reduced spore formation, an overexpression of *IME1* in dependency of Phen-DC₃ was performed. This was done in order to test, if an overexpression of *IME1* in Phen-DC₃-treated cells leads to a transition from G₁- to S-phase.

In order to overexpress *IME1* in yeast cells, the Ime1 open reading frame (ORF) was PCR amplified and cloned into pCM251 via BamHI/NotI (3.3, Appendix Table 4)²⁰². In pCM251 the *IME1* open reading frame (ORF) is under control of a tetracycline/doxycycline inducible tetO2 promoter. TRP1 acts as a selection marker. After successful insertion of *IME1* ORF into pCM251, diploid W303 cells were transfected with this construct (pCM251-*IME1*). SK1 cells yielded no positive clones after transformation. The addition of 2 μg/ml, respectively 10 μg/ml doxycycline resulted in a 4-fold, respectively 6-fold *IME1* overexpression compared to none induced expression (Figure 7b).

To test, if increased *IME1* expression can rescue the Phen-DC₃ mediated G₁ arrest, cells harboring pCM251-*IME1* were transferred to SPM. Doxycycline was added at the same time as Phen-DC₃ (time point 0). After 36 hours the cell cycle distribution was monitored (3.7). For cells with a W303 background the cell distribution was determined later as compared to SK1 cells (36 hours vs. 12 hours), because of the slower sporulation capacity of W303 compared to SK1. Interestingly, overexpression of *IME1* did not lead to tetrad formation nor to G₂ progression even without Phen-DC₃ and under favorable sporulation conditions (Figure 7c). Because the pCM251 possesses the amino acid tryptophan as a marker, I wanted to rule out that the blockage of sporulation is due to a provided nitrogen source. Therefore, additionally to doxycycline, rapamycin was simultaneously added in a concentration of 1 μg/ml. Rapamycin was previously shown to bypass the extrinsic nitrogen source signal which is mediated via the TOR pathway²⁰³. Indeed, the addition of rapamycin led to a G₂ progression after transfer to SPM in cells carrying pCM251-*IME1*, indicated by an increased G₂ (4n) peak (Figure 7c).

Nevertheless, the downregulated TOR pathway did not lead to a release of G₁ arrested cells after Phen-DC₃ treatment (Figure 7d).

Because of the impaired sporulation capacity of pCM251-*IME1* exhibiting cells, a second approach for *IME1* overexpression with an established model was performed, to confirm that a

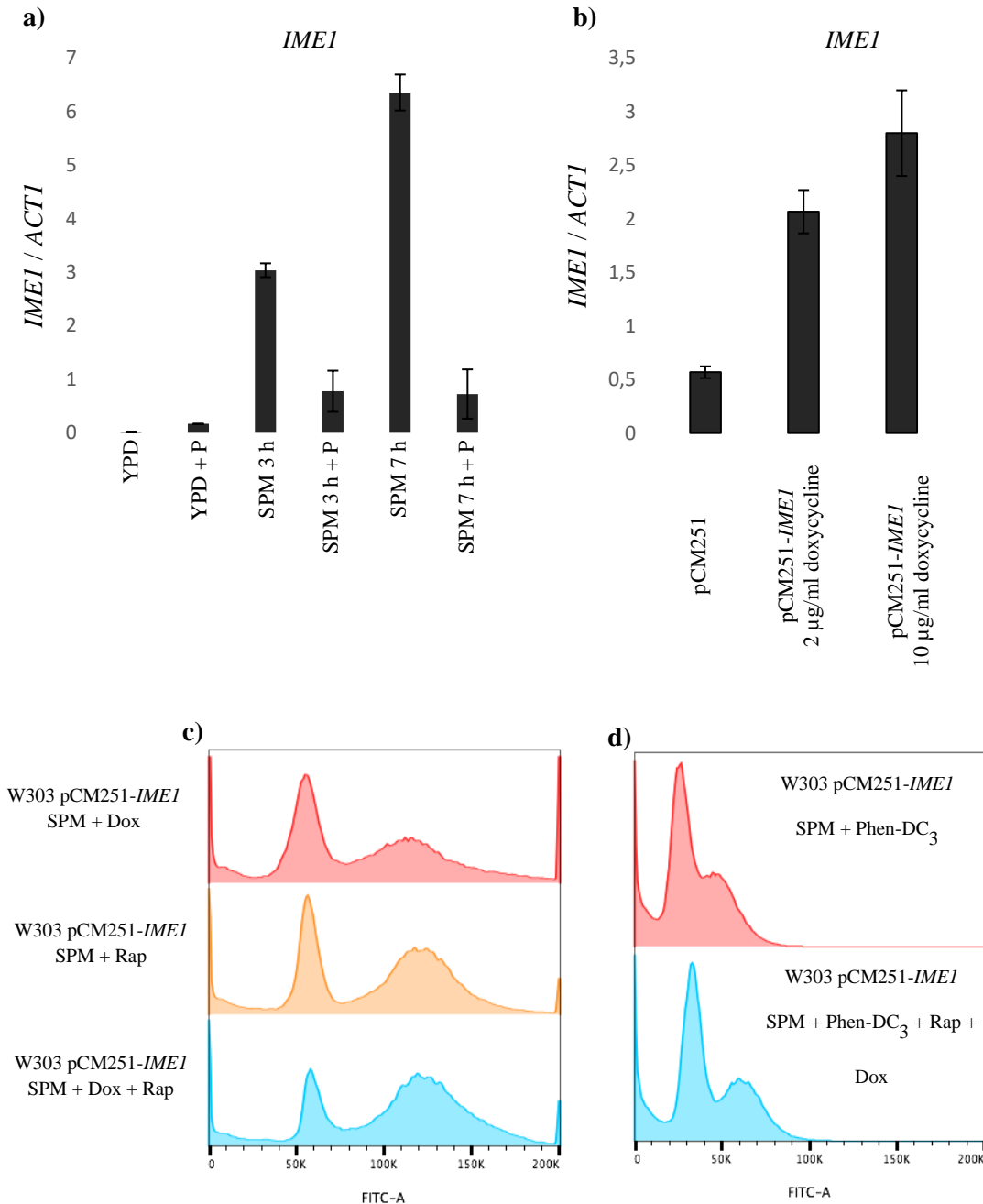


Figure 7: An overexpression of *Ime1* does not lead to G₂ progression of Phen-DC₃ arrested cells. **a)** Quantitative PCR analysis of *IME1* expression in vegetative cells (YPD) and sporulating cells (SPM) with (+P) and without Phen-DC₃. The experiment was performed in biological triplicates and technical duplicates. *IME1* expression level was normalized against expression level of housekeeping gene *ACT1*. **b)** Doxycycline induced overexpression of *IME1* via plasmid pCM251, determined via quantitative PCR 4 hours after doxycycline induction. **c)** Cell phase determination via FACS. Cells only progress to G₂-phase if additionally rapamycin (1 µg/ml) was added. **d)** No progression to G₂-phase upon *IME1* overexpression if Phen-DC₃ (10 µM) was additionally added.

IME1 overexpression does not rescue the Phen-DC₃-caused G₁ arrest. For this, the endogenous *IME1* promoter was replaced by an inducible copper promoter. The resulted strain FW2444 was provided by the van Werven lab (Appendix Table 5)²⁰⁴. Without copper, no entry into sporulation was detectable in SPM (Figure 8b). Upon addition of 50 μM copper *IME1* was expressed and cells progressed to G₂-phase during sporulation. Nevertheless, this approach also did not lead to a rescue of the G₁ arrest after G₄ stabilization (Figure 8b).

Previous studies showed that an expression of *IME1* alone is not sufficient for entry into meiosis. Ime1 also needs to accumulate in the nucleus in order to induce the expression of the early meiotic genes. This nuclear localization of Ime1 is blocked by expression of *CLN3* and by activation of the TOR pathway^{148,151}. Cln3 belongs to the G₁ cyclins and is during vegetative growth involved in cell progression and in G₁ to S-phase transition. However, during sporulation *CLN3* is down regulated¹⁴⁸. I determined the expression level of *CLN3* via quantitative PCR (3.16) to see, if *CLN3* expression is elevated in sporulating cells after Phen-DC₃ treatment.

The expression level of *CLN3* was determined from vegetative cells and sporulating cells in regard to Phen-DC₃ (Figure 8a). Similar levels of *CLN3* were detected for vegetative cells during exponential growth (OD₆₀₀ 0.5) with and without 10 μM Phen-DC₃ (Figure 8a). The expression levels in vegetative cells were between 1.5-fold and 2-fold higher compared to sporulating cells, no significant difference was observed if cells were treated with Phen-DC₃. Hence to the similar expression levels of *CLN3* in sporulating cells and sporulating cells treated with Phen-DC₃, Cln3 was excluded as a possible reason for Phen-DC₃ related G₁ arrest. Moreover, *CLN3* expression in sporulating cells should result in an unfavorable progression into mitosis under sporulation conditions and not in a G₁ arrest¹⁴⁸.

In order to down regulate TOR, the second repressor of nuclear Ime1 localization, 1 μg/ml rapamycin was simultaneously added to 50 μM copper after transfer to SPM. 12 hours after sporulation induction cell distribution was monitored via FACS (Figure 8b). Rapamycin treatment led cells progress faster to G₂-phase. However, the down regulation of TOR did not rescue the observed G₁ arrest after Phen-DC₃ treatment, indicating that not a change in Ime1 localization is the cause of G₁ arrest upon G₄ stabilization.

Taking together, repression of Ime1 by Phen-DC₃-stabilized G₄ structures does not seem to be the reason for the observed G₁ arrest.

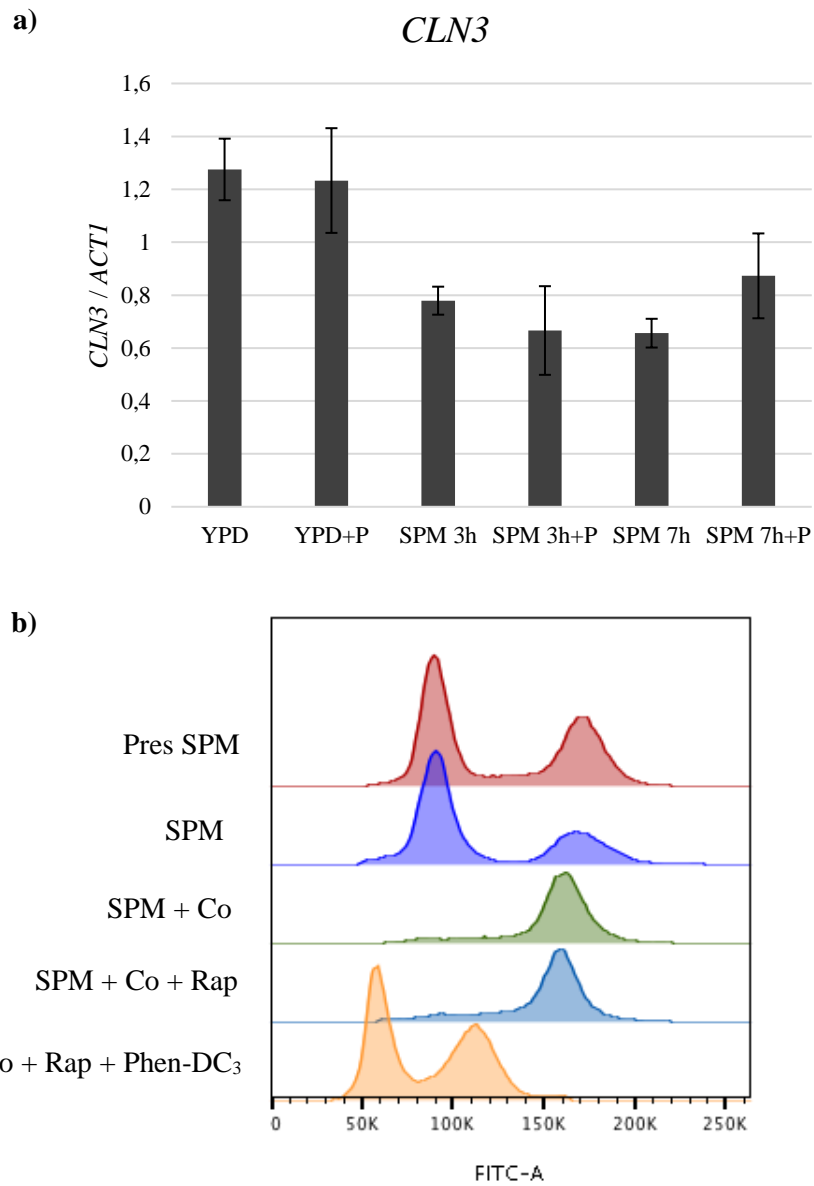


Figure 8: *Ime1* overexpression does not rescue Phen-DC₃-caused G₁ arrest. a) Quantitative *CLN3* expression in vegetative cells (YPD) and sporulating cells (SPM) with (+ P) and without Phen-DC₃. The experiment was performed in biological triplicates and technical duplicates. *CLN3* expression was normalized against expression of housekeeping gene *ACT1*. The expression level was the highest in vegetative cells (YPD) whereas it was lower in sporulating cells (SPM). No significant difference was observed for Phen-DC₃ treated (+P) and untreated cells. **b)** *IME1* overexpression via copper inducible promoter. Cell phases were determined 12 hours after inducing sporulation via FACS. Without copper, cells remained in G₁ and progressed to G₂-phase upon an addition of copper (50 μ M). Rapamycin was added to ensure the proper localization of *Ime1* to the nucleus. Nevertheless, treatment with copper and rapamycin did not lead to a G₂ progression of Phen-DC₃ arrested cells.

No elevated DNA damage response was recorded due to Phen-DC₃ treatment

Various studies have shown that G4 structures represent a risk for genome integrity^{93–95,129,205–218}. To assess the question if G₁ arrest of sporulating cells after G4 stabilization is caused by genome instability I determined the expression of established DNA damage markers.

Rnr3 is part of the ribonucleotide reductase (RNR) complex and is involved in deoxyribose nucleoside triphosphate (dNTP) synthesis²¹⁹. It plays an essential role in DNA synthesis and repair by providing all dNTPs required for these processes. Transcription of *RNR3* is inducible by DNA damage which makes it a common expression marker for DNA damage²¹⁹. To test, if *RNR3* is upregulated due to DNA damage caused by Phen-DC₃, the expression level of *RNR3* was determined via quantitative PCR in vegetative cells (cultured in YPD) and sporulating cells (culture in SPM) with and without Phen-DC₃.

Vegetative cells were collected during exponential growth (OD₆₀₀ 0.5). with and without Phen-DC₃ (10 μM) treatment. RNA was extracted and transcribed into cDNA. RNA extraction and following cDNA transcription were done as well for sporulating cells 3 and 7 hours after inducing sporulation. For the Phen-DC₃-treated cells 10 μM Phen-DC₃ was added immediately after transfer to SPM. Quantitative PCR was performed in biological triplicates and technical duplicates with specific primer against target gene and results were normalized to expression of *ACT1* (Appendix Table 4).

RNR3 was between 5- and 6-fold higher expressed after 3 and 7 hours of sporulation as compared to vegetative and Phen-DC₃-treated cells (Figure 9c). This is likely due to the focused premeiotic S-phase after prior G₁ accumulation in pre-SPM and because of meiotic recombination events that occur after premeiotic S-phase. No higher expression rates of *RNR3* were determined for vegetative cells and Phen-DC₃-treated cells. This result does not indicate higher genome instability due to Phen-DC₃ treatment.

I tested for histone H2A phosphorylation via western blot analysis (3.21). Histone H2A is one of four nucleosomes, which form together with DNA and additional proteins the chromatin²²⁰. The DNA damage-dependent phosphorylation of H2A by Mec1 facilitates DNA repair and can be used as a marker for DSBs²²¹.

Proteins were extracted from cells via trichloroacetic acid (TCA) preparation (3.18) from vegetative cells during exponential growth phase (OD₆₀₀ 0.5) and sporulating cells 16 hours after inducing sporulation without or with 10 μM Phen-DC₃. The used antibody was

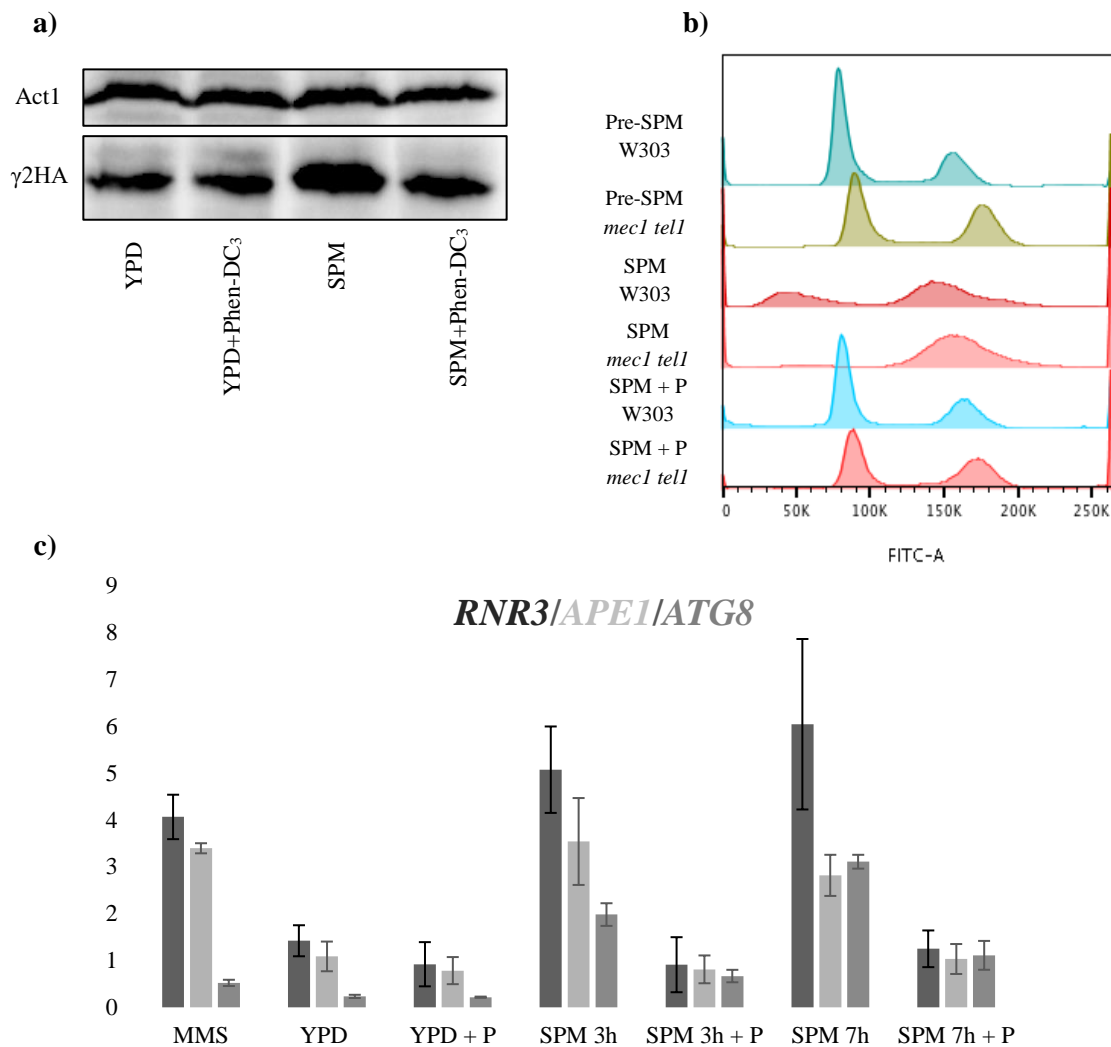


Figure 9 Determination of DNA damage in dependency of Phen-DC₃. **a)** Western blot analysis of H2A phosphorylation via anti-histone H2A (phospho S129, Abcam ab 15083). Proteins were extracted at OD₆₀₀ 0.5 from vegetative cells (YPD) and after 18 hours from sporulating cells (SPM). Phen-DC₃ was added in a concentration of 10 μ M and anti-Act1 antibody (Santa Cruz, sc-398161) was used as loading control. The SPM sample showed elevated H2A phosphorylation compared to the remaining samples, which showed a similar phosphorylation pattern. **b)** Cell phase determination of WT W303 and double mutant *mec1 tell* 36 hours after inducing sporulation with and without Phen-DC₃ (+P). **c)** Expression level of DNA damage marker *RNR3*, *APE1* and *ATG8*. Expression levels were determined via quantitative PCRs normalized against expression level of *ACT1*.

anti-histone H2A (phospho S129, Abcam ab15083). H2A phosphorylation was increased for sporulating cells (Figure 9a) which can be explained by the formation of meiotic DSBs during prophase I¹⁹⁷. In contrast, lower levels of H2A phosphorylation were detected for the remaining samples, respectively vegetative cells, vegetative cells treated with Phen-DC₃ and sporulating cells treated with Phen-DC₃, which does not speak for higher DSBs levels according to 10 μ M Phen-DC₃.

An additional response to DNA damage is driven by autophagy. Autophagy can be categorized into selective and nonselective pathways^{222,223}. The nonselective pathway also known as macrophagy is triggered by starvation in order to recycle nutrients under nutrient starvation

conditions²²⁴⁻²²⁶. The direct autophagy, also termed as genotoxin-induced targeted autophagy (GTA) is caused by DNA damage, which is distinct from the macrophage pathway^{222,223,227}. GTA requires the core components of the DNA damage response machinery (notably Mec1, Tel1 and Rad53), but these proteins do not have a significant role in starvation-induced autophagy, indicating that the signals mediating GTA are distinct from those involved in starvation-induced autophagy²²³. However, macrophagy is in a lower rate also active during GTA. Autophagy acts by regulating the level of proteins involved in DNA repair and cell progression and thereby controlling cell fate^{228,229}. One generally used marker of autophagy is the key protein Ape1 which is upregulated due to induction of mainly macrophagy and to a lower extent during GTA^{223,230}. A specific marker for GTA is Atg8 which is mainly upregulated as a result of DNA damage-induced autophagy²²³.

To test for an autophagy-induced upregulation of *APE1* (macrophagy) and *ATG8* (GTA) quantitative PCR was performed (3.16). RNA from cells under different conditions was extracted. Cells during exponential vegetative growth, cells during exponential vegetative growth treated with 10 μ M Phen-DC₃ and cells 3 and 7 hours after inducing sporulation with and without 10 μ M Phen-DC₃. Quantitative PCR was performed in biological duplicates and technical triplicates and expression levels were normalized to the housekeeping gene *ACT1*.

For *APE1* an approximately 3-fold higher expression level was detected in sporulating cells compared to vegetative cells (Figure 9c). This is in line with studies that stated an induction of autophagy due to starvation. The remaining samples show similar expression levels including the samples substituted with Phen-DC₃ indicating missing induction of macrophagy after Phen-DC₃ treatment.

To test for GTA, the expression level of *ATG8* was monitored via quantitative PCR as well. In vegetative cells, a similar low level of *ATG8* was detected with and without Phen-DC₃ (Figure 9c). Higher expression levels were observed for sporulating cells. Around 9 times higher *ATG8* expression was observed 3 hours after inducing sporulation and circa 14,5-fold higher expression after 7 hours compared to the expression level in vegetative cells. The higher expression of *ATG8* in sporulating cells is presumably due to a partially response of GTA to nitrogen starvation and because of induced meiotic DSBs.

In contrast to previous tested DNA damage marker higher levels of *ATG8* were also detected in sporulating cells upon Phen-DC₃ treatment. Around 2.5-fold higher *ATG8* expression after 3 hours and around 5-fold higher after 7 hours compared to vegetative levels. Higher level of *ATG8* in sporulating cells treated with Phen-DC₃ can be explained by a partially activation of GTA as a response to nitrogen starvation^{231,232} or as a result of remaining spore

formation (< 5%; Figure 5b). On the other hand, according to this argument, the expression level of *APE1* should then also be higher for cells in SPM plus Phen-DC₃. Thus, *ATG8* expression in SPM cells treated with Phen-DC₃ indicates an increased DNA damage after G₄ stabilization.

To address the question if a Phen-DC₃-induced G₁ arrest occurs due to G₁/S checkpoint activation in response to DNA damage, the yeast DNA damage checkpoint orthologs of ATM and ATR, named Tel1 and Mec1 were eliminated²³³. It was shown that cells, which were arrested in G₁-phase upon UV light or gamma radiation failed to arrest at G₁ checkpoint after *mec1* deletion²³⁴. Furthermore, *mec1 tel1* deletion blocks autophagy and general G₁ checkpoint arrest in response to DNA damage^{223,234,235}. Tel1 recognizes DSBs and generates ssDNAs which are recognized by Mec1, leading to phosphorylation of downstream protein kinases, causing cell cycle arrest and regulation of repair proteins²³⁶. The G₁ arrest allows cells to repair DNA damage prior to DNA replication to prevent a potentially deleterious S-phase.

The cell cycle distribution of the double mutant *mec1 tel1* strain was analyzed via FACS, using the nucleic acid stain SYTOX Green (3.7) after 36 hours of sporulation without and in dependency of Phen-DC₃. The sporulation times were in this case increased because of the W303 background which sporulates slower than the SK1 background. 10 μM Phen-DC₃ was immediately added after transfer to SPM. In SPM, both strains, wild type and *mec1 tel1* mutant, progressed to G₂-phase (Figure 9 b). The mutant strain proceeded faster to G₂-phase than wild type cells, most likely due to missing S/G₂-phase checkpoint. Meiotic DSBs trigger transient activation of the DNA damage checkpoint response machinery²³⁷. Nevertheless, also the *mec1 tel1* mutant strain was not capable to transit to premeiotic S-phase if Phen-DC₃ was added, indicated by a dominant G₁ peak.

4.4 In summary, elevated genome instability in SPM in the presence of 10 μM Phen-DC₃ appears not to be the reason for the observed G₁ arrest upon Phen-DC₃ treatment.

Phen-DC₃ treatment leads to an altered proteome in sporulating cells.

Various studies demonstrated a role of G4s in gene regulation. A computational study revealed that 42.7% of human gene promoters overlap with G4 motifs, especially proximal to the transcription start sites (TSSs)²³⁸. It was also shown that G4s have a higher tendency to form in transcription enhanced and nucleosome depleted promoter regions²³⁹. Further, genome-wide ChIP analyses revealed an overlap of gene expression associated helicases XPB and XPD with G4 motifs in promoter regions^{61,240}. The most extensively researched gene which is regulated by G4s is the human oncogene c-MYC. It was shown that stabilization of G4s via TMPyP4 led

to repression of c-MYC transcription and a mutation of the G4 motif in the promoter of c-MYC resulted in an increased expression¹⁰².

To identify proteins which show an altered appearance in response to Phen-DC₃ during sporulation proteome analyses were performed with cells at different time points during sporulation with and without Phen-DC₃. For this purpose, samples from 12 different time points were collected. From the time point 0 before transferring to SPM, 10, 20, 30, 60, 90, 120, 180, 240, 300, 360 and 420 minutes after inducing sporulation. Especially at the beginning, the time points were in small intervals to address primary changes in protein occurrence, because Phen-DC₃ seemed to affect the beginning of meiosis (Figure 6c). For this approach I chose 5 μM Phen-DC₃, which is sufficient to see a strong effect on sporulation (Figure 5b); this lower concentration was chosen, because of limited amount of Phen-DC₃ and the large amount of liquid culture, which was needed for this experiment. The mass spectroscopy was in the following performed by the Interfaculty Mass Spectrometry Center of the University of Groningen. The subsequent analysis was done using Peaks 8.0 viewer. Proteins were considered as positive using following parameters: 20% protein threshold, 0.1% False Discovery Rate for peptides, a minimum of one unique peptide, one-fold change or higher and an occurrence of peptides in at least 6 samples. Applying these parameters 575 proteins were found for the sporulation series and 328 proteins for the series containing Phen-DC₃. 350 proteins were exclusive found in the sporulation series and 103 exclusives in the Phen-DC₃ series (Appendix Table 2).

Between timepoint 0 and 420 minutes after inducing sporulation the occurrence of 71 proteins were at least 2-fold increased and 275 proteins at least 2-fold decreased in sporulation samples after 420 minutes (Appendix Table 3). For samples treated with Phen-DC₃ 27 proteins were 2-fold or higher increased and of 77 proteins 2-fold or higher decreased after 7 hours compared to the start of sporulation (Appendix Table 3). The top ten biological process GO terms (String; string-db.org) showed diverse processes in which the proteins are involved. Note, none of the identified proteins showed a clear involvement in DNA damage repair.

Genome-wide mapping of G4 structures during vegetative growth and during sporulation in *S. cerevisiae*

4.5 G4 structures are linked to fundamental biological processes such as transcription, replication and telomere maintenance^{52,60,102,240–242}. To support their involvement in biological processes and to uncover new potential regulatory sights it is crucial to map G4 structures genome-wide in a chromatin context. ChIP is a widely used method to map the genome-wide location of DNA-binding proteins in an endogenous chromatin context²⁴³. Therefore, a G4 antibody ChIP-seq approach enables the determination of G4 structures genome-wide. Two recently developed single-chain antibodies against G4 structures were used in this thesis. The antibody BG4, with a broad selectivity for a wide range of G4 structures, including parallel, antiparallel and hybrid forms⁷⁹ and the antibody D1 with a restricted specificity for parallel G4s⁷⁷.

BG4 ChIP-seq was recently established for human cells by Hänsel-Hertsch et al.¹⁸⁰, in which they mapped ~10 000 G4 structures in human chromatin. For *S. cerevisiae* a genome-wide map of G4 structures in the chromatin is missing. I performed G4 antibody ChIP-seq with the antibodies BG4 and D1 followed by high throughput sequencing for cells during vegetative growth and during sporulation with and without Phen-DC₃ in order to detect differences in G4 occurrences. I uncovered potential new G4 regulatory sites and putative regulatory differences between vegetative growth and sporulation. Moreover, G4 distribution within the chromatin changed after G4 stabilization.

The antibodies were overexpressed and purified accordingly to methods 3.8. Additionally, the specificity of BG4 for a G4 structure over unfolded DNA was determined via microscale thermophoresis (MST) (3.9). MST confirmed that BG4 bound preferred to folded G4 structures over unfolded DNA (Appendix Figure 1).

The experiment was performed in duplicates for each condition. For vegetative growth cells from the exponential growth phase in YPD (OD₆₀₀ 0.5) were used. Sporulating cells were crosslinked 3 hours after inducing sporulation. For G4 stabilizing conditions 10 μM Phen-DC₃ was added. The protocol published by Hänsel-Hertsch et al.¹⁸⁰ was used with minor changes for suitability to yeast (3.10). 1-1.5 μg of chromatin was deployed per sample. Antibodies were added in a 2:1 ratio (1 μg chromatin = 500 ng antibody). 18 samples: four samples of vegetative cells, four samples of vegetative cells plus Phen-DC₃, four samples of sporulating cells, four samples of sporulating cells plus Phen-DC₃, herein two samples of each condition with antibody BG4 and two samples of each condition with antibody D1 and further, input as control for vegetative and sporulating cells were used for library preparation (3.10). The high-throughput

sequencing was performed by the Next Generation Sequencing (NGS) Core Facility of the Medical Faculty of the University of Bonn.

Subsequent biocomputational analysis was done in accordance with Hänsel-Hertsch et al.¹⁸⁰ and is briefly described in methods (3.11). In order to call robust G4s the G4 ChIP regions from duplicates were intersected and filtered for overlaps. Only peaks present in both duplicates were used for further analysis.

ChIP-seq with the antibody BG4 yielded 623 G4 structures in vegetative cells, 381 in vegetative cells supplemented with Phen-DC₃, 239 G4 regions in sporulating cells and 408 if Phen-DC₃ was added. ChIP-seq with the antibody D1 yielded 550 G4 structures in vegetative cells, 418 in vegetative cells supplemented with Phen-DC₃, 215 G4 regions in sporulating cells and 676 if Phen-DC₃ was added.

The peaks overlapped significantly between the different conditions and between the two antibodies, especially between samples within one group (sporulating cells, sporulating cells plus Phen-DC₃, vegetative cells and vegetative cells plus Phen-DC₃) (Figure 10b). Moreover, the greatest overlap between four samples was found for vegetative cells and vegetative cells plus Phen-DC₃, implicating a smaller change in G4 appearance when Phen-DC₃ was added to vegetative cells compared to sporulating cells.

Further, bedtools jaccard revealed a high correlation between the two sets of G4 regions found by each antibody. In vegetative cells 68% of the regions were identical for the two antibodies and 65% if G4s were stabilized. In sporulating cells, the overlap was 43% and 46% if Phen-DC₃ was added.

To associate the identified G4 structures to putative regulatory functions the G4s were validated for enrichment or depletion to various genomic features by comparison to random occurrence within the yeast genome using the website yeast.genomes.nl. The mitochondrial genome, the telomere and centromere regions were excluded.

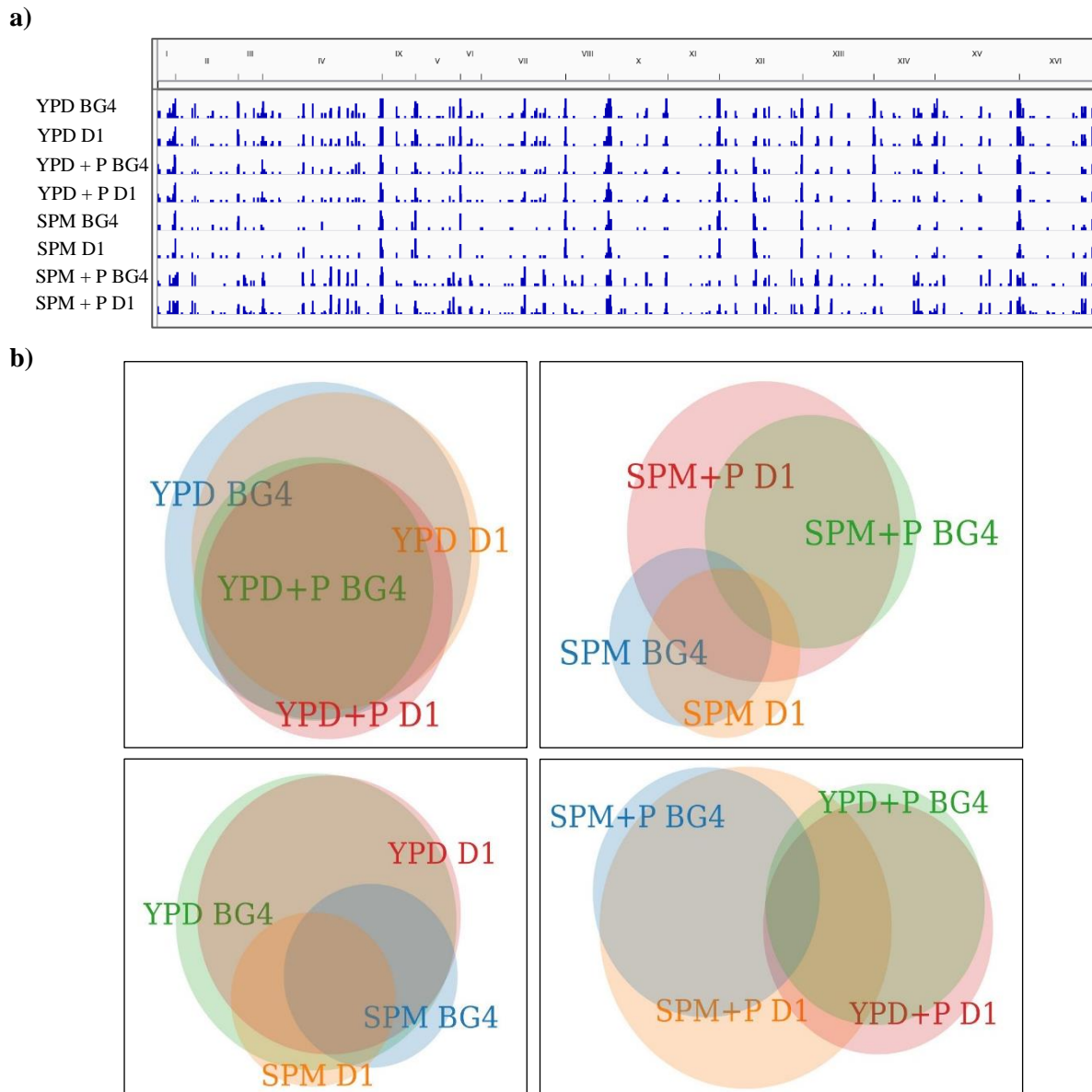


Figure 10: **a)** Genome browser screenshot for *S. cerevisiae* genome, showing common and differential G4 (BG4/D1) ChIP peaks in vegetative cells (YPD), sporulating cells (SPM), Phen-DC₃ treated cells (P); Appendix Figure 14 screenshot of chromosome XI. **b)** Venn diagrams showing the shared and unique G4 ChIP regions mapped in vegetative cells (YPD), sporulating cells (SPM), Phen-DC₃-treated cells (P). The larger the overlap between the samples, the darker the background color.

To validate the specificity of the antibodies the overlap of G4 ChIP-seq peaks with predicted G4s (*in vitro*) was determined. Genome-wide computational analyses by Capra et al.¹⁰ predicted G4 motifs along the genome of *S. cerevisiae* using an algorithm searching for G4 motifs with at least four tracts of three or more consecutive guanines separated by loop regions of 25 nucleotides or less. The ChIP-seq samples from vegetative and sporulating cells without Phen-DC₃ showed an enrichment with a $p\text{-value} \leq 0.0004$. This correlation was lost for G4-stabilized sporulation samples (Appendix Figure 2).

A different study used a G4-seq-based approach to predict G4 structures *in vitro* without G4 stabilizing and under G4 stabilizing conditions¹³. Again, by correlating the ChIP-seq data to the G4 map without G4 stabilizing conditions the vegetative and sporulating samples without Phen-

DC₃ overlap significantly, especially for the vegetative samples with Phen-DC₃ (p-value ≤ 0.0001) (Appendix Figure 3). Contrary, the sporulating cells treated with Phen-DC₃ showed again no significant overlap between the G4-seq peaks and the provided G4 map by Marssico et al.¹³. Less homogeneity was observed for the correlations between the ChIP samples and the provided G4-seq map under G4 stabilizing conditions via PDS (Appendix Figure 4)¹³. For vegetative samples the overlap was less significant or even completely missing like for D1 ChIP-seq of vegetative cells treated with Phen-DC₃. Also, the sporulating samples did not show an overlap with the PDS-stabilized G4-seq map. On the other hand, the sporulating ChIP-seq samples treated with Phen-DC₃ displayed a significant overlap (p-value ≤ 0.0183).

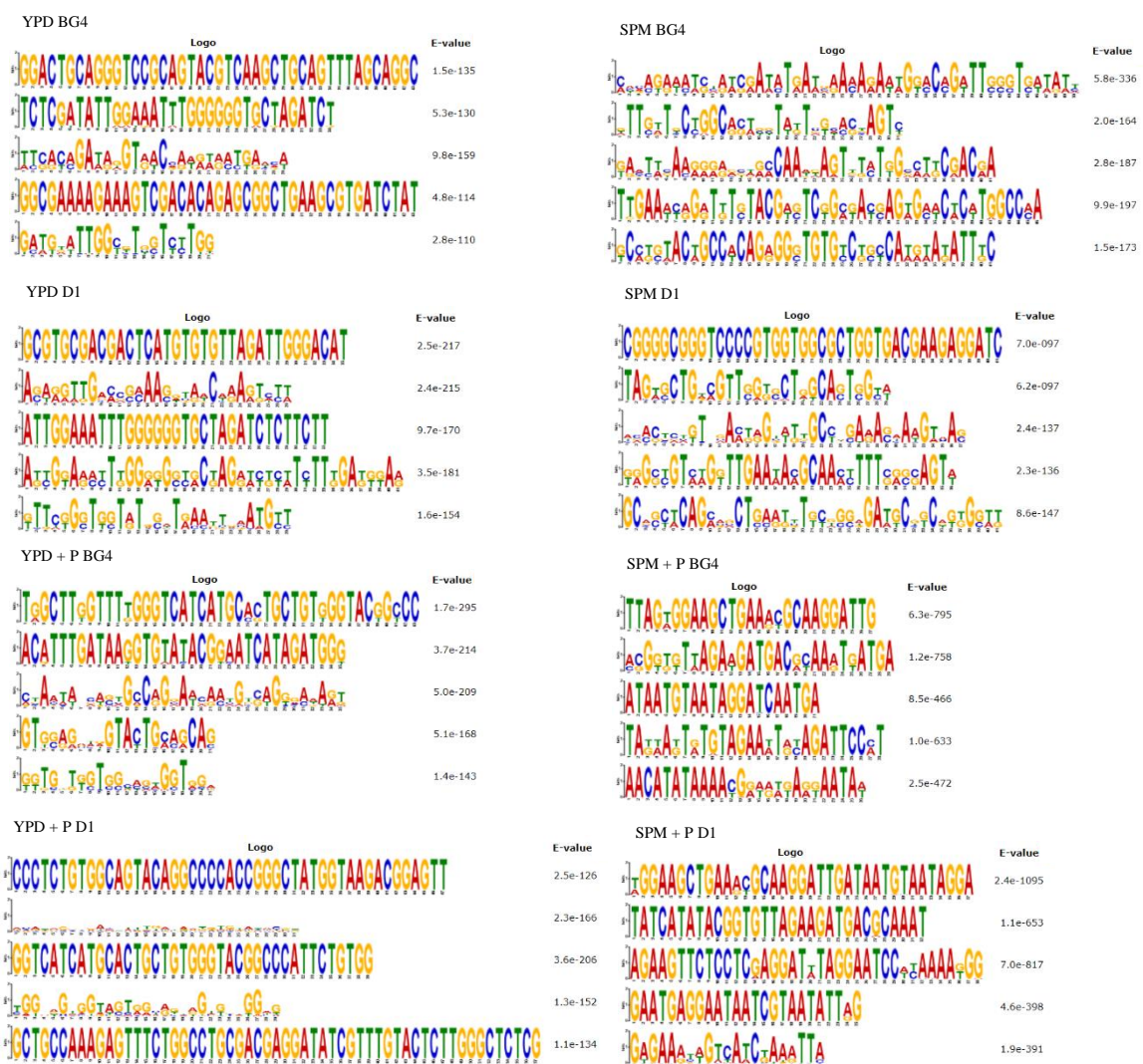


Figure 11: Motif discovery using MEME for BG4/D1 ChIP-seq peak data set reveals the presence of five possible recurring motifs (E-value < 0.1) within the entire peak file. Vegetative cells (YPD), sporulating cells (SPM), Phen-DC₃-treated cells (P).

Additionally, a motif discovery was performed using multiple expectation maximization for motif elicitation (MEME)²⁴⁴ to detect consensus binding sequences for BG4 and D1 (Figure 11). MEME is a tool for discovering motifs in a group of related DNA sequences from

a given group of DNA sequences and outputs motifs to a user-specified statistical confidence threshold. Among the top motifs for each sample extracted by MEME G-rich sequences were found to be highly prevalent within the G4 ChIP peaks as expected for a G4 antibody consensus sequence (Figure 11).

Next, the ChIP-seq-determined G4 regions were analyzed for overlaps with certain genomic regions. As expected, all G4 peaks were highly enriched for nucleosome depleted regions ($p\text{-value} \leq 0.0001$) (Appendix Figure 5), which is in line with previously found overrepresentations of G4 motifs in nucleosome free regions¹⁸⁰. G4s were also overrepresented at sub telomeric regions (Figure 10a). This is in agreement with past studies which showed that the sub telomeric regions of *S. cerevisiae* can adopt G4 structures *in vitro*²¹¹. G4 peaks also overlapped with retrotransposons ($p\text{-value} \leq 0.001$), especially the Phen-DC₃-treated sporulating cells (Appendix Figure 6). In detail, the G4-stabilized sporulation samples were also highly enriched in the retrotransposon flanking long terminal repeats (LTRs) ($p\text{-value} \leq 0.001$), whereas the G4 peaks of all other samples were depleted in the region of LTRs ($p\text{-value} \leq 0.0028$) (Appendix Figure 7). G4 structures were also found in LTRs of the human immunodeficiency virus (HIV) and further retroviruses²⁴⁵.

To assess the correlation between G4s and promoter, the overlap between G4 peaks and genomic regions 1000 bp upstream of transcription start sites (TSS) was determined. G4s were depleted ($p\text{-value} \leq 0.0001$) at these regions (Appendix Figure 8). Furthermore, ChIP-seq obtained G4 regions were underrepresented at replication start sites (ARS), 5' and 3' untranslated regions (UTRs) ($p\text{-value} \leq 0.0001$) (Appendix Figure 9 - 11). Notably, G4 peaks did not show an overlap with preferred meiotic DSB sites (Appendix Figure 12), which is in contrast to previously found predictions¹⁰. A nonuniformity within the samples was found for G4s at ORFs. At ORFs G4s in vegetative cells and G4-stabilized sporulating cells were depleted ($p\text{-value} \leq 0.0001$); this depletion did not exist in sporulating cells, even though they were not enriched either (Appendix Figure 13).

Proteins bind specifically to G4 structures

4.6 G4 structure formation and unwinding need to be regulated due to their high thermostability and slow formation and dissociation kinetics²⁴⁶. If not tightly regulated, G4 structures represent a risk for genome integrity²⁴⁶. In fact, various G4 binders, formation supporters and unwinders are known^{50,80,86,95,175,212,247}.

In order to identify novel G4-binding proteins during meiosis and potential candidates, involved in G4 stabilization caused G₁ arrest, an affinity purification with lysates from sporulating cells was performed (3.12). For this, a G4 motif was folded as described in methods (3.17) and confirmed to form parallel G4 structures via CD (Figure 12a, b). As a control, a mutated G-rich oligonucleotide was used, which was not capable of forming a G4 structure (Figure 12a, b). Only one nucleotide per G-tract was switched from G to C in order to change the sequence as less as possible and additionally maintaining the GC content. Indeed, the G4 motif showed the typical minima (245 nm) and maxima (262 nm) for parallel G4 structures, whereas the mutated G4 motif showed the characteristic wavelength of unfolded DNA²⁴⁸. The interaction partners of the mutated G4 motif were subtracted in the evaluation procedure to ensure that identified proteins are in fact specific G4 binders rather than general binders. Moreover, only G4 binding partners were considered that were detected in at least two of four G4 pull down samples. The Mass spectrometry (MS) analysis was carried out by the Interfaculty Mass Spectrometry Center (University of Groningen).

The experiment was performed in technical and biological duplicates and lysate of two different time points during sporulation were used, 3 hours and 7 hours after inducing sporulation. This timepoints were chosen to ensure that a majority of cells already entered sporulation in order to identify specifically meiotic proteins. Proteins were eluted via high salt concentration (800 mM NaCl) after prior washing with 200 mM NaCl in order to wash away unspecific, weak binder. I evaluated the obtained data using PEAKS 8.0 viewer. The identified proteins were sorted in order to identify specific G4 binder by using following parameters: 20% protein threshold, 1% False Discovery Rate (FDR) for peptides and a minimum of two unique peptides. Using the applied parameters, a total amount of 676 proteins were found of which 244 proteins were specific only in the pull-down samples with a folded G4 structure. Out of 244 specific G4 binder 129 proteins were identified in one sample, 63 proteins were present in two samples, 34 in three samples and 18 existed in all four sample (Appendix Table 1) while not being present in samples obtained from pull down with linear DNA.

To reveal robust G4 binder I focused on proteins which bound specific to G4 structures in at least 2 samples. GO term analysis (String; string-db.org) confirmed that the 115 proteins that were present in at least 2 samples were implicated in similar biological processes and molecular functions (Figure 12c, d). Of 34 RNA binding proteins 5 possessed a RGG motif (Dbp1, Gar1, Hrp1, Sbp1, Gbp2), which was connected to G4 binding^{83,84}. 4 proteins (Sbp1, Dbp1, Bre1, Air2) were also identified as G4 binders in a recently published affinity purification and quantitative mass spectroscopy study.

Several proteins with a function during meiosis were identified: Mum2, Msn2, Set3, Snt1, Hos4 and Nam8. Mum2 is needed for meiotic DNA replication and as part of the MIS complex involved in RNA methylation during induction of sporulation^{249,250}. Msn2 is a stress-responsive transcriptional activator which regulates together with Msn4 around 200 genes in response to stress, including expression of Ime1^{143,251,252}. Set3, Snt1 and Hos4 are part of the Set3 deacetylase complex, which is a meiosis-specific repressor of sporulation genes²⁵³⁻²⁵⁵ and a repressor of master regulator Ime1¹⁵⁵. The transcription of the lncRNA IRT1 recruits the Set2 histone methyltransferase and the Set3 histone deacetylase complex to establish repressive chromatin at the *IME1* promoter and thereby inhibiting *IME1* expression¹⁵⁵. Nam8 is a subunit of the yeast U1 small nuclear RNA (snRNP)²⁵⁶. It is essential for sporulation, because it promotes splicing of mRNAs that encode proteins required for sporulation such as Rec107, which is involved in meiotic DSB repair²⁵⁷. This is in line with studies showing an overrepresentation of G4 motifs at exon/intron boundaries^{258,259}. These newly identified proteins will provide a basis for detailed future characterizations of G4 binder.

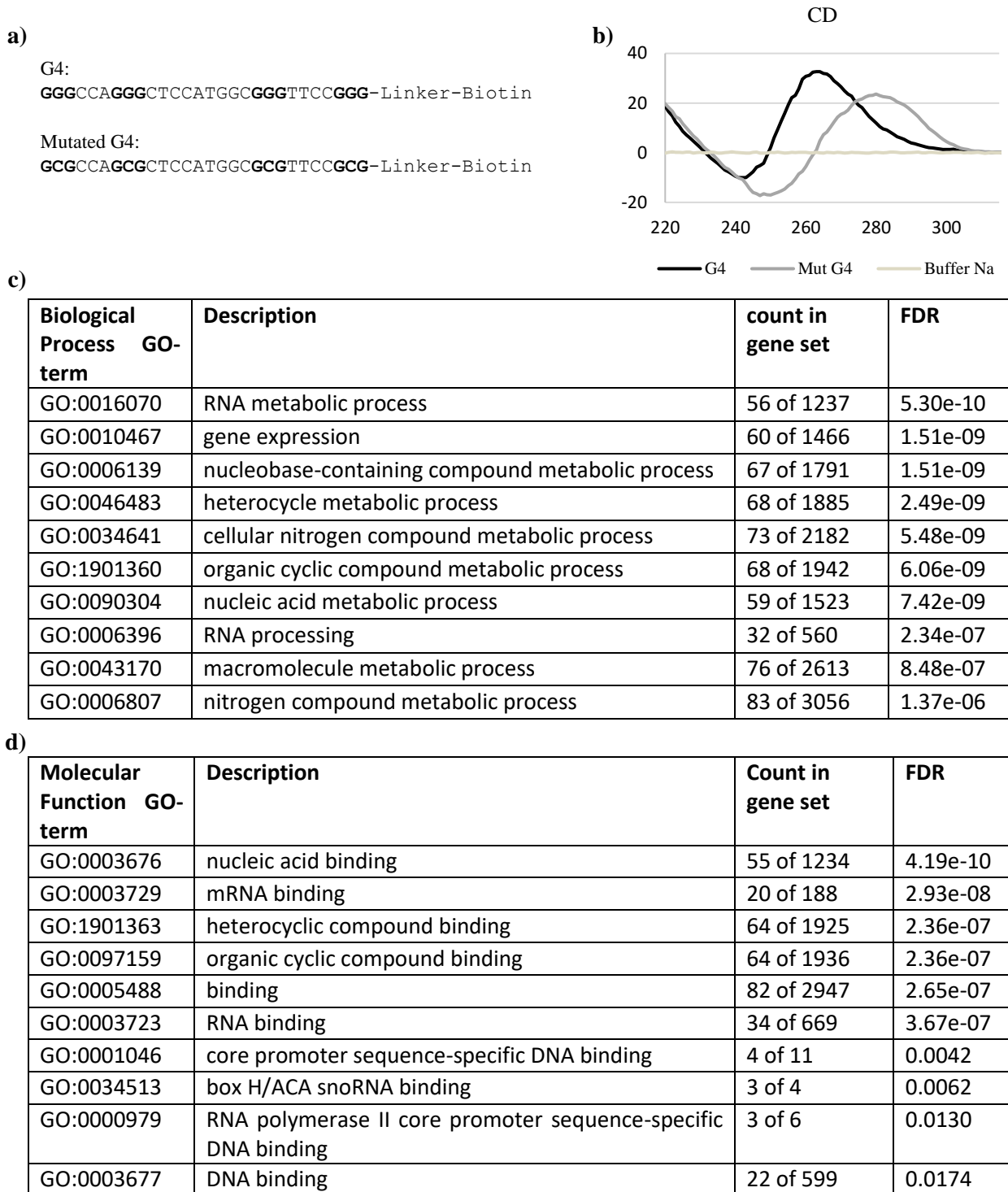


Figure 12: Affinity purification against G4 structure revealed specific G4 binder. **a)** For affinity purification used oligonucleotides. **b)** Circular dichroism spectroscopy of folded oligonucleotides. Folded G4 sequence showed the characteristic minima at 245 nm and maxima at 262 nm for parallel G4 structures, whereas the mutated G4 motif showed the characteristic wavelength of unfolded DNA. **c)** Biological Process GO-term of 115 proteins which were in at least two samples present. **d)** Molecular Function GO-term of 115 proteins present in at least 2 samples.

Telomeric insertion stimulates meiotic DSBs

As a second project I wanted to determine the correlation between G4s and meiotic DSBs. Computational analysis revealed an overrepresentation and conservation of G4 motifs at certain DNA regions such as meiotic DSB sites¹⁰. At these genome sites the meiotic DSB frequency is higher than elsewhere in the genome. Meiotic DSBs and consequently meiotic recombination events are essential for the right segregation of chromosomes during meiosis I¹³⁶⁻¹³⁸.

Further, studies showed that an insertion of yeast telomeric DNA at locus *HIS4* results in a high level of meiotic DSBs and consequently in a very strong meiotic recombination hot spot at *HIS4*^{199,260}. Because the yeast DNA sequence exhibit a G4 motif and can form G4s *in vitro*²⁶¹ one aim of my thesis was to examine if this stimulation is G4 dependent or more likely due to the specific telomere sequence. To address this question, I requested a *rad50s* mutant strain with a wildtype *HIS4* locus, named as FX3 (Appendix Table 5) and a *rad50s* strain with an additional insertion of a telomeric sequence at *HIS4*, termed FX4 (Appendix Table 5) from the University of North Carolina¹⁹⁹. The *rad50s* mutation allows the visualization of meiotic DSBs via Southern blot by the accumulation of unrepaired DSBs due to a defective MRX complex.

The parental *rad50s* mutant strains of FX3 (DNY107 × HF4) were also used to create additional strains by Cre/loxP recombination (3.5) with a telomeric G4 motif and different mutant variants of the sequence inserted at *HIS4*. The Cre/loxP site method was chosen in order to have a less severe change in the primary structure of the *HIS4* locus. The mutant variants exhibit as described followed, the telomeric sequence with disrupted G-tracts, telomeric sequence with an alternative middle loop sequence, telomeric sequence with shortened loop lengths and telomeric sequence with extended loops (Figure 13, 14). The desired oligonucleotides were designed with additional EcoRV restriction sites at the 5' and 3' end and via EcoRV digestion integrated in pUG6 plasmid. All insertions were performed in order to exhibit the G4 motif on the top strand and the bottom strand. Afterwards, the plasmid was partially amplified and inserted into the genome of DNY107 and HF4. Afterwards the strains harbored the favored sequences, a KanMX marker and two loxP sites. Subsequently, cells were transfected with plasmid pSH65, possessing a galactose inducible Cre recombinase. Finally, after Cre induction, the cells exhibited the different inserts and two loxP sites. Genomic DNA was extracted (3.1) from diploid mutant strains after 24 hours of sporulation. At this time point, the majority of meiotic DSBs occurred¹⁹⁹. After following BglII (NEB) digestion, the meiotic DSBs were visualized via southern blot analysis as described in methods (3.22). As a probe, a DIG labeled PCR product of ORF *HIS4* was used (used primer see Table 4).

The strongest stimulation of meiotic DSBs at locus *HIS4* showed the strains with a telomeric insertion and the G4 motif with short loop length (Figure 13). Lower activation of the meiotic hot spot was seen for strains with longer loops and more decreased for strains possessing the mutated G-tracts. However, these strains still showed a higher frequency of meiotic DSBs than the strain with the wild type *HIS4* locus. The low meiotic DSB frequency for the wild type *HIS4* compared to the publication resulted presumably from the here used lower sensitivity of DIG labeling compared to the publication used P³² isotope¹⁹⁹. For the increased meiotic DSB frequency it does not matter in which orientation the sequence was inserted. The only strains which did not show observable meiotic DSBs are the strains with the alternative loop sequence.

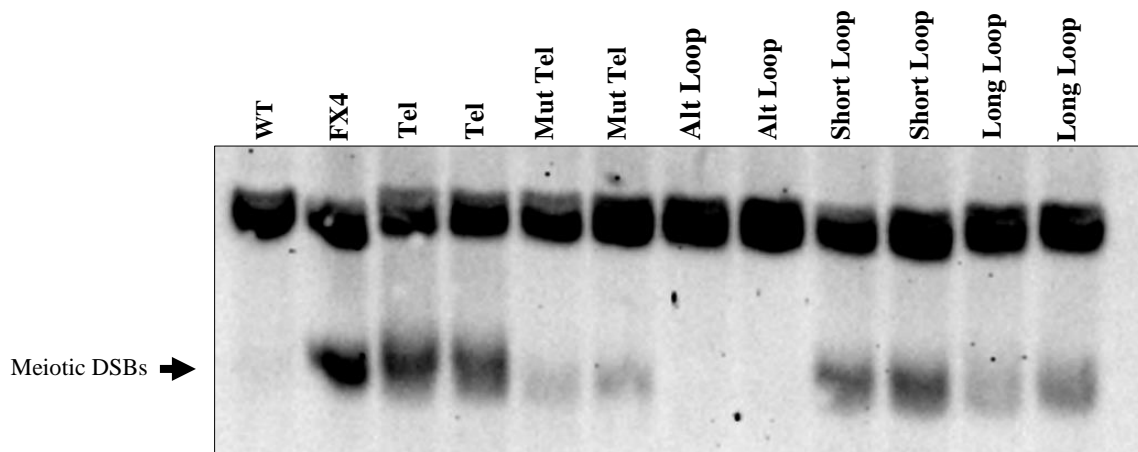


Figure 13: Southern blot analysis of meiotic DSBs at *HIS4* locus. Genomic DNA were extracted 24 hours after inducing sporulation and subsequently digested with BglIII. Labeled PCR probe served as probe using primer against *HIS4* (Appendix Table 4). Strongest meiotic DSB stimulation were visualized in cells containing a telomer insertion at *HIS4* (FX4, Tel) and strains containing a G4 motif with short loop length. Also, high level of meiotic DSBs showed the strains containing a G4 motif with extended loop lengths. Lower intensities were displayed by strains exhibiting a mutated G4 motif. DSBs were hardly visible for the WT *HIS4* and absent for cells containing telomeric G4 motif with an alternative loop sequence.

5 Discussion

Effect of G4s on meiotic DSB formation

G4 structures were shown to overlap with preferred meiotic DSB sites¹⁰. At these “hot spots”, between 1-2 kb in size, the meiotic DSBs and consequently the recombination frequency is 5.1 higher than anywhere else in the genome^{262,263}. The meiotic recombination starts with the formation of DSBs in order to ensure the proper segregation of chromosomes during metaphase I, by establishing connections between the homologue chromosomes¹³⁶⁻¹³⁹. A genome-wide map of preferred meiotic DSBs in *S. cerevisiae* shows a significant overlap of meiotic DSB hot spots with G4 motifs¹⁰. In addition, the MRX complex, which is involved in meiotic DSB formation, binds to G4 structures *in vitro*^{175,247}. Furthermore, it was demonstrated that a telomeric sequence inserted in the meiotic DSB hot spot site *HIS4* resulted in an increase of meiotic DSBs at this site^{199,260}. It was shown that the telomeric sequence of *S. cerevisiae* can form G4 structures *in vitro*, with the potential to form G4s *in vivo*^{50,240,264}. Proteins that are essential for telomere maintenance and function, such as the potent G4 unwinder Pif1, are known G4 binder^{265,266}.

These findings let me look closer into the correlation of G4 structures and meiotic DSBs. In line with the hypothesis that observed DSBs are G4 mediated I expected that telomeric G4 motifs, as well as alternative telomeric G4 motifs, stimulate DSB formation during meiosis. Previously, telomeric DSB stimulation was explained by Rap1 binding^{260,267}. Rap1 binds and promotes G4 formation⁵⁰. To test, if G4 formation triggers DSB formation I inserted alternative versions of the telomeric G4 motif with either short, long or alternative loops. According to the QGRS Mapper all of these inserts can form G4 structures. Surprisingly, the telomeric G4 motif with the alternative middle loop sequence did not show detectable meiotic DSBs, even though the motif has the potential to form a G4 structure (Figure 13, 14). Moreover, the mutated G4 motif with G to C conversions in their G-tracts showed meiotic DSBs, regardless of a missing potential to form G4 (provided by QGRS mapper).

From these results I concluded that G4s alone do not trigger meiotic DSBs. The results agree with findings during vegetative growth. Here, in wild type cells G4s alone do not stimulate recombination, they were shown to only trigger recombination events in the absence of helicases or if stabilized^{94,129}.

Furthermore, my results are supported by previous findings, which demonstrated that Rap1 binding can stimulate meiotic recombination events at locus *HIS4*^{260,267}. They demonstrated that the hot spot region upstream of *HIS4* possesses a Rap1 binding site and that a mutation in that binding site resulted in a lower meiotic recombination frequency. Moreover, the overexpression of Rap1 led to an increase of meiotic recombination frequency at locus *HIS4*. This effect cannot be indirect, because an overexpression of Rap1 did not lead to a higher meiotic recombination frequency when the Rap1 binding site was mutated²⁶⁷.

Later on, White et al. observed that the insertion of additional Rap1 binding sites by inserting a telomeric sequence proximal to *HIS4* resulted in an elevation of meiotic recombination events and consequently in a higher meiotic DSBs frequency at this site^{199,260}, even if the telomeric sequence does not represent a perfect Rap1 binding consensus sequence²⁶⁸. It exhibits 2 binding sites, which match in 11 out of 13 bases to the consensus sequence. It is likely that this binding site is sufficient for Rap1 binding, because it was shown that Rap1 binds to yeast telomeric repeats²⁶⁹. Additionally, the verified Rap1 binding site at *HIS4* exhibits the same sequence identity to the Rap1 consensus sequence than the telomeric sequence.

The potential Rap1-caused stimulation of meiotic DSBs at *HIS4* could also provide a favorable explanation for the results observed in this thesis. The highest meiotic DSB frequencies are observed at the telomeric inserts and the G4 motifs with a short loop length, followed by the G4 motifs with an extended loop length (Figure 13, 14). All three sequences match in 11 bases to the Rap1 consensus sequence. In case of the insert with the extended loop length the distance between the two Rap1 binding sites is larger compared to the telomere sequence and to the sequence with the short loops (Figure 14). The lower DSB frequency can be caused by a weaker interaction between Rap1 and the binding site due to a greater distance between the binding sites.

Lower DSBs frequency was observed for the mutated G4 motif, which possesses 2 binding sites with one nucleotide less overlap to the Rap1 consensus sequence (10 nt) (Figure 13, 14). A possible explanation is a weaker binding of Rap1 to the sequence. The least identity with the Rap1 consensus sequence (8 nt) was also the insert that did not show any detectable meiotic DSB formation. It is conceivable that 8 consistent bases are not sufficient for Rap1 binding and consequently no Rap1-stimulated meiotic DSB formation took place.

How Rap1 stimulates meiotic recombination is not known. It was excluded that it is correlated to transcription of *HIS4*, because silencing of *HIS4* did not result in a change of DSB frequency²⁶⁰. There are several possible suggestions how Rap1 could facilitate meiotic DSB formation¹⁹⁹. The favored hypothesis is that Rap1 provides an open chromatin structure leading

to an increased accessibility for the recombination machinery. This is supported by the fact that Rap1 affects DNA bending²⁷⁰, stimulates the formation of DNA loops²⁷¹ and nucleosome positioning²⁶⁸. Another possible explanation is an interaction between Rap1 and one or more proteins of the recombination machinery, although there are hot spots that do not exhibit a Rap1 binding site¹⁹⁹. A third option is that Rap1 localizes the genomic DNA to a nuclear position where meiotic DSBs occur, which is supported by the characteristic of Rap1 to localize to the nuclear periphery²⁷².

Discarding the mechanism by which Rap1 stimulates meiotic DSB formation, the meiotic DSB analysis used in this thesis does not answer if Rap1 binds to the sequences used in this thesis or not. Nor it gives a conclusion if these sequences are forming G4 structures *in vivo*.

Our conclusion about G4 formation during meiosis is based on predictions. It is not possible to foresee which sequences form G4 structures *in vivo* due to the high polymorphism of G4 structures with their variable loop length and their ability to form stable G4s even with bulges. Also, the presence or absence of G4 interaction proteins during meiosis could alter the formation of G4s.

In my genome-wide ChIP-seq experiments no overlap of G4 peaks to preferred meiotic DSB sites was detected. This argues against an involvement of G4s at meiotic DSB hot spots. However, the BG4/D1 ChIP-seq has been started 3 hours after inducing sporulation and it could be that G4s that stimulate DSBs were not folded, yet. There are different phases during meiosis, which require the activation and silencing of specific proteins¹³⁴. If G4s are a regulatory tool involved in meiotic DSB formation, then they need to be tightly regulated and specifically formed during prophase I, when DSBs are needed^{140,197}. This implies that proteins that are active in this phase, such as Hop1, Kem1 or the MRX complex, which were shown to bind or promote G4 formation *in vitro* and which are involved in meiosis could regulate G4 formation^{175-177,179,247}. However, there is not yet *in vivo* evidence that Hop1, Kem1 or the MRX complex carry out their meiotic functions by acting at G4 structures. Also, none of these proteins were found in the affinity purification performed in this thesis. Additionally, Spo11, that creates the meiotic DSBs, does not cleave at G4 motifs²⁷³.

Future experiments require the detection of G4s at later stages of meiosis to determine the changes of the G4 landscape according to meiosis progression. It is also interesting to address, if Rap1 is binding to the sequences used in this thesis and if G4 structures are present at *HIS4*. One possibility to address these questions can be provided by different ChIP approaches. A Rap1 ChIP could examine, if Rap1 binds in a chromatin context to the sequences used in this thesis and a BG4/D1 ChIP during prophase I could deliver the answer, if G4 structures are

Further interaction partners belong to the class of proteins involved in splicing. Pre-mRNA splicing is crucial for the proper expression of eukaryotic genes. Despite the fact that *S. cerevisiae* belongs to the relatively intron-poor species with a more compact genome, it still possesses about 300 annotated intron-containing genes^{301,302}. The spliceosome components are highly conserved from yeast to mammals at the sequence, structure and functional level^{303,304}. Also, G4-binding proteins involved in splicing were found in previous studies^{299,300}. A role of G-quadruplexes in alternative splicing was for instance shown for the tumor suppressor gene TP53 mRNA³⁰⁵. In the mRNA of TP53 a G4 structure in intron 3 modulates the splicing of intron 2 and treatment with the specific G4 ligand 360A altered the ratio of two different splice forms.

Nam8, a meiosis-specific splicing factor, was identified in this thesis. Nam8 is a subunit of the yeast U1 small nuclear RNA (snRNP)²⁵⁶. It is essential for sporulation due to its splicing of mRNAs that encode proteins required for sporulation like Rec107²⁵⁷, which is also involved in meiotic DSB repair.

The identification of RNP components and splicing factors as G4 binder verifies the specificity of the performed G4 pull-down. Four identified proteins (Sbp1, Dbp1, Bre1, Air2) were also identified in a recently published study³⁰⁶. Moreover, of 34 RNA binding proteins 5 possessed an RGG motif (Dbp1, Gar1, Hrp1, Sbp1, Gbp2), which is indicative for G4 binder^{83,84}.

Despite the mentioned parameters to ensure specific G4 binding over general capacity to interact with guanine-rich sequences, future additional controls of selected proteins could confirm their G4 specificity. For instance, proteins enriched by the G4 pull-down could be analyzed by western blotting to confirm G4 binding. Thereby address additionally the direct binding to G4 structures. Even though the stringent washing steps during the G4 pull-down assay are removing indirect false positive binding proteins. It cannot be completely ruled out that proteins bind indirect to G4 structures, for instance in case of the Set3 deacetylase complex, Snt1 was suggested to be the DNA binding domain³⁰⁷.

Further, pull-down assays with sequences forming different G4 structures could cover more potential G4 binding proteins. Due to the high polymorphism of G4 structures it is likely that organisms require specific proteins to selectively modulate a given G4 structure.

Early effects of G4 formation on meiosis

It was shown that 500 μM Phen-DC₃ is triggering genome instability in yeast at human minisatellite CEB1 inserts, without having an effect on vegetative growth¹²⁹. CEB1 are G-rich tandem repeats with the potential to form G4 structures²¹².

5.3

Here it was demonstrated that significant lower amounts of Phen-DC₃ (10 μM) had no effect on vegetative growth but a severe effect on sporulation. Cells did not only form hardly spores (< 5%) when treated with Phen-DC₃, but they also arrested in G₁-phase after transfer to SPM (Figure 6b).

Ime1, the master regulator of meiosis is crucial for the G₁/S-phase transition

5.4

In budding yeast, initiation of sporulation is mediated by a single master regulatory transcription factor, termed inducer of meiosis 1 (IME1)¹⁴⁵. It activates the transcription of early meiotic genes, which transit cells from G₁-phase of the mitotic cell cycle into the meiotic program²⁷⁴. I speculated that reduced spore formation and G₁ arrest were due to changes in *IME1* expression. The regulation of *IME1* expression is very complex, mainly due to its long promoter region and two regulatory RNA molecules. In agreement with my hypothesis, it has been shown that Ime1 deficient cells are also arrested in G₁-phase^{145,201}. Two regulators of Ime1 (Msn2, Set3 complex) were identified in the G4 affinity purification executed in this thesis. That and the fact that the Ime1 promoter region has the potential to form G4s, according to the QGRS Mapper, supported the theory that Ime1 could be regulated by G4s. Stabilization of G4s in this case would in turn result in a repression of Ime1.

Previously, G4 structures in promoter regions of HER2, MET and c-MYC have been shown to repress the expression of their genes^{102,275,276}. The addition of G4-specific ligands in yeast and humans has been linked to changes in gene expression^{11,102,103,277-279}. I speculated that G4 formation and stabilization by Phen-DC₃ prevents *IME1* expression. Quantitative PCR analysis of RNA levels of treated versus untreated cells after 3 and 7 hours of sporulation revealed that *IME1* expression is ~4-fold respectively ~9-fold reduced in Phen-DC₃-treated cells as compared to untreated cells (Figure 7a). If low amounts of Ime1 is the cause of G₁ arrest, reintroduction and stimulation of *IME1* expression would lead to transition into S-phase.

I overexpressed *IME1* in two different ways (Figure 7b, c, d, 8b). The first approach was via a tetracycline inducible plasmid and the second via an endogenous copper inducible promoter. Chia and van Werven²⁰⁴ demonstrated with the copper-inducible system that an induction of *IME1* expression in SPM is sufficient to induce meiosis in Ime1-deficient cells. However, both

overexpression experiments did not lead to a rescue of Phen-DC₃-caused G₁ arrest (Figure 7c, d, 8b). It is unlikely that this is because of a mislocalization of Ime1 outside of the nucleus. The downregulation of the TOR pathway, which was demonstrated to cause a delocalization of Ime1 via rapamycin, did not lead to a rescue of Phen-DC₃-caused G₁ arrest (Figure 7c, d, 8b). Further, Cln3, a second factor that is responsible for the localization of Ime1 is not higher expressed in Phen-DC₃-treated cells (Figure 8a). In addition, that Ime1 is not the reason for the observed G₁ arrest is supported by the fact that the replacement of the endogenous *IME1* promoter by a copper-inducible promoter and thereby eliminating the potential effect of G4 structures on the *IME1* promoter regions did not lead to S-phase progression.

DNA damage accumulation can stop G₁/S transition during meiosis

5.5 10 μM Phen-DC₃ is not sufficient to cause severe genome instability in cells growing in YPD. But it was demonstrated that an addition of 20 μM Phen-DC₃ to synthetic complete media (SC media), was sufficient to increase CEB1 instability to a similar extent as 500 μM Phen-DC₃ in YPD. Additionally, 20 μM Phen-DC₃ in SC media causes a drop in the growth rate of around 50%. For 10 μM and 5 μM Phen-DC₃ the growth slowdown was approximately 20% and 10%, respectively¹²⁹. The results from this work are indicating that Phen-DC₃ could have a more severe effect on cells in SPM as well.

Additionally to CEB1 instability, it has been shown that accumulating DNA damage, for example by 200 mM HU, stalls cells in G₁/early S-phase²⁸⁰. Further, G4 motifs are prone to mutations in pif1-deficient yeast cells⁹⁴. These joint observations led me to the speculation that my observed G₁/S arrest might be due to accumulating DNA damage.

The preferred repair pathway in *S. cerevisiae* is affected by the mating type. A heterozygote mating type (diploid) is favoring homologous recombination (HR) over non-homologous end joining (NHEJ)^{281,282}. During HR an identical or similar DNA molecule, such as a sister chromatid or a homologous chromosome serves as template²⁸³. This repair mechanism is less error prone than NHEJ, which only uses a short single-strand overlap to repair a DNA-DSB²⁸⁴. For this reason, NHEJ is only predominately active in haploid G₁ cells when no homologous chromosomes or sister chromatids are available²⁸⁵. In a/alpha diploids NHEJ is repressed, thus promoting HR. Sporulating cells show the capacity of DNA repair by HR. As a result of meiotic DSBs cells perform extensive HR events¹³⁸. Therefore, sporulating cells should have the ability to repair DSBs via HR.

I tested by quantitative PCR and western blot analysis, if more DNA damage accumulates in sporulating cell treated with Phen-DC₃ compared to untreated. DNA damage marker *RNR3*,

APE1 and H2A did not show higher expression levels or phosphorylation in treated compared to untreated cells, arguing for no increased DNA damage due to Phen-DC₃. However, the GTA expression marker *ATG8* showed higher expression levels in sporulating cells treated with Phen-DC₃ compared to vegetative cells and to vegetative cell treated with Phen-DC₃, indicating genome instability. GTA is a selective autophagy pathway which is induced as response to DNA damage in order to regulate proteins involved in DNA repair and cell progression²²³. I speculated that elevated DNA damage occurred in the cell after G4 stabilization and that this activated the G₁/S-phase checkpoint, which consequently leads to G₁ arrest. The ATM and ATR orthologs Tel1 and Mec1 perform an important role in DNA damage sensing, as well as in transduction of DNA damage^{286,287}. In particular Mec1 is a very important transducer of DNA damage and replication stress signals. It transmits the signal due to UV damage, DSBs, and stalled replication forks via Mec1-dependent phosphorylation of Rad53, which is in turn necessary for a full checkpoint response²⁸⁸⁻²⁹⁰. Mec1 mutants are not only sensitive to DNA damaging agents, but also fail to arrest the cell cycle in response to DNA damage via UV radiation or in response to inhibition of DNA synthesis by hydroxy urea²⁹⁰⁻²⁹³. Tel1 is similar to ATM likely only involved in response to DSBs. Tel1 deletion is not connected to a higher sensitivity to DNA damage reagents, its enhances the sensitivity of *mec1* mutants though, indicating an overlap in function^{294,295}. Therefore, I hypothesized that *mec1 tell* mutants should fail to arrest after Phen-DC₃ treatment, if G4-caused genome instability is the reason for the G₁ arrest.

Deletion of these kinases did not release cells from the G₁ arrest as indicated by a strong G₁ peak in the FACS analysis (Figure 9b). This argues against a Phen-DC₃ mediated genome instability caused arrest via activation of the G₁/S checkpoint. This fits to the results of the other tested DNA damage marker such as *RNR3*, *APE1* and γ 2HAX, which did not indicate DNA damage.

As indicated before, these data are to some extent in contrast to studies in vegetative cells. Treatment with the G4 stabilization agent RHPS4 in human fibroblast led to elevated γ H2Ax foci²⁹⁶. Phen-DC₃ triggered genome instability at CEB1 integrated into the yeast genome¹²⁹. Multiple studies in cancer cell lines demonstrated DNA damage and proliferation suppression after G4 stabilization^{74,100,113,124}. This is explained by the nature of cancerous cells, such as active telomerase, which is blocked by stabilized G4s and due to the impaired DNA repair capacity in many cancerous cells. In contrast, elevated G4 levels caused by deletions of helicases in yeast did not lead to increased γ H2Ax phosphorylation⁹⁴. Helicase deletion and

consequently G4 accumulation in the absence of Pif1 and increasing genome instability also did not activate DNA damage checkpoints (unpublished findings, Prof. Dr. Katrin Paeschke). The data presented in this thesis demonstrates that it is unlikely that the observed G₁ arrest by Phen-DC₃ is caused by severe genome instability and downstream checkpoint activation.

Changes in transcriptional level of essential meiotic genes

5.6 By computational and G4 sequencing methods it was demonstrated that G4 motifs are overrepresented in promoter regions of human, yeast and *C. elegans*¹⁰. Contrary, a recent G4 sequencing approach did not indicate G4 enrichment in promoter regions of *S. cerevisiae*¹³. Also, the BG4/D1 ChIP-seq data from this thesis did not exhibit an overrepresentation of G4s in promoter regions. Nevertheless, G4s are still present in promoter regions where they might have a regulating effect. Previous studies have shown that the addition of G4 ligands, including Phen-DC₃, resulted in up and down regulation of gene expression in human cells¹⁸⁹. If a G4 stabilization causes a positive or negative effect on transcription is dependent on the position of the G4 structure. Two putative scenarios were suggested, either G4s form upstream of the transcription start site (TSS) or G4s form downstream of the TSS. Upstream they can cause a positive or negative effect on transcription, depending on their capability of interfering with the transcription machinery, transcription factors binding, recruiting G4 binding proteins, representing an obstacle for protein binding or maintaining an open chromatin conformation. If G4 structures are present downstream of the TSS they are proposed to have an enhancing effect on transcription when located in the coding strand due to an open, transcription-favoring strand confirmation, or a suppressing effect on transcription, if located in the template strand due to stalling the progression of RNA Pol II²⁹⁷. For example, it has been demonstrated by luciferase reporter assays that stabilization of G4s by TMPyP4 leads to significant downregulation of the particular reporter gene²⁹⁸.

I speculated that essential early meiotic genes, which drive meiotic S-phase, are blocked or inhibitors are upregulated by G4 stabilization. For example, with the Set3 deacetylase complex one such factor was identified during this thesis to bind specific to G4s (Appendix Table 1). The Set3 complex is involved in the repression of Ime1 in haploid cells¹⁵⁵. Also, the findings that a distinct amount of found G4 binder are involved in gene expression shows the potential of G4s in regulating transcription and supports the theory that G4 stabilizing could alter the transcriptome to sporulation unfavorable conditions.

A proteome analysis of sporulating cells with and without Phen-DC₃ did not provide a clear conclusion that could explain the Phen-DC₃-caused arrest. Proteome analyses have the

limitation that upon the absence/lack of proteins it is not clear, if this is caused by technical problems or by a regulatory effect. This problem is indicated by the fact that I could not detect key proteins essential for meiosis, such as Ime1, Ime2, Ime4, Hop1, Spo1, etc., even without Phen-DC₃. Other proteins specific for sporulation were present, like Rim4, demonstrating that cells entered sporulation. Comparison of the existing proteins with genes exhibiting G4s in their promoter via G4 ChIP-seq did not show an obvious regulator. For a deeper analysis of the altered regulation after G4 stabilization a complementing method like a transcriptome analysis would be necessary and of great interest to identify the missing puzzle pieces.

Genome-wide mapping of G4 structures in chromatin of *S. cerevisiae*

5.7 A bioinformatical approach revealed 668 G4 motifs in the genome of *S. cerevisiae*¹⁰. More recently, a G4 sequencing method identified 103 G4s, with a potential of 498 G4s when G4s were stabilized with PDS¹³. They provide an experimental reference map of potential G4 structures but do not provide a map of potential G4s in a chromatin context. By using a G4-specific antibody ChIP-seq approach, I mapped the genome-wide location of G4 structures in the chromatin of *S. cerevisiae*. The amount of detected G4s was comparable to the expected amount of G4s according to Capra et al. but higher than expected from Marsico et al.^{10,13}. G4 stabilization did not result in increased G4 structure formation in vegetative cells. Additionally, the overlap between the four vegetative samples, vegetative cells BG4/D1 and vegetative cells + Phen-DC₃ BG4/D1 was the highest (Figure 10b). One explanation is that G4 motifs might not be available for forming G4 structures in a chromatin context under this condition. Another possibility is that the used Phen-DC₃ concentration of 10 μ M was not high enough in YPD media to ensure a significant G4 stabilization. In studies which showed genome instability after Phen-DC₃ treatment the concentration was up to 500 μ M in YPD media¹²⁹. G4 signals differ between different cell types. This argues against mapped G4 structures being an artifact caused by antibody binding. Additionally, it shows the potential different regulation capacity mediated by G4s between vegetative and sporulating cells and the possible impact of G4 stabilization. Cells within one population showed always the most overlap between BG4 and D1 compared to cells of another population (vegetative cells, sporulating cells, sporulating cells treated with Phen-DC₃). G4 signals between different populations demonstrated a significant overlap as well, with additional distinct signals, but significant for the given population (Figure 10b). Sporulating cells showed significantly less G4s compared to the other samples, indicating a less frequent occurrence of G4s during sporulation.

Correlations between the identified G4 structures and the reference G4 maps of Capra et al.¹⁰ and Marscico et al.¹³ showed a significant overlap between the predicted G4s and the observed G4 peaks via ChIP-seq arguing for the correctness of the identified G4s. However, this enrichment was missing for sporulating cells treated with Phen-DC₃. An argument for the specificity of the BG4/D1 ChIP-seq in these samples is the high repeatability between SPM samples treated with Phen-DC₃. One explanation is that Phen-DC₃ is might supporting in these cases the formation of G4s that would otherwise be unlikely to form. This could also be true for the G4-seq under PDS stabilizing conditions¹³. The less significant overlap between the ChIP-seq data and the list of G4s obtained from G4-seq under G4 stabilizing conditions by Marscico et al.¹³ is supporting this possibility.

The identification of G4 structures in a chromatin context by BG4/D1 ChIP-seq has the prospect to uncover new regulatory insights. G4s were overlapping nucleosome-depleted regions (NDRs) which are generally transcriptionally more active, because of a higher accessibility for proteins of the transcription machinery. According to previous studies, G4s were also enriched at sub telomeric regions which show an overrepresentation of G4 motifs¹⁰. Whereas G4s were enriched at promoters in the human genome and especially at promoters of highly expressed genes⁶¹ G4s did not significantly overlap promoter regions in *S. cerevisiae*. Moreover, genes which overlap with G4s in their promoter regions did not show particular high or low expression rates according to Nagalakshmi et al. and Miura et al.^{308,309}.

G4s were suggested to be involved in meiotic DSBs because of an observed overlap of G4 motifs with preferred meiotic DSB sites¹⁰. This overlap could not be confirmed in this thesis. Nonetheless, for the case that these G4s would be highly dynamic and only existing during meiotic recombination, there is a chance that these G4 structures could have been overseen via BG4/D1 ChIP-seq, because this approach represents a snapshot of cells in their current cellular state. Sporulating cells were cross linked 3 hours after inducing sporulation where the vast majority of cells should not have ended premeiotic S-phase according to FACS analysis (Figure 6b) which is crucial before meiotic DSB formation.

G4 peaks were overrepresented in LTR retrotransposons for all samples. This could be partially explained by the wide span which LTR retrotransposons cover within the genome. LTR retrotransposons represent dynamic segments of DNA that can move from one position to another in the genome via an RNA intermediate. They are flanked by two LTRs and encode a minimum of two genes, *gag* and *pol*, to ensure its replication³¹⁰. A significant proportion of the genome in eukaryotes consist of LTR retrotransposons³¹¹. The 12.2 Mb *S. cerevisiae* genome for instance harbors 483 conserved LTR retrotransposon insertions³¹².

I observed a striking enrichment of G4 signals in the flanking LTRs for Phen-DC₃-treated SPM samples whereas G4 peaks were depleted in other samples. The identified presence of G4s in LTRs is in line with previous findings in plants and lentiviruses^{313,314}. Studies in plants showed that G4 motifs are preferentially located inside of LTRs, upstream and downstream of predicted promoters³¹⁴. Two models were proposed: the formation of a G4 upstream of the promoter in the minus strand can open the DNA double helix and promote transcription, while formation of a G4 downstream of the promoter in the plus strand can inhibit or stop elongation of nascent RNA strands. The second option is supported by observed viral transcription silencing due to G4 stabilization in HIV-1³¹⁵. Moreover, G4 ligands were shown to strongly reduce virus propagation^{316,317}.

Work from a broad range of host organisms suggests that LTR retrotransposon insertions are generally deleterious and that natural selection acts to suppress proliferation in host populations. They mediate many types of simple and complex chromosomal rearrangements, including deletions, segmental duplications, inversions and reciprocal and nonreciprocal translocations^{318–333}. Different kinds of environmental stress, such as ionizing radiation, DNA damage, nitrogen starvation, and severe adenine starvation activate LTR transcription and mobility in *S. cerevisiae*^{334–339}. In diploid cells it was demonstrated that nitrogen starvation activates the LTR retrotransposon promoter³³⁶. Further, under conditions of severe adenine starvation it was observed that an insertion of a LTR retrotransposon adjacent to a gene coactivates its transcription, indicating that LTR retrotransposon-driven transcription of coding and noncoding sequences could regulate yeast gene expression in response to stress³⁴⁰. In line, fusion of the control gene *lacZ* to a 5' LTR leads to *lacZ* expression in response to adenine starvation³⁴⁰. In the same study, the activation of adjacent genes by LTR retrotransposons transcription was also confirmed at the endogenous gene *ESF1*. *ESF1*, which is naturally located in proximity to a full-length endogenous LTR retrotransposon element is differently expressed in response to adenine starvation. Under adenine starvation conditions a second class of *ESF1* mRNAs were transcribed with 5' ends in the LTR of the retrotransposon. Albeit the mRNAs are most probably not functional in this case, because of several short ORFs upstream of the *ESF1* initiation codon, it shows that LTR retrotransposons can influence the transcription of adjacent genes. Further, important regulatory functions have been assigned to antisense transcripts such as IRT1¹⁵⁵, which led to the hypothesis that LTR retrotransposon-driven transcription could contribute to the production of noncoding RNAs, which in turn could influence the reprogramming of yeast gene expression in response to nitrogen starvation, such

as during sporulation. Moreover, it was revealed that an activation of LTR transposons is dependent on open chromatin³⁴⁰.

One favorable hypothesis is that LTR retrotransposon are activated in sporulating samples due to nitrogen starvation. This results in a favorable environment for G4 formation either due to chromatin remodeling or due to LTR retrotransposon transcription. That in turn permits G4 formation and stabilization by Phen-DC₃. Or Phen-DC₃ itself would lead to LTR retrotransposon transcription, because it was shown that LTR retrotransposons become active in response to various stress conditions. Which then would result again in supportive G4 formation conditions. However, the observed missing distinct DNA damage response in Phen-DC₃-treated cells is not supporting this option, but it cannot be completely ruled out. Either ways, stabilized G4s would most likely result in blockage of LTR retrotransposon transcription according to discoveries of G4 stabilizing on viral transcription^{315–317}.

In the past only parallel G4 structures could be specifically detected using the D1 antibody. Due to the universal specificity of BG4 to a wide range of G4 structures, including parallel, antiparallel and hybrid G4 structures, it cannot be determined, which structure the G4s possessed that were identified by BG4 ChIP-seq. The G4 signals of the two antibodies BG4 and D1 were highly overlapping, arguing for G4-specific binding of the antibodies and indicating a high abundance of parallel G4 structures in the chromatin of *S. cerevisiae*. To note, some G4 structures might be unavailable for BG4/D1 ChIP-seq, because of G4 structures being masked by bound proteins.

There are a few conceivable hypotheses how Phen-DC₃ stabilization leads to impaired meiosis (Figure 15). One is that G4 structure-stabilization causes genome instability and consequently G₁/S checkpoint activation and G₁ arrest. This hypothesis is not supported by my data, because deletion of the checkpoint proteins Mec1 and Tel1 did not result in a rescue of G₁ arrest upon G4 stabilization. The other hypotheses are in connection with the potential regulation capacity of G4 structures on gene expression. Recruitment of an activator or repressor to a stabilized G4 structure next to a TSS leads to an activation or repression of meiosis-associated genes. Supporting data for the hypothesis that G4 structures are involved in transcription factor recruitment came from studies of the G4-binding proteins CNBP and NM23-H2^{341–343}. The binding of these proteins is related to G4 structures unwinding and structural changes within the proximal genomic regions. These conditions are supposed to be favorable for the recruitment of transcription factors, which can subsequently activate transcription.

Stabilized G4 structures can also represent obstacles, which block the transcription of meiosis-associated genes for example by preventing the binding of a transcription enhancer or by

blocking the progression of the transcription machinery. It was demonstrated that G4 structure formation in the c-MYC promoter results in its downregulation and a mutation of the G4 motif in the c-MYC promoter resulted in a 3-fold higher transcriptional activity of the promoter¹⁰². Another possibility is that Phen-DC₃ might blocks the binding of an activator to a regulatory G4 in a promoter region.

To address these open questions, an expression analysis will be performed, including Phen-DC₃-treated vegetative and sporulating cells and as a reference cells without stabilized G4s. This will provide more detailed information about the expressed genes in response to Phen-DC₃ treatment. Moreover, this analysis will yield, which genes that are involved in DNA damage response are upregulated.

In my thesis I focused on DNA G4 structures, but a regulatory effect caused by Phen-DC₃-stabilized RNA G4 structures on meiosis in *S. cerevisiae* is conceivable as well. In untranslated regions (UTRs) and ORFs of many mRNAs are G4 motifs³⁴⁴. They are considered to be putative translation inhibitors, because formed G4 structures would act as barriers for ribosomal scanning or translocation. Hence, the unwinding of G4 structures in G4 containing genes by helicases, such as human DHX36 or human eIF4A, is essential^{345,346}.

Furthermore, G4 structures can also affect translation by supporting the binding or localization of translation-related proteins to mRNAs³⁴³. The consequent effects are translational stimulation or repression depending on the protein. G4 structures were also considered to play a role in cap-independent translation. Cap-independent translation largely depends on internal ribosomal entry sites (IRESs) in the 5' UTRs of mRNAs. A recent study showed that the mutation of a G4 motif in the IRES abolished the initiation activity of the IRES site completely³⁴⁷. However, another study suggested an inhibitory role of G4 structures on cap-independent translation³⁴⁸. Besides mRNAs, studies have indicated a role of G4 structures in noncoding RNAs (ncRNAs) as well. ncRNAs are functional molecules that interact with various targets and have diverse regulatory functions such as the repressive effect of lncRNA IRT1 on *IME1* expression^{82,155,343}.

In summary, in this thesis G4 structures were for the first time identified in a chromatin context in *S. cerevisiae*. The G4 landscape will serve in the future as a reference for not only meiotic but also for vegetative cells. Novel G4 binder in *S. cerevisiae*, including meiosis-specific proteins were identified. Further, genome-wide approaches performed in this thesis such as proteomics, G4 affinity purification and G4 ChIP-seq will help to provide a global overview of G4 structures during meiosis and their potential regulatory capacity.

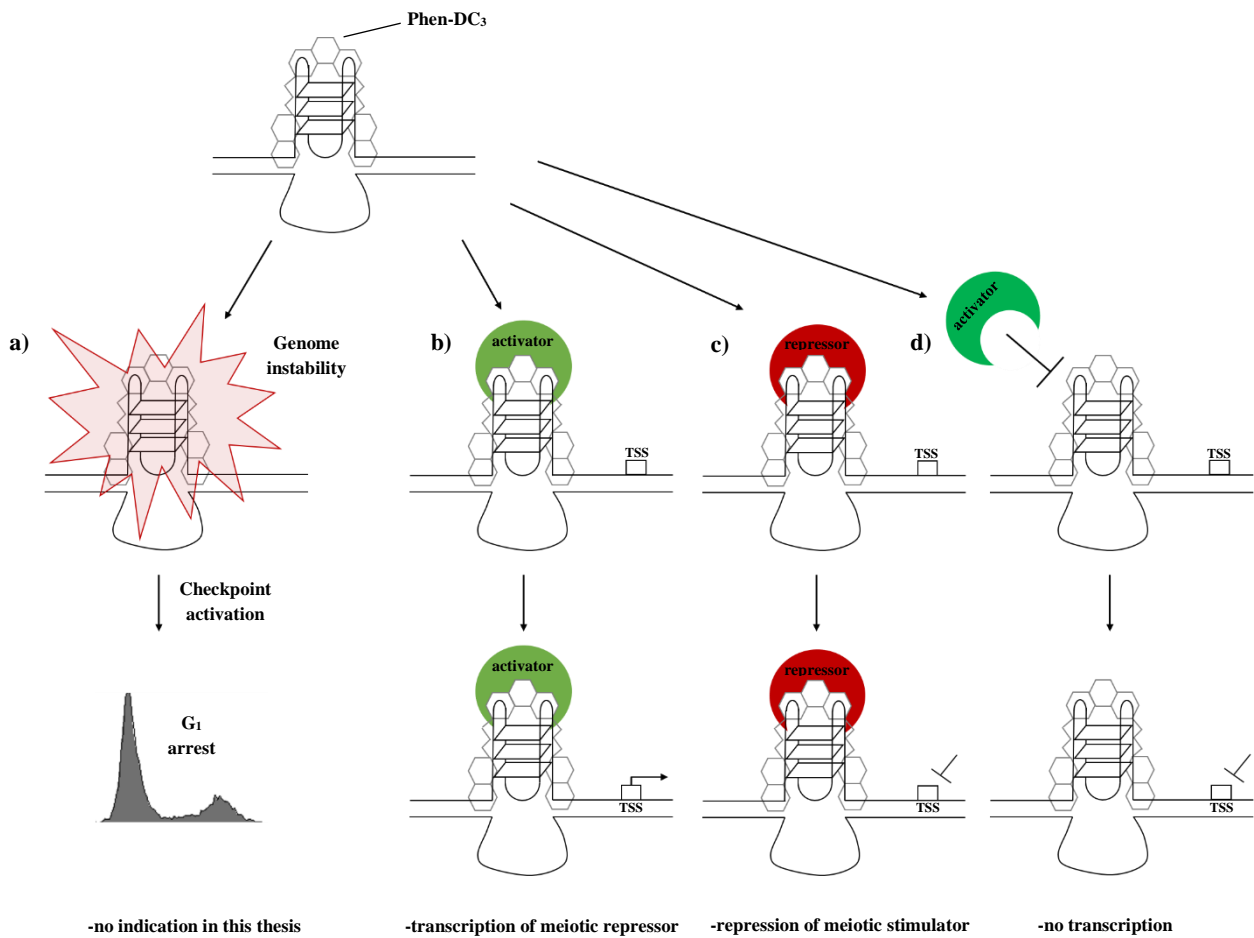


Figure 15: Models for impact of G4 structure stabilization on meiosis in *S. cerevisiae*. a) G4 structure stabilization leads to genome instability during G₁-phase prior to meiosis. Thereby induce G₁/S checkpoint activation, resulting in G₁ arrest. Results in this study do not support this hypothesis. b) A transcription activator binds to a stabilized G4 structure next to a transcription start site (TSS), resulting in expression of meiosis repressor and by that inhibits meiosis. c) A transcription repressor binds to a stabilized G4 structure next to a TSS, resulting in repression of meiosis activator and by that inhibits meiosis. d) Stabilization of G4 structures by Phen-DC₃ blocks the transcription either by the structure itself or by masking of a regulatory G4 structure by Phen-DC₃ and by that inhibits meiosis.

References

1. GELLERT, M., LIPSETT, M. N. & DAVIES, D. R. Helix formation by guanylic acid. *Proceedings of the National Academy of Sciences of the United States of America* **48**, 2013–2018 (1962).
2. Sen, D. & Gilbert, W. Formation of parallel four-stranded complexes by guanine-rich motifs in DNA and its implications for meiosis. *Nature* **334**, 364–366; 10.1038/334364a0 (1988).
3. Sundquist, W. I. & Klug, A. Telomeric DNA dimerizes by formation of guanine tetrads between hairpin loops. *Nature* **342**, 825–829; 10.1038/342825a0 (1989).
4. Kim, J., Cheong, C. & Moore, P. B. Tetramerization of an RNA oligonucleotide containing a GGGG sequence. *Nature* **351**, 331–332; 10.1038/351331a0 (1991).
5. Hoogsteen, K. The crystal and molecular structure of a hydrogen-bonded complex between 1-methylthymine and 9-methyladenine. *Acta Cryst* **16**, 907–916; 10.1107/S0365110X63002437 (1963).
6. Bishop, J. S. *et al.* Intramolecular G-quartet motifs confer nuclease resistance to a potent anti-HIV oligonucleotide. *The Journal of biological chemistry* **271**, 5698–5703 (1996).
7. Jin, R., Gaffney, B. L., Wang, C., Jones, R. A. & Breslauer, K. J. Thermodynamics and structure of a DNA tetraplex: a spectroscopic and calorimetric study of the tetramolecular complexes of d(TG3T) and d(TG3T2G3T). *Proceedings of the National Academy of Sciences of the United States of America* **89**, 8832–8836 (1992).
8. Huppert, J. L. & Balasubramanian, S. Prevalence of quadruplexes in the human genome. *Nucleic acids research* **33**, 2908–2916; 10.1093/nar/gki609 (2005).
9. Todd, A. K., Johnston, M. & Neidle, S. Highly prevalent putative quadruplex sequence motifs in human DNA. *Nucleic acids research* **33**, 2901–2907; 10.1093/nar/gki553 (2005).
10. Capra, J. A., Paeschke, K., Singh, M. & Zakian, V. A. G-quadruplex DNA sequences are evolutionarily conserved and associated with distinct genomic features in *Saccharomyces cerevisiae*. *PLoS computational biology* **6**, e1000861; 10.1371/journal.pcbi.1000861 (2010).
11. Hershman, S. G. *et al.* Genomic distribution and functional analyses of potential G-quadruplex-forming sequences in *Saccharomyces cerevisiae*. *Nucleic acids research* **36**, 144–156; 10.1093/nar/gkm986 (2008).
12. Chambers, V. S. *et al.* High-throughput sequencing of DNA G-quadruplex structures in the human genome. *Nature biotechnology* **33**, 877–881; 10.1038/nbt.3295 (2015).
13. Marsico, G. *et al.* Whole genome experimental maps of DNA G-quadruplexes in multiple species. *Nucleic acids research* **47**, 3862–3874; 10.1093/nar/gkz179 (2019).
14. Guédin, A., Gros, J., Alberti, P. & Mergny, J.-L. How long is too long? Effects of loop size on G-quadruplex stability. *Nucleic acids research* **38**, 7858–7868; 10.1093/nar/gkq639 (2010).
15. Agrawal, P., Lin, C., Mathad, R. I., Carver, M. & Yang, D. The major G-quadruplex formed in the human BCL-2 proximal promoter adopts a parallel structure with a 13-nt loop in K⁺ solution. *Journal of the American Chemical Society* **136**, 1750–1753; 10.1021/ja4118945 (2014).
16. Tippana, R., Xiao, W. & Myong, S. G-quadruplex conformation and dynamics are determined by loop length and sequence. *Nucleic acids research* **42**, 8106–8114; 10.1093/nar/gku464 (2014).

17. McManus, S. A. & Li, Y. Assessing the amount of quadruplex structures present within G₂-tract synthetic random-sequence DNA libraries. *PLoS one* **8**, e64131; 10.1371/journal.pone.0064131 (2013).
18. Hazel, P., Huppert, J., Balasubramanian, S. & Neidle, S. Loop-length-dependent folding of G-quadruplexes. *Journal of the American Chemical Society* **126**, 16405–16415; 10.1021/ja045154j (2004).
19. Smirnov, I. & Shafer, R. H. Effect of loop sequence and size on DNA aptamer stability. *Biochemistry* **39**, 1462–1468 (2000).
20. Guédin, A., Alberti, P. & Mergny, J.-L. Stability of intramolecular quadruplexes: sequence effects in the central loop. *Nucleic acids research* **37**, 5559–5567; 10.1093/nar/gkp563 (2009).
21. Špačková, N. a., Berger, I. & Šponer, J. Nanosecond Molecular Dynamics Simulations of Parallel and Antiparallel Guanine Quadruplex DNA Molecules. *Journal of the American Chemical Society* **121**, 5519–5534; 10.1021/ja984449s (1999).
22. Clay, E. H. & Gould, I. R. A combined QM and MM investigation into guanine quadruplexes. *Journal of molecular graphics & modelling* **24**, 138–146; 10.1016/j.jmgm.2005.08.009 (2005).
23. Fahlman, R. P. & Sen, D. Cation-regulated self-association of "synapsable" DNA duplexes. *Journal of molecular biology* **280**, 237–244; 10.1006/jmbi.1998.1875 (1998).
24. Tateishi-Karimata, H. & Sugimoto, N. Structure, stability and behaviour of nucleic acids in ionic liquids. *Nucleic acids research* **42**, 8831–8844; 10.1093/nar/gku499 (2014).
25. Bhattacharyya, D., Mirihana Arachchilage, G. & Basu, S. Metal Cations in G-Quadruplex Folding and Stability. *Frontiers in chemistry* **4**, 38; 10.3389/fchem.2016.00038 (2016).
26. Howard, F. B., Frazier, J. & Miles, H. T. Stable and metastable forms of poly(G). *Biopolymers* **16**, 791–809; 10.1002/bip.1977.360160407 (1977).
27. van Mourik, T. & Dingley, A. J. Characterization of the monovalent ion position and hydrogen-bond network in guanine quartets by DFT calculations of NMR parameters. *Chemistry (Weinheim an der Bergstrasse, Germany)* **11**, 6064–6079; 10.1002/chem.200500198 (2005).
28. Chen, Y. & Yang, D. Sequence, stability, and structure of G-quadruplexes and their interactions with drugs. *Current protocols in nucleic acid chemistry* **Chapter 17**, Unit17.5; 10.1002/0471142700.nc1705s50 (2012).
29. Phillips, K., Dauter, Z., Murchie, A. I., Lilley, D. M. & Luisi, B. The crystal structure of a parallel-stranded guanine tetraplex at 0.95 Å resolution. *Journal of molecular biology* **273**, 171–182; 10.1006/jmbi.1997.1292 (1997).
30. Davis, J. T. G-quartets 40 years later: from 5'-GMP to molecular biology and supramolecular chemistry. *Angewandte Chemie (International ed. in English)* **43**, 668–698; 10.1002/anie.200300589 (2004).
31. You, J. *et al.* Effects of monovalent cations on folding kinetics of G-quadruplexes. *Bioscience reports* **37**; 10.1042/BSR20170771 (2017).
32. Ambrus, A. *et al.* Human telomeric sequence forms a hybrid-type intramolecular G-quadruplex structure with mixed parallel/antiparallel strands in potassium solution. *Nucleic acids research* **34**, 2723–2735; 10.1093/nar/gkl348 (2006).

33. Mukundan, V. T. & Phan, A. T. Bulges in G-quadruplexes: broadening the definition of G-quadruplex-forming sequences. *Journal of the American Chemical Society* **135**, 5017–5028; 10.1021/ja310251r (2013).
34. Rachwal, P. A., Brown, T. & Fox, K. R. Sequence effects of single base loops in intramolecular quadruplex DNA. *FEBS letters* **581**, 1657–1660; 10.1016/j.febslet.2007.03.040 (2007).
35. Patel, D. J., Phan, A. T. & Kuryavyi, V. Human telomere, oncogenic promoter and 5'-UTR G-quadruplexes: diverse higher order DNA and RNA targets for cancer therapeutics. *Nucleic acids research* **35**, 7429–7455; 10.1093/nar/gkm711 (2007).
36. Burge, S., Parkinson, G. N., Hazel, P., Todd, A. K. & Neidle, S. Quadruplex DNA: sequence, topology and structure. *Nucleic acids research* **34**, 5402–5415; 10.1093/nar/gkl655 (2006).
37. Neidle, S. The structures of quadruplex nucleic acids and their drug complexes. *Current opinion in structural biology* **19**, 239–250; 10.1016/j.sbi.2009.04.001 (2009).
38. Parkinson, G. N., Lee, M. P. H. & Neidle, S. Crystal structure of parallel quadruplexes from human telomeric DNA. *Nature* **417**, 876–880; 10.1038/nature755 (2002).
39. Wang, Y. & Patel, D. J. Solution structure of the human telomeric repeat dAG3(T2AG3)3 G-tetraplex. *Structure (London, England : 1993)* **1**, 263–282 (1993).
40. Yan Xu, Yuki Noguchi & Hiroshi Sugiyama. The new models of the human telomere d[AGGG(TTAGGG)3] in K⁺ solution. *Bioorganic & Medicinal Chemistry* **14**, 5584–5591; 10.1016/j.bmc.2006.04.033 (2006).
41. Luu, K. N., Phan, A. T., Kuryavyi, V., Lacroix, L. & Patel, D. J. Structure of the Human Telomere in K⁺ Solution: An Intramolecular (3 + 1) G-Quadruplex Scaffold. *Journal of the American Chemical Society* **128**, 9963–9970; 10.1021/ja062791w (2006).
42. Yu, H., Gu, X., Nakano, S.-i., Miyoshi, D. & Sugimoto, N. Beads-on-a-String Structure of Long Telomeric DNAs under Molecular Crowding Conditions. *Journal of the American Chemical Society* **134**, 20060–20069; 10.1021/ja305384c (2012).
43. Webba da Silva, M. Geometric formalism for DNA quadruplex folding. *Chemistry (Weinheim an der Bergstrasse, Germany)* **13**, 9738–9745; 10.1002/chem.200701255 (2007).
44. Zhang, N., Phan, A. T. & Patel, D. J. (3 + 1) Assembly of three human telomeric repeats into an asymmetric dimeric G-quadruplex. *Journal of the American Chemical Society* **127**, 17277–17285; 10.1021/ja0543090 (2005).
45. Dai, J., Carver, M., Punchihewa, C., Jones, R. A. & Yang, D. Structure of the Hybrid-2 type intramolecular human telomeric G-quadruplex in K⁺ solution: insights into structure polymorphism of the human telomeric sequence. *Nucleic acids research* **35**, 4927–4940; 10.1093/nar/gkm522 (2007).
46. Phan, A. T., Luu, K. N. & Patel, D. J. Different loop arrangements of intramolecular human telomeric (3+1) G-quadruplexes in K⁺ solution. *Nucleic acids research* **34**, 5715–5719; 10.1093/nar/gkl726 (2006).
47. Dhakal, S. *et al.* Structural and mechanical properties of individual human telomeric G-quadruplexes in molecularly crowded solutions. *Nucleic acids research* **41**, 3915–3923; 10.1093/nar/gkt038 (2013).

48. Heddi, B. & Phan, A. T. Structure of human telomeric DNA in crowded solution. *Journal of the American Chemical Society* **133**, 9824–9833; 10.1021/ja200786q (2011).
49. Lim, K. W., Ng, V. C. M., Martín-Pintado, N., Heddi, B. & Phan, A. T. Structure of the human telomere in Na⁺ solution: an antiparallel (2+2) G-quadruplex scaffold reveals additional diversity. *Nucleic acids research* **41**, 10556–10562; 10.1093/nar/gkt771 (2013).
50. Giraldo, R. & Rhodes, D. The yeast telomere-binding protein RAP1 binds to and promotes the formation of DNA quadruplexes in telomeric DNA. *The EMBO journal* **13**, 2411–2420 (1994).
51. Giraldo, R., Suzuki, M., Chapman, L. & Rhodes, D. Promotion of parallel DNA quadruplexes by a yeast telomere binding protein: a circular dichroism study. *Proceedings of the National Academy of Sciences of the United States of America* **91**, 7658–7662 (1994).
52. Paeschke, K., Simonsson, T., Postberg, J., Rhodes, D. & Lipps, H. J. Telomere end-binding proteins control the formation of G-quadruplex DNA structures in vivo. *Nature structural & molecular biology* **12**, 847–854; 10.1038/nsmb982 (2005).
53. Fang, G. & Cech, T. R. The beta subunit of Oxytricha telomere-binding protein promotes G-quartet formation by telomeric DNA. *Cell* **74**, 875–885 (1993).
54. Bugaut, A. & Balasubramanian, S. A sequence-independent study of the influence of short loop lengths on the stability and topology of intramolecular DNA G-quadruplexes. *Biochemistry* **47**, 689–697; 10.1021/bi701873c (2008).
55. Huppert, J. L. Structure, location and interactions of G-quadruplexes. *The FEBS journal* **277**, 3452–3458; 10.1111/j.1742-4658.2010.07758.x (2010).
56. Eddy, J. & Maizels, N. Gene function correlates with potential for G4 DNA formation in the human genome. *Nucleic acids research* **34**, 3887–3896; 10.1093/nar/gkl529 (2006).
57. König, S. L. B., Evans, A. C. & Huppert, J. L. Seven essential questions on G-quadruplexes. *Biomolecular concepts* **1**, 197–213; 10.1515/bmc.2010.011 (2010).
58. Rawal, P. *et al.* Genome-wide prediction of G4 DNA as regulatory motifs: role in Escherichia coli global regulation. *Genome research* **16**, 644–655; 10.1101/gr.4508806 (2006).
59. Frees, S., Menendez, C., Crum, M. & Bagga, P. S. QGRS-Conserve: a computational method for discovering evolutionarily conserved G-quadruplex motifs. *Human genomics* **8**, 8; 10.1186/1479-7364-8-8 (2014).
60. Besnard, E. *et al.* Unraveling cell type-specific and reprogrammable human replication origin signatures associated with G-quadruplex consensus motifs. *Nature structural & molecular biology* **19**, 837–844; 10.1038/nsmb.2339 (2012).
61. Hänsel-Hertsch, R. *et al.* G-quadruplex structures mark human regulatory chromatin. *Nature genetics* **48**, 1267–1272; 10.1038/ng.3662 (2016).
62. Li, W., Wu, P., Ohmichi, T. & Sugimoto, N. Characterization and thermodynamic properties of quadruplex/duplex competition. *FEBS letters* **526**, 77–81 (2002).
63. Nikolova, E. N. *et al.* Transient Hoogsteen base pairs in canonical duplex DNA. *Nature* **470**, 498–502; 10.1038/nature09775 (2011).

64. Rhodes, D. & Lipps, H. J. G-quadruplexes and their regulatory roles in biology. *Nucleic acids research* **43**, 8627–8637; 10.1093/nar/gkv862 (2015).
65. Wang, S. S. & Zakian, V. A. Sequencing of *Saccharomyces* telomeres cloned using T4 DNA polymerase reveals two domains. *Molecular and cellular biology* **10**, 4415–4419 (1990).
66. Zakian, V. A. Telomeres: the beginnings and ends of eukaryotic chromosomes. *Experimental cell research* **318**, 1456–1460; 10.1016/j.yexcr.2012.02.015 (2012).
67. Schaffitzel, C. *et al.* In vitro generated antibodies specific for telomeric guanine-quadruplex DNA react with *Stylonychia lemnae* macronuclei. *Proceedings of the National Academy of Sciences of the United States of America* **98**, 8572–8577; 10.1073/pnas.141229498 (2001).
68. Paeschke, K. *et al.* Telomerase recruitment by the telomere end binding protein-beta facilitates G-quadruplex DNA unfolding in ciliates. *Nature structural & molecular biology* **15**, 598–604; 10.1038/nsmb.1422 (2008).
69. Postberg, J., Tsytlonok, M., Sparvoli, D., Rhodes, D. & Lipps, H. J. A telomerase-associated RecQ protein-like helicase resolves telomeric G-quadruplex structures during replication. *Gene* **497**, 147–154; 10.1016/j.gene.2012.01.068 (2012).
70. Lipps, H. J. & Rhodes, D. G-quadruplex structures: in vivo evidence and function. *Trends in cell biology* **19**, 414–422; 10.1016/j.tcb.2009.05.002 (2009).
71. Sun, D. *et al.* Inhibition of human telomerase by a G-quadruplex-interactive compound. *Journal of medicinal chemistry* **40**, 2113–2116; 10.1021/jm970199z (1997).
72. Read, M. *et al.* Structure-based design of selective and potent G quadruplex-mediated telomerase inhibitors. *Proceedings of the National Academy of Sciences* **98**, 4844; 10.1073/pnas.081560598 (2001).
73. Burger, A. M. *et al.* The G-quadruplex-interactive molecule BRACO-19 inhibits tumor growth, consistent with telomere targeting and interference with telomerase function. *Cancer research* **65**, 1489–1496; 10.1158/0008-5472.CAN-04-2910 (2005).
74. Gowan, S. M. *et al.* A G-quadruplex-interactive potent small-molecule inhibitor of telomerase exhibiting in vitro and in vivo antitumor activity. *Molecular pharmacology* **61**, 1154–1162 (2002).
75. Bryan, T. M. & Cech, T. R. Telomerase and the maintenance of chromosome ends. *Current opinion in cell biology* **11**, 318–324; 10.1016/S0955-0674(99)80043-X (1999).
76. Harley, C. B., Futcher, A. B. & Greider, C. W. Telomeres shorten during ageing of human fibroblasts. *Nature* **345**, 458–460; 10.1038/345458a0 (1990).
77. Liu, H.-Y. *et al.* Conformation Selective Antibody Enables Genome Profiling and Leads to Discovery of Parallel G-Quadruplex in Human Telomeres. *Cell chemical biology* **23**, 1261–1270; 10.1016/j.chembiol.2016.08.013 (2016).
78. Biffi, G., Di Antonio, M., Tannahill, D. & Balasubramanian, S. Visualization and selective chemical targeting of RNA G-quadruplex structures in the cytoplasm of human cells. *Nature chemistry* **6**, 75–80; 10.1038/nchem.1805 (2014).
79. Biffi, G., Tannahill, D., McCafferty, J. & Balasubramanian, S. Quantitative visualization of DNA G-quadruplex structures in human cells. *Nature chemistry* **5**, 182–186; 10.1038/nchem.1548 (2013).

80. Li, Q.-J., Tong, X.-J., Duan, Y.-M. & Zhou, J.-Q. Characterization of the intramolecular G-quadruplex promoting activity of Est1. *FEBS letters* **587**, 659–665; 10.1016/j.febslet.2013.01.024 (2013).
81. Jansson, L. I. *et al.* Telomere DNA G-quadruplex folding within actively extending human telomerase. *Proceedings of the National Academy of Sciences of the United States of America* **116**, 9350–9359; 10.1073/pnas.1814777116 (2019).
82. Biffi, G., Tannahill, D. & Balasubramanian, S. An intramolecular G-quadruplex structure is required for binding of telomeric repeat-containing RNA to the telomeric protein TRF2. *Journal of the American Chemical Society* **134**, 11974–11976; 10.1021/ja305734x (2012).
83. Brázda, V. *et al.* The Amino Acid Composition of Quadruplex Binding Proteins Reveals a Shared Motif and Predicts New Potential Quadruplex Interactors. *Molecules (Basel, Switzerland)* **23**; 10.3390/molecules23092341 (2018).
84. Huang, Z.-L. *et al.* Identification of G-Quadruplex-Binding Protein from the Exploration of RGG Motif/G-Quadruplex Interactions. *Journal of the American Chemical Society*; 10.1021/jacs.8b09329 (2018).
85. Lane, A. N., Chaires, J. B., Gray, R. D. & Trent, J. O. Stability and kinetics of G-quadruplex structures. *Nucleic acids research* **36**, 5482–5515; 10.1093/nar/gkn517 (2008).
86. Sanders, C. M. Human Pif1 helicase is a G-quadruplex DNA-binding protein with G-quadruplex DNA-unwinding activity. *The Biochemical journal* **430**, 119–128; 10.1042/BJ20100612 (2010).
87. Lin, W. *et al.* Mammalian DNA2 helicase/nuclease cleaves G-quadruplex DNA and is required for telomere integrity. *The EMBO journal* **32**, 1425–1439; 10.1038/emboj.2013.88 (2013).
88. Guo, M. *et al.* A distinct triplex DNA unwinding activity of ChIR1 helicase. *The Journal of biological chemistry* **290**, 5174–5189; 10.1074/jbc.M114.634923 (2015).
89. Vannier, J.-B. *et al.* RTEL1 is a replisome-associated helicase that promotes telomere and genome-wide replication. *Science (New York, N.Y.)* **342**, 239–242; 10.1126/science.1241779 (2013).
90. Sun, H., Karow, J. K., Hickson, I. D. & Maizels, N. The Bloom's syndrome helicase unwinds G4 DNA. *The Journal of biological chemistry* **273**, 27587–27592; 10.1074/jbc.273.42.27587 (1998).
91. Fry, M. & Loeb, L. A. Human werner syndrome DNA helicase unwinds tetrahelical structures of the fragile X syndrome repeat sequence d(CGG)_n. *The Journal of biological chemistry* **274**, 12797–12802; 10.1074/jbc.274.18.12797 (1999).
92. Sun, H., Bennett, R. J. & Maizels, N. The *Saccharomyces cerevisiae* Sgs1 helicase efficiently unwinds G-G paired DNAs. *Nucleic acids research* **27**, 1978–1984; 10.1093/nar/27.9.1978 (1999).
93. London, T. B. C. *et al.* FANCD1 is a structure-specific DNA helicase associated with the maintenance of genomic G/C tracts. *The Journal of biological chemistry* **283**, 36132–36139; 10.1074/jbc.M808152200 (2008).
94. Paeschke, K. *et al.* Pif1 family helicases suppress genome instability at G-quadruplex motifs. *Nature* **497**, 458–462; 10.1038/nature12149 (2013).

95. Paeschke, K., Capra, J. A. & Zakian, V. A. DNA replication through G-quadruplex motifs is promoted by the *Saccharomyces cerevisiae* Pif1 DNA helicase. *Cell* **145**, 678–691; 10.1016/j.cell.2011.04.015 (2011).
96. Cahoon, L. A. & Seifert, H. S. An alternative DNA structure is necessary for pilin antigenic variation in *Neisseria gonorrhoeae*. *Science (New York, N.Y.)* **325**, 764–767; 10.1126/science.1175653 (2009).
97. Qin, Y. & Hurley, L. H. Structures, folding patterns, and functions of intramolecular DNA G-quadruplexes found in eukaryotic promoter regions. *Biochimie* **90**, 1149–1171; 10.1016/j.biochi.2008.02.020 (2008).
98. Huppert, J. L. & Balasubramanian, S. G-quadruplexes in promoters throughout the human genome. *Nucleic acids research* **35**, 406–413; 10.1093/nar/gkl1057 (2007).
99. Lim, K. W. *et al.* Coexistence of two distinct G-quadruplex conformations in the hTERT promoter. *Journal of the American Chemical Society* **132**, 12331–12342; 10.1021/ja101252n (2010).
100. Xu, Y. Chemistry in human telomere biology: structure, function and targeting of telomere DNA/RNA. *Chemical Society reviews* **40**, 2719–2740; 10.1039/c0cs00134a (2011).
101. Phan, A. T., Kuryavyi, V., Gaw, H. Y. & Patel, D. J. Small-molecule interaction with a five-guanine-tract G-quadruplex structure from the human MYC promoter. *Nature chemical biology* **1**, 167–173; 10.1038/nchembio723 (2005).
102. Siddiqui-Jain, A., Grand, C. L., Bearss, D. J. & Hurley, L. H. Direct evidence for a G-quadruplex in a promoter region and its targeting with a small molecule to repress c-MYC transcription. *Proceedings of the National Academy of Sciences of the United States of America* **99**, 11593–11598; 10.1073/pnas.182256799 (2002).
103. Hurley, L. H., Hoff, D. D. von, Siddiqui-Jain, A. & Yang, D. Drug targeting of the c-MYC promoter to repress gene expression via a G-quadruplex silencer element. *Seminars in oncology* **33**, 498–512; 10.1053/j.seminoncol.2006.04.012 (2006).
104. Yang, D. & Hurley, L. H. Structure of the biologically relevant G-quadruplex in the c-MYC promoter. *Nucleosides, nucleotides & nucleic acids* **25**, 951–968; 10.1080/15257770600809913 (2006).
105. Marcu, K. B., Bossone, S. A. & Patel, A. J. myc function and regulation. *Annual review of biochemistry* **61**, 809–860; 10.1146/annurev.bi.61.070192.004113 (1992).
106. D'Cruz, C. M. *et al.* c-MYC induces mammary tumorigenesis by means of a preferred pathway involving spontaneous Kras2 mutations. *Nature medicine* **7**, 235–239; 10.1038/84691 (2001).
107. Strieder, V. & Lutz, W. Regulation of N-myc expression in development and disease. *Cancer letters* **180**, 107–119 (2002).
108. Lutz, W., Leon, J. & Eilers, M. Contributions of Myc to tumorigenesis. *Biochimica et biophysica acta* **1602**, 61–71 (2002).
109. Pelengaris, S., Khan, M. & Evan, G. I. Suppression of Myc-induced apoptosis in beta cells exposes multiple oncogenic properties of Myc and triggers carcinogenic progression. *Cell* **109**, 321–334 (2002).

110. Pelengaris, S., Khan, M. & Evan, G. c-MYC: more than just a matter of life and death. *Nature reviews. Cancer* **2**, 764–776; 10.1038/nrc904 (2002).
111. Allain, J.-E. *et al.* Immortalization of a primate bipotent epithelial liver stem cell. *Proceedings of the National Academy of Sciences of the United States of America* **99**, 3639–3644; 10.1073/pnas.062038599 (2002).
112. Hiyama, E. *et al.* Correlating telomerase activity levels with human neuroblastoma outcomes. *Nature medicine* **1**, 249–255 (1995).
113. Neidle, S. & Kelland, L. R. Telomerase as an anti-cancer target: current status and future prospects. *Anti-cancer drug design* **14**, 341–347 (1999).
114. Cian, A. de *et al.* Targeting telomeres and telomerase. *Biochimie* **90**, 131–155; 10.1016/j.biochi.2007.07.011 (2008).
115. Gowan, S. M., Heald, R., Stevens, M. F. & Kelland, L. R. Potent inhibition of telomerase by small-molecule pentacyclic acridines capable of interacting with G-quadruplexes. *Molecular pharmacology* **60**, 981–988 (2001).
116. Gunaratnam, M. *et al.* Mechanism of acridine-based telomerase inhibition and telomere shortening. *Biochemical pharmacology* **74**, 679–689; 10.1016/j.bcp.2007.06.011 (2007).
117. Neidle, S. Quadruplex Nucleic Acids as Novel Therapeutic Targets. *Journal of medicinal chemistry* **59**, 5987–6011; 10.1021/acs.jmedchem.5b01835 (2016).
118. Ali, A. & Bhattacharya, S. DNA binders in clinical trials and chemotherapy. *Bioorganic & Medicinal Chemistry* **22**, 4506–4521; 10.1016/j.bmc.2014.05.030 (2014).
119. Arthanari, H., Basu, S., Kawano, T. L. & Bolton, P. H. Fluorescent dyes specific for quadruplex DNA. *Nucleic acids research* **26**, 3724–3728 (1998).
120. Paramasivan, S. & Bolton, P. H. Mix and measure fluorescence screening for selective quadruplex binders. *Nucleic acids research* **36**, e106; 10.1093/nar/gkn487 (2008).
121. Cian, A. de, Delemos, E., Mergny, J.-L., Teulade-Fichou, M.-P. & Monchaud, D. Highly efficient G-quadruplex recognition by bisquinolinium compounds. *Journal of the American Chemical Society* **129**, 1856–1857; 10.1021/ja067352b (2007).
122. Monchaud, D. *et al.* Ligands playing musical chairs with G-quadruplex DNA: a rapid and simple displacement assay for identifying selective G-quadruplex binders. *Biochimie* **90**, 1207–1223; 10.1016/j.biochi.2008.02.019 (2008).
123. Cian, A. de *et al.* Reevaluation of telomerase inhibition by quadruplex ligands and their mechanisms of action. *Proceedings of the National Academy of Sciences of the United States of America* **104**, 17347–17352; 10.1073/pnas.0707365104 (2007).
124. Xu, H. *et al.* CX-5461 is a DNA G-quadruplex stabilizer with selective lethality in BRCA1/2 deficient tumours. *Nature communications* **8**, 14432; 10.1038/ncomms14432 (2017).
125. Nicoludis, J. M., Barrett, S. P., Mergny, J.-L. & Yatsunyk, L. A. Interaction of human telomeric DNA with N-methyl mesoporphyrin IX. *Nucleic acids research* **40**, 5432–5447; 10.1093/nar/gks152 (2012).

126. Huber, M. D., Lee, D. C. & Maizels, N. G4 DNA unwinding by BLM and Sgs1p: substrate specificity and substrate-specific inhibition. *Nucleic acids research* **30**, 3954–3961 (2002).
127. Wu, X. & Maizels, N. Substrate-specific inhibition of RecQ helicase. *Nucleic acids research* **29**, 1765–1771 (2001).
128. Chung, W. J., Heddi, B., Hamon, F., Teulade-Fichou, M.-P. & Phan, A. T. Solution structure of a G-quadruplex bound to the bisquinolinium compound Phen-DC(3). *Angewandte Chemie (International ed. in English)* **53**, 999–1002; 10.1002/anie.201308063 (2014).
129. Piazza, A. *et al.* Genetic instability triggered by G-quadruplex interacting Phen-DC compounds in *Saccharomyces cerevisiae*. *Nucleic acids research* **38**, 4337–4348; 10.1093/nar/gkq136 (2010).
130. Wallgren, M. *et al.* G-rich telomeric and ribosomal DNA sequences from the fission yeast genome form stable G-quadruplex DNA structures in vitro and are unwound by the Pfh1 DNA helicase. *Nucleic acids research* **44**, 6213–6231; 10.1093/nar/gkw349 (2016).
131. Doi, T., Yoshida, M., Shin-ya, K. & Takahashi, T. Total synthesis of (R)-telomestatin. *Organic letters* **8**, 4165–4167; 10.1021/ol061793i (2006).
132. Sullivan, H.-J. *et al.* Binding of Telomestatin, TMPyP4, BSU6037, and BRACO19 to a Telomeric G-Quadruplex-Duplex Hybrid Probed by All-Atom Molecular Dynamics Simulations with Explicit Solvent. *ACS omega* **3**, 14788–14806; 10.1021/acsomega.8b01574 (2018).
133. Maynard Smith, J. *The Evolution of Sex*. Cambridge University Press, (1978).
134. Primig, M. *et al.* The core meiotic transcriptome in budding yeasts. *Nature genetics* **26**, 415–423; 10.1038/82539 (2000).
135. Freese, E. B., Chu, M. I. & Freese, E. Initiation of yeast sporulation of partial carbon, nitrogen, or phosphate deprivation. *Journal of bacteriology* **149**, 840–851 (1982).
136. Lam, I. & Keeney, S. Mechanism and regulation of meiotic recombination initiation. *Cold Spring Harbor perspectives in biology* **7**, a016634; 10.1101/cshperspect.a016634 (2014).
137. Keeney, S. Spo11 and the Formation of DNA Double-Strand Breaks in Meiosis. *Genome dynamics and stability* **2**, 81–123; 10.1007/7050_2007_026 (2008).
138. Pâques, F. & Haber, J. E. Multiple pathways of recombination induced by double-strand breaks in *Saccharomyces cerevisiae*. *Microbiology and molecular biology reviews : MMBR* **63**, 349–404 (1999).
139. Bergerat, A. *et al.* An atypical topoisomerase II from Archaea with implications for meiotic recombination. *Nature* **386**, 414–417; 10.1038/386414a0 (1997).
140. Keeney, S., Giroux, C. N. & Kleckner, N. Meiosis-specific DNA double-strand breaks are catalyzed by Spo11, a member of a widely conserved protein family. *Cell* **88**, 375–384 (1997).
141. Keeney, S. Mechanism and control of meiotic recombination initiation. *Current topics in developmental biology* **52**, 1–53 (2001).
142. Mitchell, A. P. Control of meiotic gene expression in *Saccharomyces cerevisiae*. *Microbiological reviews* **58**, 56–70 (1994).

143. Sagee, S. *et al.* Multiple and distinct activation and repression sequences mediate the regulated transcription of IME1, a transcriptional activator of meiosis-specific genes in *Saccharomyces cerevisiae*. *Molecular and cellular biology* **18**, 1985–1995 (1998).
144. Kahana, S. *et al.* Functional dissection of IME1 transcription using quantitative promoter-reporter screening. *Genetics* **186**, 829–841; 10.1534/genetics.110.122200 (2010).
145. Kassir, Y., Granot, D. & Simchen, G. IME1, a positive regulator gene of meiosis in *S. cerevisiae*. *Cell* **52**, 853–862 (1988).
146. Cross, F. R. Cell cycle arrest caused by CLN gene deficiency in *Saccharomyces cerevisiae* resembles START-I arrest and is independent of the mating-pheromone signalling pathway. *Molecular and cellular biology* **10**, 6482–6490 (1990).
147. Dirick, L., Böhm, T. & Nasmyth, K. Roles and regulation of Cln-Cdc28 kinases at the start of the cell cycle of *Saccharomyces cerevisiae*. *The EMBO journal* **14**, 4803–4813 (1995).
148. Colomina, N., Garí, E., Gallego, C., Herrero, E. & Aldea, M. G1 cyclins block the Ime1 pathway to make mitosis and meiosis incompatible in budding yeast. *The EMBO journal* **18**, 320–329; 10.1093/emboj/18.2.320 (1999).
149. Lee, R. H. & Honigberg, S. M. Nutritional regulation of late meiotic events in *Saccharomyces cerevisiae* through a pathway distinct from initiation. *Molecular and cellular biology* **16**, 3222–3232 (1996).
150. Smith, H. E., Su, S. S., Neigeborn, L., Driscoll, S. E. & Mitchell, A. P. Role of IME1 expression in regulation of meiosis in *Saccharomyces cerevisiae*. *Molecular and cellular biology* **10**, 6103–6113 (1990).
151. Colomina, N., Liu, Y., Aldea, M. & Garí, E. TOR regulates the subcellular localization of Ime1, a transcriptional activator of meiotic development in budding yeast. *Molecular and cellular biology* **23**, 7415–7424 (2003).
152. Kunoh, T., Kaneko, Y. & Harashima, S. YHP1 encodes a new homeoprotein that binds to the IME1 promoter in *Saccharomyces cerevisiae*. *Yeast (Chichester, England)* **16**, 439–449; 10.1002/(SICI)1097-0061(20000330)16:5<439::AID-YEA536>3.0.CO;2-M (2000).
153. Shenhar, G. & Kassir, Y. A positive regulator of mitosis, Sok2, functions as a negative regulator of meiosis in *Saccharomyces cerevisiae*. *Molecular and cellular biology* **21**, 1603–1612; 10.1128/MCB.21.5.1603-1612.2001 (2001).
154. Toone, W. M. *et al.* Rme1, a negative regulator of meiosis, is also a positive activator of G1 cyclin gene expression. *The EMBO journal* **14**, 5824–5832 (1995).
155. van Werven, F. J. *et al.* Transcription of two long noncoding RNAs mediates mating-type control of gametogenesis in budding yeast. *Cell* **150**, 1170–1181; 10.1016/j.cell.2012.06.049 (2012).
156. Park, H. D., Luche, R. M. & Cooper, T. G. The yeast UME6 gene product is required for transcriptional repression mediated by the CAR1 URS1 repressor binding site. *Nucleic acids research* **20**, 1909–1915 (1992).
157. Strich, R. *et al.* UME6 is a key regulator of nitrogen repression and meiotic development. *Genes & development* **8**, 796–810 (1994).

158. Steber, C. M. & Esposito, R. E. UME6 is a central component of a developmental regulatory switch controlling meiosis-specific gene expression. *Proceedings of the National Academy of Sciences of the United States of America* **92**, 12490–12494 (1995).
159. Washburn, B. K. & Esposito, R. E. Identification of the Sin3-binding site in Ume6 defines a two-step process for conversion of Ume6 from a transcriptional repressor to an activator in yeast. *Molecular and cellular biology* **21**, 2057–2069; 10.1128/MCB.21.6.2057-2069.2001 (2001).
160. Malathi, K., Xiao, Y. & Mitchell, A. P. Interaction of yeast repressor-activator protein Ume6p with glycogen synthase kinase 3 homolog Rim11p. *Molecular and cellular biology* **17**, 7230–7236 (1997).
161. Xiao, Y. & Mitchell, A. P. Shared roles of yeast glycogen synthase kinase 3 family members in nitrogen-responsive phosphorylation of meiotic regulator Ume6p. *Molecular and cellular biology* **20**, 5447–5453 (2000).
162. Bowdish, K. S., Yuan, H. E. & Mitchell, A. P. Analysis of RIM11, a yeast protein kinase that phosphorylates the meiotic activator IME1. *Molecular and cellular biology* **14**, 7909–7919 (1994).
163. Malathi, K., Xiao, Y. & Mitchell, A. P. Catalytic roles of yeast GSK3beta/shaggy homolog Rim11p in meiotic activation. *Genetics* **153**, 1145–1152 (1999).
164. Mitchell, A. P., Driscoll, S. E. & Smith, H. E. Positive control of sporulation-specific genes by the IME1 and IME2 products in *Saccharomyces cerevisiae*. *Molecular and cellular biology* **10**, 2104–2110 (1990).
165. Dirick, L., Goetsch, L., Ammerer, G. & Byers, B. Regulation of meiotic S phase by Ime2 and a Clb5,6-associated kinase in *Saccharomyces cerevisiae*. *Science (New York, N.Y.)* **281**, 1854–1857 (1998).
166. Collins, I. & Newlon, C. S. Chromosomal DNA replication initiates at the same origins in meiosis and mitosis. *Molecular and cellular biology* **14**, 3524–3534 (1994).
167. Callan, H. G. DNA replication in the chromosomes of eukaryotes. *Cold Spring Harbor symposia on quantitative biology* **38**, 195–203 (1974).
168. Cha, R. S., Weiner, B. M., Keeney, S., Dekker, J. & Kleckner, N. Progression of meiotic DNA replication is modulated by interchromosomal interaction proteins, negatively by Spo11p and positively by Rec8p. *Genes & development* **14**, 493–503 (2000).
169. Wijnen, H., Landman, A. & Futcher, B. The G(1) cyclin Cln3 promotes cell cycle entry via the transcription factor Swi6. *Molecular and cellular biology* **22**, 4402–4418 (2002).
170. Bruin, R. A. M. de, McDonald, W. H., Kalashnikova, T. I., Yates, J. & Wittenberg, C. Cln3 activates G1-specific transcription via phosphorylation of the SBF bound repressor Whi5. *Cell* **117**, 887–898; 10.1016/j.cell.2004.05.025 (2004).
171. Costanzo, M. *et al.* CDK activity antagonizes Whi5, an inhibitor of G1/S transcription in yeast. *Cell* **117**, 899–913; 10.1016/j.cell.2004.05.024 (2004).
172. Ferrezuelo, F., Colomina, N., Futcher, B. & Aldea, M. The transcriptional network activated by Cln3 cyclin at the G1-to-S transition of the yeast cell cycle. *Genome biology* **11**, R67; 10.1186/gb-2010-11-6-r67 (2010).

173. Stuart, D. & Wittenberg, C. CLB5 and CLB6 are required for premeiotic DNA replication and activation of the meiotic S/M checkpoint. *Genes & development* **12**, 2698–2710; 10.1101/gad.12.17.2698 (1998).
174. Richardson, H. E., Wittenberg, C., Cross, F. & Reed, S. I. An essential G1 function for cyclin-like proteins in yeast. *Cell* **59**, 1127–1133 (1989).
175. Ghosal, G. & Muniyappa, K. *Saccharomyces cerevisiae* Mre11 is a high-affinity G4 DNA-binding protein and a G-rich DNA-specific endonuclease: implications for replication of telomeric DNA. *Nucleic acids research* **33**, 4692–4703; 10.1093/nar/gki777 (2005).
176. Liu, Z. & Gilbert, W. The yeast KEM1 gene encodes a nuclease specific for G4 tetraplex DNA: implication of in vivo functions for this novel DNA structure. *Cell* **77**, 1083–1092 (1994).
177. Muniyappa, K., Anuradha, S. & Byers, B. Yeast meiosis-specific protein Hop1 binds to G4 DNA and promotes its formation. *Molecular and cellular biology* **20**, 1361–1369 (2000).
178. Borde, V. The multiple roles of the Mre11 complex for meiotic recombination. *Chromosome research : an international journal on the molecular, supramolecular and evolutionary aspects of chromosome biology* **15**, 551–563; 10.1007/s10577-007-1147-9 (2007).
179. Anuradha, S. & Muniyappa, K. Meiosis-specific yeast Hop1 protein promotes synapsis of double-stranded DNA helices via the formation of guanine quartets. *Nucleic acids research* **32**, 2378–2385; 10.1093/nar/gkh559 (2004).
180. Hänsel-Hertsch, R., Spiegel, J., Marsico, G., Tannahill, D. & Balasubramanian, S. Genome-wide mapping of endogenous G-quadruplex DNA structures by chromatin immunoprecipitation and high-throughput sequencing. *Nature protocols* **13**, 551–564; 10.1038/nprot.2017.150 (2018).
181. Martin, M. Cutadapt removes adapter sequences from high-throughput sequencing reads. *EMBnet j.* **17**, 10; 10.14806/ej.17.1.200 (2011).
182. Li, H. & Durbin, R. Fast and accurate short read alignment with Burrows-Wheeler transform. *Bioinformatics (Oxford, England)* **25**, 1754–1760; 10.1093/bioinformatics/btp324 (2009).
183. Li, H. & Durbin, R. Fast and accurate long-read alignment with Burrows-Wheeler transform. *Bioinformatics (Oxford, England)* **26**, 589–595; 10.1093/bioinformatics/btp698 (2010).
184. Zhang, Y. *et al.* Model-based analysis of ChIP-Seq (MACS). *Genome biology* **9**, R137; 10.1186/gb-2008-9-9-r137 (2008).
185. Feng, J., Liu, T., Qin, B., Zhang, Y. & Liu, X. S. Identifying ChIP-seq enrichment using MACS. *Nature protocols* **7**, 1728–1740; 10.1038/nprot.2012.101 (2012).
186. Foiani, M., Liberi, G., Piatti, S. and Plevani, P. Eukaryotic DNA Replication. A Practical Approach. *Saccharomyces cerevisiae* as a model system to study DNA replication. *Oxford University Press*, 185–200 (1999).
187. Kane, S. M. & Roth, R. Carbohydrate metabolism during ascospore development in yeast. *Journal of bacteriology* **118**, 8–14 (1974).
188. Voth, W. P., Olsen, A. E., Sbia, M., Freedman, K. H. & Stillman, D. J. ACE2, CBK1, and BUD4 in budding and cell separation. *Eukaryotic cell* **4**, 1018–1028; 10.1128/EC.4.6.1018-1028.2005 (2005).

189. Halder, R., Riou, J.-F., Teulade-Fichou, M.-P., Frickey, T. & Hartig, J. S. Bisquinolinium compounds induce quadruplex-specific transcriptome changes in HeLa S3 cell lines. *BMC research notes* **5**, 138; 10.1186/1756-0500-5-138 (2012).
190. Fleming, A. M. *et al.* Human DNA Repair Genes Possess Potential G-Quadruplex Sequences in Their Promoters and 5'-Untranslated Regions. *Biochemistry* **57**, 991–1002; 10.1021/acs.biochem.7b01172 (2018).
191. GANESAN, A. T., HOLTER, H. & ROBERTS, C. Some observations on sporulation in *Saccharomyces*. *Comptes rendus des travaux du Laboratoire Carlsberg. Serie chimique* **31**, 1–6 (1958).
192. SHERMAN, F. & ROMAN, H. Evidence for two types of allelic recombination in yeast. *Genetics* **48**, 255–261 (1963).
193. Simchen, G., Piñon, R. & Salts, Y. Sporulation in *Saccharomyces cerevisiae*: premeiotic DNA synthesis, readiness and commitment. *Experimental cell research* **75**, 207–218; 10.1016/0014-4827(72)90538-1 (1972).
194. Winter, E. The Sum1/Ndt80 transcriptional switch and commitment to meiosis in *Saccharomyces cerevisiae*. *Microbiology and molecular biology reviews : MMBR* **76**, 1–15; 10.1128/MMBR.05010-11 (2012).
195. Ballew, O. & Lacefield, S. The DNA damage checkpoint and the spindle position checkpoint: guardians of meiotic commitment. *Current genetics*; 10.1007/s00294-019-00981-z (2019).
196. PETES, T., MALONE, R., SYMINGTON, L. 8 Recombination in Yeast. *Cold Spring Harbor Monograph Archive*, 407–521 (1991).
197. Borde, V., Goldman, A. S. & Lichten, M. Direct coupling between meiotic DNA replication and recombination initiation. *Science (New York, N.Y.)* **290**, 806–809 (2000).
198. Alani, E., Padmore, R. & Kleckner, N. Analysis of wild-type and rad50 mutants of yeast suggests an intimate relationship between meiotic chromosome synapsis and recombination. *Cell* **61**, 419–436 (1990).
199. Fan, Q., Xu, F. & Petes, T. D. Meiosis-specific double-strand DNA breaks at the HIS4 recombination hot spot in the yeast *Saccharomyces cerevisiae*: control in cis and trans. *Molecular and cellular biology* **15**, 1679–1688; 10.1128/mcb.15.3.1679 (1995).
200. Buhler, C., Borde, V. & Lichten, M. Mapping meiotic single-strand DNA reveals a new landscape of DNA double-strand breaks in *Saccharomyces cerevisiae*. *PLoS biology* **5**, e324; 10.1371/journal.pbio.0050324 (2007).
201. Foiani, M. *et al.* A meiosis-specific protein kinase, Ime2, is required for the correct timing of DNA replication and for spore formation in yeast meiosis. *Molecular & general genetics : MGG* **253**, 278–288 (1996).
202. Bellí, G., Garí, E., Piedrafita, L., Aldea, M. & Herrero, E. An activator/repressor dual system allows tight tetracycline-regulated gene expression in budding yeast. *Nucleic acids research* **26**, 942–947; 10.1093/nar/26.4.942 (1998).

203. Cardenas, M. E., Cutler, N. S., Lorenz, M. C., Di Como, C. J. & Heitman, J. The TOR signaling cascade regulates gene expression in response to nutrients. *Genes & development* **13**, 3271–3279; 10.1101/gad.13.24.3271 (1999).
204. Chia, M. & van Werven, F. J. Temporal Expression of a Master Regulator Drives Synchronous Sporulation in Budding Yeast. *G3 (Bethesda, Md.)* **6**, 3553–3560; 10.1534/g3.116.034983 (2016).
205. Castillo Bosch, P. *et al.* FANCI promotes DNA synthesis through G-quadruplex structures. *The EMBO journal* **33**, 2521–2533; 10.15252/embj.201488663 (2014).
206. Crabbe, L., Verdun, R. E., Haggblom, C. I. & Karlseder, J. Defective telomere lagging strand synthesis in cells lacking WRN helicase activity. *Science (New York, N.Y.)* **306**, 1951–1953; 10.1126/science.1103619 (2004).
207. Koole, W. *et al.* A Polymerase Theta-dependent repair pathway suppresses extensive genomic instability at endogenous G4 DNA sites. *Nature communications* **5**, 3216; 10.1038/ncomms4216 (2014).
208. Kruisselbrink, E. *et al.* Mutagenic capacity of endogenous G4 DNA underlies genome instability in FANCI-defective *C. elegans*. *Current biology : CB* **18**, 900–905; 10.1016/j.cub.2008.05.013 (2008).
209. Lopes, J. *et al.* G-quadruplex-induced instability during leading-strand replication. *The EMBO journal* **30**, 4033–4046; 10.1038/emboj.2011.316 (2011).
210. Piazza, A. *et al.* Short loop length and high thermal stability determine genomic instability induced by G-quadruplex-forming minisatellites. *The EMBO journal* **34**, 1718–1734; 10.15252/embj.201490702 (2015).
211. Piazza, A. *et al.* Stimulation of gross chromosomal rearrangements by the human CEB1 and CEB25 minisatellites in *Saccharomyces cerevisiae* depends on G-quadruplexes or Cdc13. *PLoS genetics* **8**, e1003033; 10.1371/journal.pgen.1003033 (2012).
212. Ribeyre, C. *et al.* The yeast Pif1 helicase prevents genomic instability caused by G-quadruplex-forming CEB1 sequences in vivo. *PLoS genetics* **5**, e1000475; 10.1371/journal.pgen.1000475 (2009).
213. Sabouri, N., Capra, J. A. & Zakian, V. A. The essential *Schizosaccharomyces pombe* Pfh1 DNA helicase promotes fork movement past G-quadruplex motifs to prevent DNA damage. *BMC biology* **12**, 101; 10.1186/s12915-014-0101-5 (2014).
214. Sarkies, P. *et al.* FANCI coordinates two pathways that maintain epigenetic stability at G-quadruplex DNA. *Nucleic acids research* **40**, 1485–1498; 10.1093/nar/gkr868 (2012).
215. Sarkies, P., Reams, C., Simpson, L. J. & Sale, J. E. Epigenetic instability due to defective replication of structured DNA. *Molecular cell* **40**, 703–713; 10.1016/j.molcel.2010.11.009 (2010).
216. Schiavone, D. *et al.* Determinants of G quadruplex-induced epigenetic instability in REV1-deficient cells. *The EMBO journal* **33**, 2507–2520; 10.15252/embj.201488398 (2014).
217. Wu, C. G. & Spies, M. G-quadruplex recognition and remodeling by the FANCI helicase. *Nucleic acids research* **44**, 8742–8753; 10.1093/nar/gkw574 (2016).
218. Zimmer, J. *et al.* Targeting BRCA1 and BRCA2 Deficiencies with G-Quadruplex-Interacting Compounds. *Molecular cell* **61**, 449–460; 10.1016/j.molcel.2015.12.004 (2016).

219. Elledge, S. J. & Davis, R. W. Two genes differentially regulated in the cell cycle and by DNA-damaging agents encode alternative regulatory subunits of ribonucleotide reductase. *Genes & development* **4**, 740–751; 10.1101/gad.4.5.740 (1990).
220. Kornberg, R. D. Chromatin Structure: A Repeating Unit of Histones and DNA. *Science (New York, N.Y.)* **184**, 868–871; 10.1126/science.184.4139.868 (1974).
221. Downs, J. A., Lowndes, N. F. & Jackson, S. P. A role for *Saccharomyces cerevisiae* histone H2A in DNA repair. *Nature* **408**, 1001–1004; 10.1038/35050000 (2000).
222. Ueda, S. *et al.* TORC1, Tel1/Mec1, and Mpk1 regulate autophagy induction after DNA damage in budding yeast. *Cellular signalling* **62**, 109344; 10.1016/j.cellsig.2019.109344 (2019).
223. Eapen, V. V. *et al.* A pathway of targeted autophagy is induced by DNA damage in budding yeast. *Proceedings of the National Academy of Sciences of the United States of America* **114**, E1158–E1167; 10.1073/pnas.1614364114 (2017).
224. Nakatogawa, H., Suzuki, K., Kamada, Y. & Ohsumi, Y. Dynamics and diversity in autophagy mechanisms: lessons from yeast. *Nature reviews. Molecular cell biology* **10**, 458–467; 10.1038/nrm2708 (2009).
225. Kaur, J. & Debnath, J. Autophagy at the crossroads of catabolism and anabolism. *Nature reviews. Molecular cell biology* **16**, 461–472; 10.1038/nrm4024 (2015).
226. Wen, X. & Klionsky, D. J. An overview of macroautophagy in yeast. *Journal of molecular biology* **428**, 1681–1699; 10.1016/j.jmb.2016.02.021 (2016).
227. Vessoni, A. T., Filippi-Chiela, E. C., Menck, C. F. & Lenz, G. Autophagy and genomic integrity. *Cell death and differentiation* **20**, 1444–1454; 10.1038/cdd.2013.103 (2013).
228. Dotiwala, F. *et al.* DNA damage checkpoint triggers autophagy to regulate the initiation of anaphase. *Proceedings of the National Academy of Sciences of the United States of America* **110**, E41–9; 10.1073/pnas.1218065109 (2013).
229. Eapen, V. V. & Haber, J. E. DNA damage signaling triggers the cytoplasm-to-vacuole pathway of autophagy to regulate cell cycle progression. *Autophagy* **9**, 440–441; 10.4161/auto.23280 (2013).
230. Suzuki, K., Kamada, Y. & Ohsumi, Y. Studies of cargo delivery to the vacuole mediated by autophagosomes in *Saccharomyces cerevisiae*. *Developmental cell* **3**, 815–824 (2002).
231. Huang, W. P., Scott, S. V., Kim, J. & Klionsky, D. J. The itinerary of a vesicle component, Aut7p/Cvt5p, terminates in the yeast vacuole via the autophagy/Cvt pathways. *The Journal of biological chemistry* **275**, 5845–5851; 10.1074/jbc.275.8.5845 (2000).
232. Kirisako, T. *et al.* Formation process of autophagosome is traced with Apg8/Aut7p in yeast. *The Journal of cell biology* **147**, 435–446; 10.1083/jcb.147.2.435 (1999).
233. Harrison, J. C. & Haber, J. E. Surviving the breakup: the DNA damage checkpoint. *Annual review of genetics* **40**, 209–235; 10.1146/annurev.genet.40.051206.105231 (2006).
234. Siede, W., Allen, J. B., Elledge, S. J. & Friedberg, E. C. The *Saccharomyces cerevisiae* MEC1 gene, which encodes a homolog of the human ATM gene product, is required for G1 arrest following radiation treatment. *Journal of bacteriology* **178**, 5841–5843; 10.1128/jb.178.19.5841-5843.1996 (1996).

235. Gerald, J. N. F., Benjamin, J. M. & Kron, S. J. Robust G1 checkpoint arrest in budding yeast: dependence on DNA damage signaling and repair. *Journal of cell science* **115**, 1749–1757 (2002).
236. Gobbin, E., Cesena, D., Galbiati, A., Lockhart, A. & Longhese, M. P. Interplays between ATM/Tel1 and ATR/Mec1 in sensing and signaling DNA double-strand breaks. *DNA repair* **12**, 791–799; 10.1016/j.dnarep.2013.07.009 (2013).
237. Lydall, D., Nikolsky, Y., Bishop, D. K. & Weinert, T. A meiotic recombination checkpoint controlled by mitotic checkpoint genes. *Nature* **383**, 840–843; 10.1038/383840a0 (1996).
238. Huppert, J. L. & Balasubramanian, S. G-quadruplexes in promoters throughout the human genome. *Nucleic acids research* **35**, 406–413; 10.1093/nar/gkl1057 (2007).
239. Yuan, G.-C. *et al.* Genome-scale identification of nucleosome positions in *S. cerevisiae*. *Science (New York, N.Y.)* **309**, 626–630; 10.1126/science.1112178 (2005).
240. Smith, J. S. *et al.* Rudimentary G-quadruplex-based telomere capping in *Saccharomyces cerevisiae*. *Nature structural & molecular biology* **18**, 478–485; 10.1038/nsmb.2033 (2011).
241. Cayrou, C. *et al.* Genome-scale analysis of metazoan replication origins reveals their organization in specific but flexible sites defined by conserved features. *Genome research* **21**, 1438–1449; 10.1101/gr.121830.111 (2011).
242. Valton, A.-L. *et al.* G4 motifs affect origin positioning and efficiency in two vertebrate replicators. *The EMBO journal* **33**, 732–746; 10.1002/embj.201387506 (2014).
243. Ren, B. *et al.* Genome-wide location and function of DNA binding proteins. *Science (New York, N.Y.)* **290**, 2306–2309; 10.1126/science.290.5500.2306 (2000).
244. Bailey, T. L. & Elkan, C. Fitting a mixture model by expectation maximization to discover motifs in biopolymers. *Proceedings. International Conference on Intelligent Systems for Molecular Biology* **2**, 28–36 (1994).
245. Ruggiero, E., Tassinari, M., Perrone, R., Nadai, M. & Richter, S. N. Stable and Conserved G-Quadruplexes in the Long Terminal Repeat Promoter of Retroviruses. *ACS infectious diseases* **5**, 1150–1159; 10.1021/acsinfecdis.9b00011 (2019).
246. Bochman, M. L., Paeschke, K. & Zakian, V. A. DNA secondary structures: stability and function of G-quadruplex structures. *Nature reviews. Genetics* **13**, 770–780; 10.1038/nrg3296 (2012).
247. Ghosal, G. & Muniyappa, K. The characterization of *Saccharomyces cerevisiae* Mre11/Rad50/Xrs2 complex reveals that Rad50 negatively regulates Mre11 endonucleolytic but not the exonucleolytic activity. *Journal of molecular biology* **372**, 864–882; 10.1016/j.jmb.2007.07.013 (2007).
248. Gray, D. M. *et al.* Measured and calculated CD spectra of G-quartets stacked with the same or opposite polarities. *Chirality* **20**, 431–440; 10.1002/chir.20455 (2008).
249. Davis, L. *et al.* The *Saccharomyces cerevisiae* MUM2 gene interacts with the DNA replication machinery and is required for meiotic levels of double strand breaks. *Genetics* **157**, 1179–1189 (2001).
250. Agarwala, S. D., Blitzblau, H. G., Hochwagen, A. & Fink, G. R. RNA methylation by the MIS complex regulates a cell fate decision in yeast. *PLoS genetics* **8**, e1002732; 10.1371/journal.pgen.1002732 (2012).

251. Martínez-Pastor, M. T. *et al.* The *Saccharomyces cerevisiae* zinc finger proteins Msn2p and Msn4p are required for transcriptional induction through the stress response element (STRE). *The EMBO journal* **15**, 2227–2235 (1996).
252. Schmitt, A. P. & McEntee, K. Msn2p, a zinc finger DNA-binding protein, is the transcriptional activator of the multistress response in *Saccharomyces cerevisiae*. *Proceedings of the National Academy of Sciences of the United States of America* **93**, 5777–5782; 10.1073/pnas.93.12.5777 (1996).
253. Keogh, M.-C. *et al.* Cotranscriptional set2 methylation of histone H3 lysine 36 recruits a repressive Rpd3 complex. *Cell* **123**, 593–605; 10.1016/j.cell.2005.10.025 (2005).
254. Carrozza, M. J. *et al.* Histone H3 methylation by Set2 directs deacetylation of coding regions by Rpd3S to suppress spurious intragenic transcription. *Cell* **123**, 581–592; 10.1016/j.cell.2005.10.023 (2005).
255. Kim, T. & Buratowski, S. Dimethylation of H3K4 by Set1 recruits the Set3 histone deacetylase complex to 5' transcribed regions. *Cell* **137**, 259–272; 10.1016/j.cell.2009.02.045 (2009).
256. Gottschalk, A. *et al.* A comprehensive biochemical and genetic analysis of the yeast U1 snRNP reveals five novel proteins. *RNA (New York, N.Y.)* **4**, 374–393 (1998).
257. Qiu, Z. R., Schwer, B. & Shuman, S. Determinants of Nam8-dependent splicing of meiotic pre-mRNAs. *Nucleic acids research* **39**, 3427–3445; 10.1093/nar/gkq1328 (2011).
258. Eddy, J. & Maizels, N. Conserved elements with potential to form polymorphic G-quadruplex structures in the first intron of human genes. *Nucleic acids research* **36**, 1321–1333; 10.1093/nar/gkm1138 (2008).
259. Varizhuk, A. *et al.* The expanding repertoire of G4 DNA structures. *Biochimie* **135**, 54–62; 10.1016/j.biochi.2017.01.003 (2017).
260. White, M. A., Dominska, M. & Petes, T. D. Transcription factors are required for the meiotic recombination hotspot at the HIS4 locus in *Saccharomyces cerevisiae*. *Proceedings of the National Academy of Sciences of the United States of America* **90**, 6621–6625; 10.1073/pnas.90.14.6621 (1993).
261. Tran, P. L. T., Mergny, J.-L. & Alberti, P. Stability of telomeric G-quadruplexes. *Nucleic acids research* **39**, 3282–3294; 10.1093/nar/gkq1292 (2011).
262. Petes, T. D. Meiotic recombination hot spots and cold spots. *Nature reviews. Genetics* **2**, 360–369; 10.1038/35072078 (2001).
263. Kauppi, L., Jeffreys, A. J. & Keeney, S. Where the crossovers are: recombination distributions in mammals. *Nature reviews. Genetics* **5**, 413–424; 10.1038/nrg1346 (2004).
264. Patel, P. K. & Hosur, R. V. NMR observation of T-tetrads in a parallel stranded DNA quadruplex formed by *Saccharomyces cerevisiae* telomere repeats. *Nucleic acids research* **27**, 2457–2464; 10.1093/nar/27.12.2457 (1999).
265. Schulz, V. P. & Zakian, V. A. The *saccharomyces* PIF1 DNA helicase inhibits telomere elongation and de novo telomere formation. *Cell* **76**, 145–155; 10.1016/0092-8674(94)90179-1 (1994).

266. Paeschke, K., McDonald, K. R. & Zakian, V. A. Telomeres: structures in need of unwinding. *FEBS letters* **584**, 3760–3772; 10.1016/j.febslet.2010.07.007 (2010).
267. White, M. A., Wierdl, M., Detloff, P. & Petes, T. D. DNA-binding protein RAP1 stimulates meiotic recombination at the HIS4 locus in yeast. *Proceedings of the National Academy of Sciences of the United States of America* **88**, 9755–9759; 10.1073/pnas.88.21.9755 (1991).
268. Devlin, C., Tice-Baldwin, K., Shore, D. & Arndt, K. T. RAP1 is required for BAS1/BAS2- and GCN4-dependent transcription of the yeast HIS4 gene. *Molecular and cellular biology* **11**, 3642–3651; 10.1128/mcb.11.7.3642 (1991).
269. Buchman, A. R., Kimmerly, W. J., Rine, J. & Kornberg, R. D. Two DNA-binding factors recognize specific sequences at silencers, upstream activating sequences, autonomously replicating sequences, and telomeres in *Saccharomyces cerevisiae*. *Molecular and cellular biology* **8**, 210–225; 10.1128/mcb.8.1.210 (1988).
270. Vignais, M. L. & Sentenac, A. Asymmetric DNA bending induced by the yeast multifunctional factor TUF. *The Journal of biological chemistry* **264**, 8463–8466 (1989).
271. Hofmann, J. F.-X., Laroche, T., Brand, A. H. & Gasser, S. M. RAP-1 factor is necessary for DNA loop formation in vitro at the silent mating type locus HML. *Cell* **57**, 725–737; 10.1016/0092-8674(89)90788-5 (1989).
272. Runge, K. W. & Zakian, V. A. Properties of the transcriptional enhancer in *Saccharomyces cerevisiae* telomeres. *Nucleic acids research* **18**, 1783–1787; 10.1093/nar/18.7.1783 (1990).
273. Pan, J. *et al.* A hierarchical combination of factors shapes the genome-wide topography of yeast meiotic recombination initiation. *Cell* **144**, 719–731; 10.1016/j.cell.2011.02.009 (2011).
274. Serikawa, T. *et al.* Comprehensive identification of proteins binding to RNA G-quadruplex motifs in the 5' UTR of tumor-associated mRNAs. *Biochimie* **144**, 169–184; 10.1016/j.biochi.2017.11.003 (2018).
275. Hacht, A. von *et al.* Identification and characterization of RNA guanine-quadruplex binding proteins. *Nucleic acids research* **42**, 6630–6644; 10.1093/nar/gku290 (2014).
276. Juneau, K., Nislow, C. & Davis, R. W. Alternative splicing of PTC7 in *Saccharomyces cerevisiae* determines protein localization. *Genetics* **183**, 185–194; 10.1534/genetics.109.105155 (2009).
277. Hossain, M. A., Rodriguez, C. M. & Johnson, T. L. Key features of the two-intron *Saccharomyces cerevisiae* gene SUS1 contribute to its alternative splicing. *Nucleic acids research* **39**, 8612–8627; 10.1093/nar/gkr497 (2011).
278. Wahl, M. C., Will, C. L. & Lührmann, R. The spliceosome: design principles of a dynamic RNP machine. *Cell* **136**, 701–718; 10.1016/j.cell.2009.02.009 (2009).
279. Li, X. *et al.* CryoEM structure of *Saccharomyces cerevisiae* U1 snRNP offers insight into alternative splicing. *Nature communications* **8**, 1035; 10.1038/s41467-017-01241-9 (2017).
280. Marcel, V. *et al.* G-quadruplex structures in TP53 intron 3: role in alternative splicing and in production of p53 mRNA isoforms. *Carcinogenesis* **32**, 271–278; 10.1093/carcin/bgq253 (2011).
281. Gao, J. *et al.* DEAD-box RNA helicases Dbp2, Ded1 and Mss116 bind to G-quadruplex nucleic acids and destabilize G-quadruplex RNA. *Chemical communications (Cambridge, England)* **55**, 4467–4470; 10.1039/c8cc10091h (2019).

282. Pijnappel, W. W. *et al.* The *S. cerevisiae* SET3 complex includes two histone deacetylases, Hos2 and Hst1, and is a meiotic-specific repressor of the sporulation gene program. *Genes & development* **15**, 2991–3004; 10.1101/gad.207401 (2001).
283. Honigberg, S. M. & Purnapatre, K. Signal pathway integration in the switch from the mitotic cell cycle to meiosis in yeast. *Journal of cell science* **116**, 2137–2147; 10.1242/jcs.00460 (2003).
284. Cui, X. *et al.* Exploration of the Structure and Recognition of a G-quadruplex in the her2 Proto-oncogene Promoter and Its Transcriptional Regulation. *Scientific reports* **9**, 3966; 10.1038/s41598-019-39941-5 (2019).
285. Yan, J., Zhao, X., Liu, B., Yuan, Y. & Guan, Y. An intramolecular G-quadruplex structure formed in the human MET promoter region and its biological relevance. *Molecular carcinogenesis* **55**, 897–909; 10.1002/mc.22330 (2016).
286. Sun, D., Guo, K., Rusche, J. J. & Hurley, L. H. Facilitation of a structural transition in the polypurine/polypyrimidine tract within the proximal promoter region of the human VEGF gene by the presence of potassium and G-quadruplex-interactive agents. *Nucleic acids research* **33**, 6070–6080; 10.1093/nar/gki917 (2005).
287. Qin, Y., Rezler, E. M., Gokhale, V., Sun, D. & Hurley, L. H. Characterization of the G-quadruplexes in the duplex nuclease hypersensitive element of the PDGF-A promoter and modulation of PDGF-A promoter activity by TMPyP4. *Nucleic acids research* **35**, 7698–7713; 10.1093/nar/gkm538 (2007).
288. Verma, A. *et al.* Genome-wide computational and expression analyses reveal G-quadruplex DNA motifs as conserved cis-regulatory elements in human and related species. *Journal of medicinal chemistry* **51**, 5641–5649; 10.1021/jm800448a (2008).
289. Paillé, A. *et al.* Analyses of rRNA gene chromatin in cell cycle arrested *Saccharomyces cerevisiae* cells. *Data in brief* **25**, 104083; 10.1016/j.dib.2019.104083 (2019).
290. Heude, M. & Fabre, F. α -control of DNA repair in the yeast *Saccharomyces cerevisiae*: genetic and physiological aspects. *Genetics* **133**, 489–498 (1993).
291. Fasullo, M., Bennett, T. & Dave, P. Expression of *Saccharomyces cerevisiae* MAT α and MAT α enhances the HO endonuclease-stimulation of chromosomal rearrangements directed by his3 recombinational substrates. *Mutation Research/DNA Repair* **433**, 33–44; 10.1016/s0921-8777(98)00059-7 (1999).
292. CHAFFEY, N. Alberts, B., Johnson, A., Lewis, J., Raff, M., Roberts, K. and Walter, P. Molecular biology of the cell. 4th edn. *Annals of Botany* **91**, 401; 10.1093/aob/mcg023 (2003).
293. Moore, J. K. & Haber, J. E. Cell cycle and genetic requirements of two pathways of nonhomologous end-joining repair of double-strand breaks in *Saccharomyces cerevisiae*. *Molecular and cellular biology* **16**, 2164–2173 (1996).
294. Shrivastav, M., Haro, L. P. de & Nickoloff, J. A. Regulation of DNA double-strand break repair pathway choice. *Cell research* **18**, 134–147; 10.1038/cr.2007.111. (2008).
295. Melo, J. & Toczyski, D. A unified view of the DNA-damage checkpoint. *Current opinion in cell biology* **14**, 237–245; 10.1016/S0955-0674(02)00312-5 (2002).

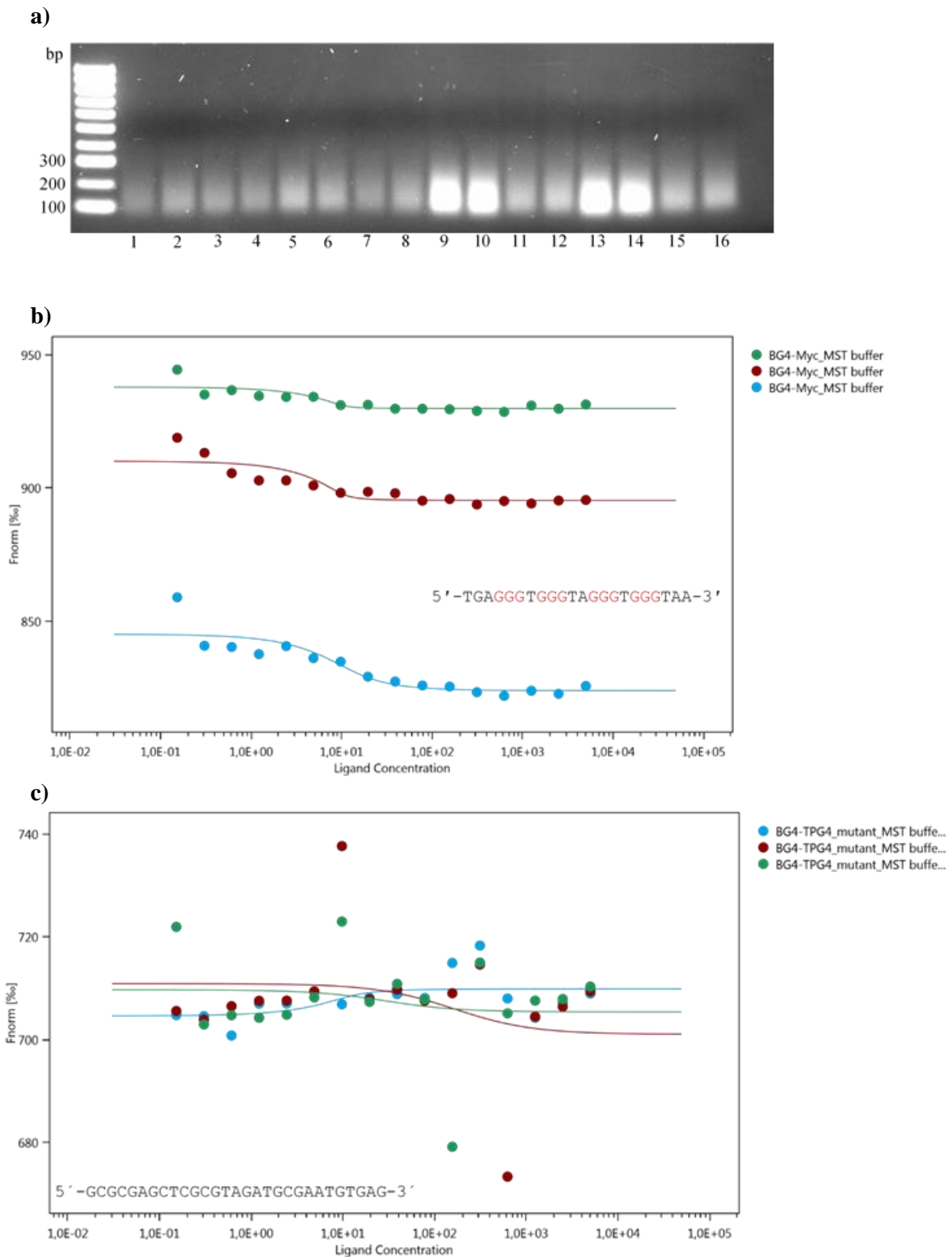
296. Paciotti, V., Clerici, M., Scotti, M., Lucchini, G. & Longhese, M. P. Characterization of *mec1* kinase-deficient mutants and of new hypomorphic *mec1* alleles impairing subsets of the DNA damage response pathway. *Molecular and cellular biology* **21**, 3913–3925; 10.1128/MCB.21.12.3913-3925.2001 (2001).
297. Zou, L., Cortez, D. & Elledge, S. J. Regulation of ATR substrate selection by Rad17-dependent loading of Rad9 complexes onto chromatin. *Genes & development* **16**, 198–208; 10.1101/gad.950302 (2002).
298. Mallory, J. C. & Petes, T. D. Protein kinase activity of Tel1p and Mec1p, two *Saccharomyces cerevisiae* proteins related to the human ATM protein kinase. *Proceedings of the National Academy of Sciences of the United States of America* **97**, 13749–13754; 10.1073/pnas.250475697 (2000).
299. Weinert, T. A., Kiser, G. L. & Hartwell, L. H. Mitotic checkpoint genes in budding yeast and the dependence of mitosis on DNA replication and repair. *Genes & development* **8**, 652–665; 10.1101/gad.8.6.652 (1994).
300. Grenon, M., Gilbert, C. & Lowndes, N. F. Checkpoint activation in response to double-strand breaks requires the Mre11/Rad50/Xrs2 complex. *Nature cell biology* **3**, 844–847; 10.1038/ncb0901-844 (2001).
301. D'Amours, D. & Jackson, S. P. The yeast Xrs2 complex functions in S phase checkpoint regulation. *Genes & development* **15**, 2238–2249; 10.1101/gad.208701 (2001).
302. Allen, J. B., Zhou, Z., Siede, W., Friedberg, E. C. & Elledge, S. J. The SAD1/RAD53 protein kinase controls multiple checkpoints and DNA damage-induced transcription in yeast. *Genes & development* **8**, 2401–2415; 10.1101/gad.8.20.2401 (1994).
303. Morrow, D. M., Tagle, D. A., Shiloh, Y., Collins, F. S. & Hieter, P. TEL1, an *S. cerevisiae* homolog of the human gene mutated in ataxia telangiectasia, is functionally related to the yeast checkpoint gene MEC1. *Cell* **82**, 831–840; 10.1016/0092-8674(95)90480-8 (1995).
304. Sanchez, Y. *et al.* Regulation of RAD53 by the ATM-like kinases MEC1 and TEL1 in yeast cell cycle checkpoint pathways. *Science (New York, N.Y.)* **271**, 357–360; 10.1126/science.271.5247.357 (1996).
305. Salvati, E. *et al.* Telomere damage induced by the G-quadruplex ligand RHPS4 has an antitumor effect. *The Journal of clinical investigation* **117**, 3236–3247; 10.1172/JCI32461 (2007).
306. Armas, P., David, A. & Calcaterra, N. B. Transcriptional control by G-quadruplexes: In vivo roles and perspectives for specific intervention. *Transcription* **8**, 21–25; 10.1080/21541264.2016.1243505 (2017).
307. Seenisamy, J. *et al.* The dynamic character of the G-quadruplex element in the c-MYC promoter and modification by TMPyP4. *Journal of the American Chemical Society* **126**, 8702–8709; 10.1021/ja040022b (2004).
308. Ito, T., Miura, F. & Onda, M. Unexpected complexity of the budding yeast transcriptome. *IUBMB life* **60**, 775–781; 10.1002/iub.121. (2008).
309. Nagalakshmi, U. *et al.* The transcriptional landscape of the yeast genome defined by RNA sequencing. *Science (New York, N.Y.)* **320**, 1344–1349; 10.1126/science.1158441. (2008).

310. Sandmeyer, S. B. & Clemens, K. A. Function of a retrotransposon nucleocapsid protein. *RNA biology* **7**, 642–654; 10.4161/rna.7.6.14117 (2010).
311. Pritham, E. J. Transposable elements and factors influencing their success in eukaryotes. *The Journal of heredity* **100**, 648–655; 10.1093/jhered/esp065 (2009).
312. Carr, M., Bensasson, D. & Bergman, C. M. Evolutionary genomics of transposable elements in *Saccharomyces cerevisiae*. *PloS one* **7**, e50978; 10.1371/journal.pone.0050978 (2012).
313. Perrone, R., Lavezzo, E., Palù, G. & Richter, S. N. Conserved presence of G-quadruplex forming sequences in the Long Terminal Repeat Promoter of Lentiviruses. *Scientific reports* **7**, 2018; 10.1038/s41598-017-02291-1 (2017).
314. Lexa, M. *et al.* Quadruplex-forming sequences occupy discrete regions inside plant LTR retrotransposons. *Nucleic acids research* **42**, 968–978; 10.1093/nar/gkt893 (2014).
315. Tosoni, E. *et al.* Nucleolin stabilizes G-quadruplex structures folded by the LTR promoter and silences HIV-1 viral transcription. *Nucleic acids research* **43**, 8884–8897; 10.1093/nar/gkv897. (2015).
316. Perrone, R. *et al.* Anti-HIV-1 activity of the G-quadruplex ligand BRACO-19. *The Journal of antimicrobial chemotherapy* **69**, 3248–3258; 10.1093/jac/dku280 (2014).
317. Perrone, R. *et al.* Synthesis, Binding and Antiviral Properties of Potent Core-Extended Naphthalene Diimides Targeting the HIV-1 Long Terminal Repeat Promoter G-Quadruplexes. *Journal of medicinal chemistry* **58**, 9639–9652; 10.1021/acs.jmedchem.5b01283 (2015).
318. Montgomery, E., Charlesworth, B. & Langley, C. H. A test for the role of natural selection in the stabilization of transposable element copy number in a population of *Drosophila melanogaster*. *Genetical research* **49**, 31–41 (1987).
319. Biémont, C., Tsitroni, A., Vieira, C. & Hoogland, C. Transposable Element Distribution in *Drosophila*. *Genetics* **147**, 1997–1999 (1997).
320. Hollister, J. D. & Gaut, B. S. Population and evolutionary dynamics of Helitron transposable elements in *Arabidopsis thaliana*. *Molecular biology and evolution* **24**, 2515–2524; 10.1093/molbev/msm197 (2007).
321. Song, M. & Boissinot, S. Selection against LINE-1 retrotransposons results principally from their ability to mediate ectopic recombination. *Gene* **390**, 206–213; 10.1016/j.gene.2006.09.033 (2007).
322. Carr, M., Nelson, M., Leadbeater, B. S. C. & Baldauf, S. L. Three families of LTR retrotransposons are present in the genome of the choanoflagellate *Monosiga brevicollis*. *Protist* **159**, 579–590; 10.1016/j.protis.2008.05.001 (2008).
323. Chan, J. E. & Kolodner, R. D. A genetic and structural study of genome rearrangements mediated by high copy repeat Ty1 elements. *PLoS genetics* **7**, e1002089; 10.1371/journal.pgen.1002089 (2011).
324. Koszul, R., Caburet, S., Dujon, B. & Fischer, G. Eucaryotic genome evolution through the spontaneous duplication of large chromosomal segments. *The EMBO journal* **23**, 234–243; 10.1038/sj.emboj.7600024 (2004).

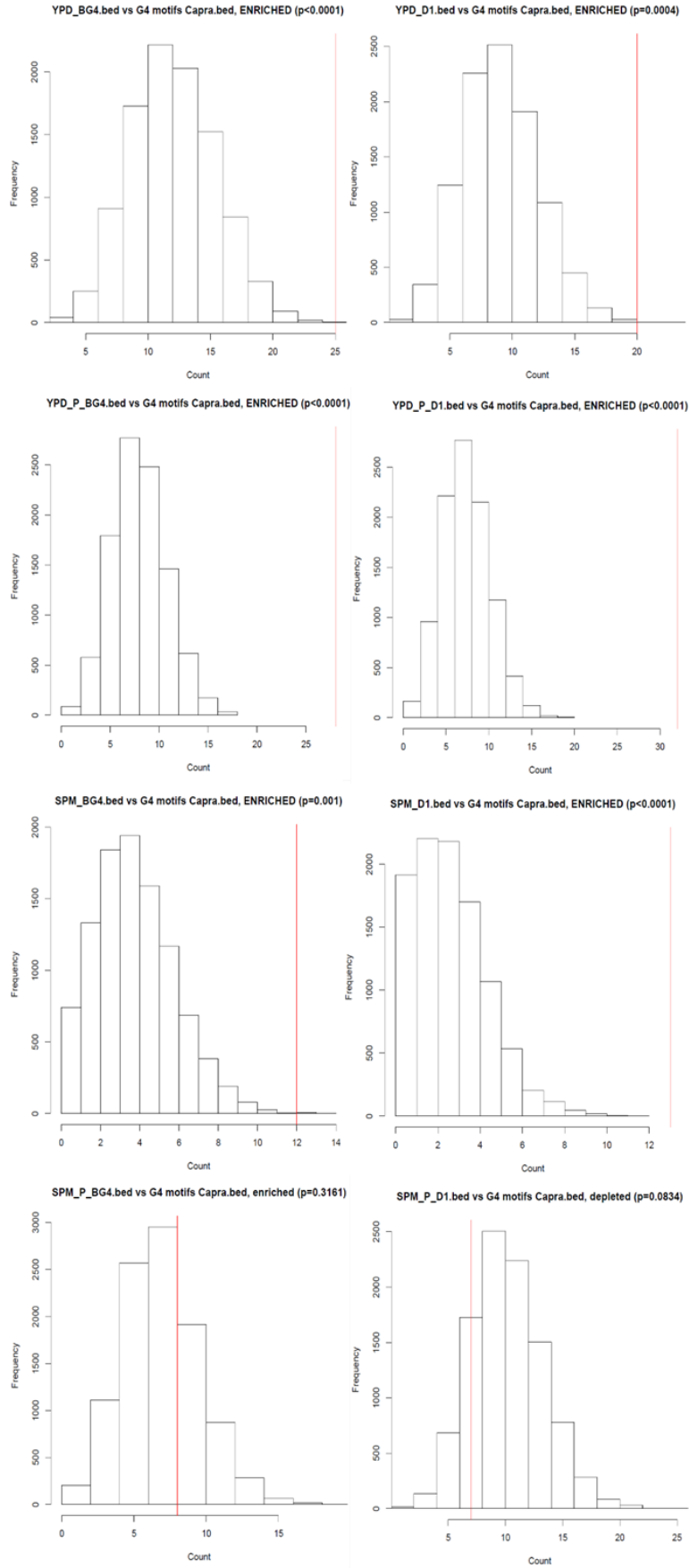
325. Chaleff, D. T. & Fink, G. R. Genetic events associated with an insertion mutation in yeast. *Cell* **21**, 227–237; 10.1016/0092-8674(80)90130-0 (1980).
326. Roeder, G.S. & Fink, G. R. DNA rearrangements associated with a transposable element in yeast. *Cell* **21**, 239–249; 10.1016/0092-8674(80)90131-2 (1980).
327. Roeder, G. S. & Fink, G. R. Movement of yeast transposable elements by gene conversion. *Proceedings of the National Academy of Sciences of the United States of America* **79**, 5621–5625; 10.1073/pnas.79.18.5621 (1982).
328. Downs, K. M., Brennan, G. & Liebman, S. W. Deletions extending from a single Ty1 element in *Saccharomyces cerevisiae*. *Molecular and cellular biology* **5**, 3451–3457; 10.1128/mcb.5.12.3451 (1985).
329. Dunham, M. J. *et al.* Characteristic genome rearrangements in experimental evolution of *Saccharomyces cerevisiae*. *Proceedings of the National Academy of Sciences of the United States of America* **99**, 16144–16149; 10.1073/pnas.242624799 (2002).
330. Putnam, C. D., Pennaneach, V. & Kolodner, R. D. *Saccharomyces cerevisiae* as a model system to define the chromosomal instability phenotype. *Molecular and cellular biology* **25**, 7226–7238; 10.1128/MCB.25.16.7226-7238.2005 (2005).
331. Surosky, R. T. & Tye, B. K. Resolution of dicentric chromosomes by Ty-mediated recombination in yeast. *Genetics* **110**, 397–419 (1985).
332. Umezu, K., Hiraoka, M., Mori, M. & Maki, H. Structural analysis of aberrant chromosomes that occur spontaneously in diploid *Saccharomyces cerevisiae*: retrotransposon Ty1 plays a crucial role in chromosomal rearrangements. *Genetics* **160**, 97–110 (2002).
333. Zhang, H. *et al.* Gene copy-number variation in haploid and diploid strains of the yeast *Saccharomyces cerevisiae*. *Genetics* **193**, 785–801; 10.1534/genetics.112.146522 (2013).
334. Bradshaw, V. A. & McEntee, K. DNA damage activates transcription and transposition of yeast Ty retrotransposons. *Molecular & general genetics : MGG* **218**, 465–474; 10.1007/bf00332411 (1989).
335. McClanahan, T. & McEntee, K. Specific transcripts are elevated in *Saccharomyces cerevisiae* in response to DNA damage. *Molecular and cellular biology* **4**, 2356–2363; 10.1128/mcb.4.11.2356 (1984).
336. Morillon, A., Springer, M. & Lesage, P. Activation of the Kss1 invasive-filamentous growth pathway induces Ty1 transcription and retrotransposition in *Saccharomyces cerevisiae*. *Molecular and cellular biology* **20**, 5766–5776; 10.1128/mcb.20.15.5766-5776.2000 (2000).
337. Rolfe, M., Spanos, A. & Banks, G. Induction of yeast Ty element transcription by ultraviolet light. *Nature* **319**, 339–340; 10.1038/319339a0 (1986).
338. Staleva Staleva, L. & Venkov, P. Activation of Ty transposition by mutagens. *Mutation research* **474**, 93–103; 10.1016/s0027-5107(00)00165-2 (2001).
339. Todeschini, A.-L., Morillon, A., Springer, M. & Lesage, P. Severe adenine starvation activates Ty1 transcription and retrotransposition in *Saccharomyces cerevisiae*. *Molecular and cellular biology* **25**, 7459–7472; 10.1128/MCB.25.17.7459-7472.2005 (2005).

340. Servant, G., Pannetier, C. & Lesage, P. Remodeling yeast gene transcription by activating the Ty1 long terminal repeat retrotransposon under severe adenine deficiency. *Molecular and cellular biology* **28**, 5543–5554; 10.1128/MCB.00416-08 (2008).
341. Chen, S. *et al.* Mechanistic studies for the role of cellular nucleic-acid-binding protein (CNBP) in regulation of c-myc transcription. *Biochimica et biophysica acta* **1830**, 4769–4777; 10.1016/j.bbagen.2013.06.007 (2013).
342. Thakur, R. K. *et al.* Metastases suppressor NM23-H2 interaction with G-quadruplex DNA within c-MYC promoter nuclease hypersensitive element induces c-MYC expression. *Nucleic acids research* **37**, 172–183; 10.1093/nar/gkn919 (2009).
343. Tian, T., Chen, Y.-Q., Wang, S.-R. & Zhou, X. G-Quadruplex: A Regulator of Gene Expression and Its Chemical Targeting. *Chem* **4**, 1314–1344; 10.1016/j.chempr.2018.02.014 (2018).
344. Kwok, C. K., Marsico, G., Sahakyan, A. B., Chambers, V. S. & Balasubramanian, S. rG4-seq reveals widespread formation of G-quadruplex structures in the human transcriptome. *Nature methods* **13**, 841–844; 10.1038/nmeth.3965 (2016).
345. Nie, J. *et al.* Post-transcriptional Regulation of Nkx2-5 by RHAU in Heart Development. *Cell reports* **13**, 723–732; 10.1016/j.celrep.2015.09.043 (2015).
346. Wolfe, A. L. *et al.* RNA G-quadruplexes cause eIF4A-dependent oncogene translation in cancer. *Nature* **513**, 65–70; 10.1038/nature13485 (2014).
347. Morris, M. J., Negishi, Y., Pazsint, C., Schonhoft, J. D. & Basu, S. An RNA G-quadruplex is essential for cap-independent translation initiation in human VEGF IRES. *Journal of the American Chemical Society* **132**, 17831–17839; 10.1021/ja106287x (2010).
348. Cammas, A. *et al.* Stabilization of the G-quadruplex at the VEGF IRES represses cap-independent translation. *RNA biology* **12**, 320–329; 10.1080/15476286.2015.1017236 (2015).
349. Jiang, C. & Pugh, B. F. A compiled and systematic reference map of nucleosome positions across the *Saccharomyces cerevisiae* genome. *Genome biology* **10**, R109; 10.1186/gb-2009-10-10-r109 (2009).
350. Robine, N. *et al.* Genome-wide redistribution of meiotic double-strand breaks in *Saccharomyces cerevisiae*. *Molecular and cellular biology* **27**, 1868–1880; 10.1128/MCB.02063-06 (2007).

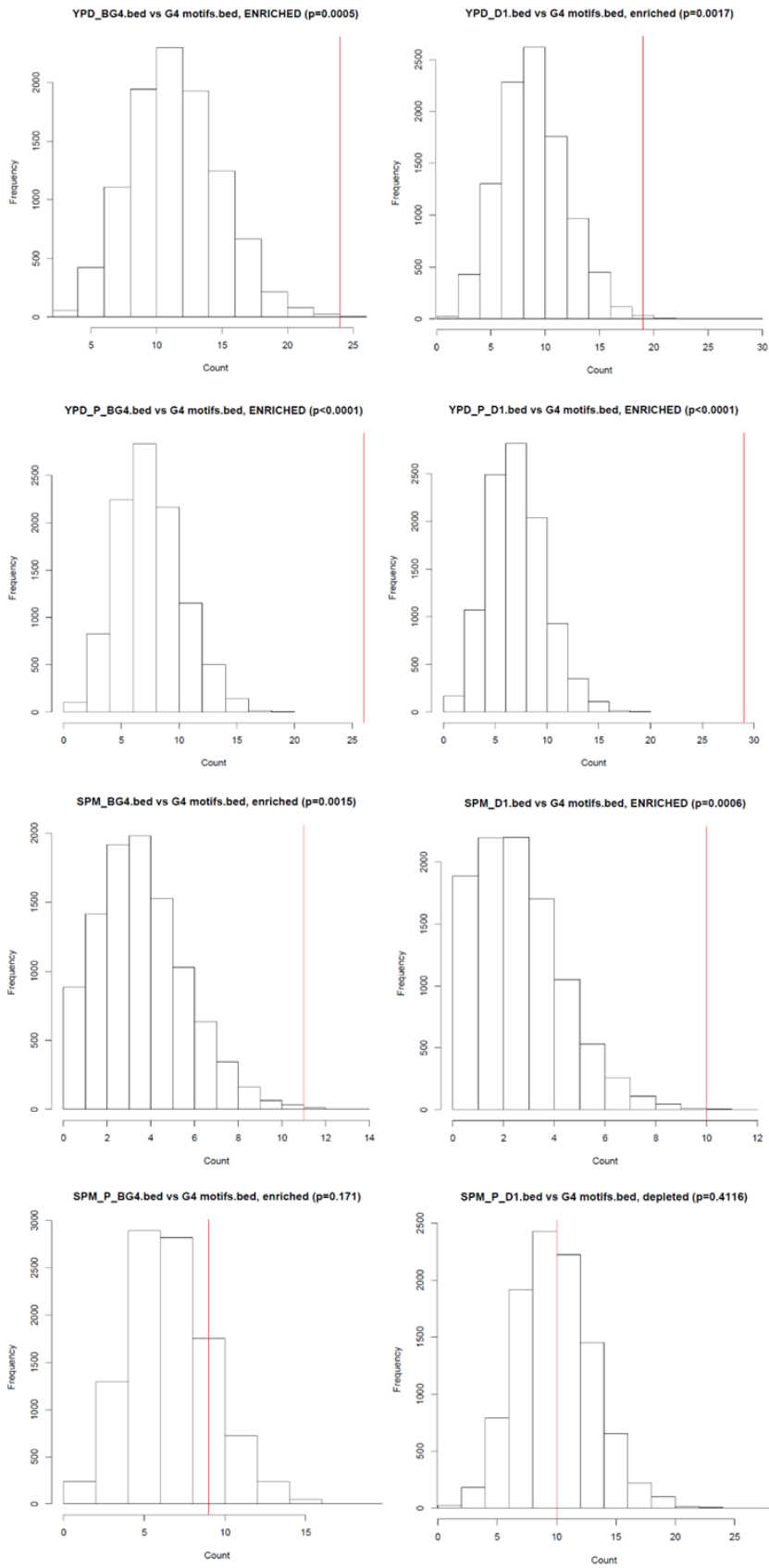
6 Appendix



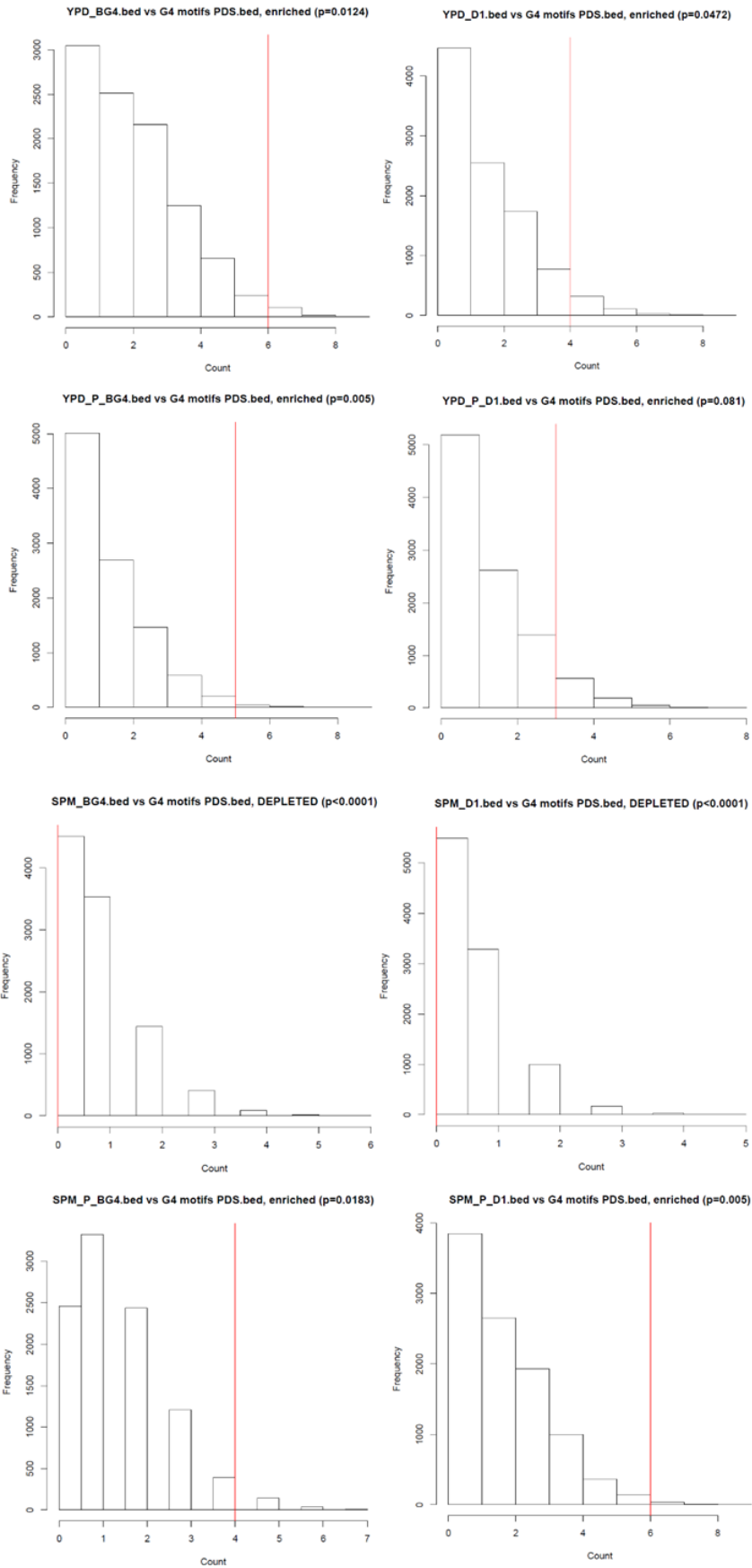
Appendix Figure 1: BG4/D1 ChIP-seq. a) sheared ChIP-seq samples. Majority of chromatin fragments between 100-200 bp. b) binding of BG4 to G4 motif. c) BG4 binding to mutated G4 motif.



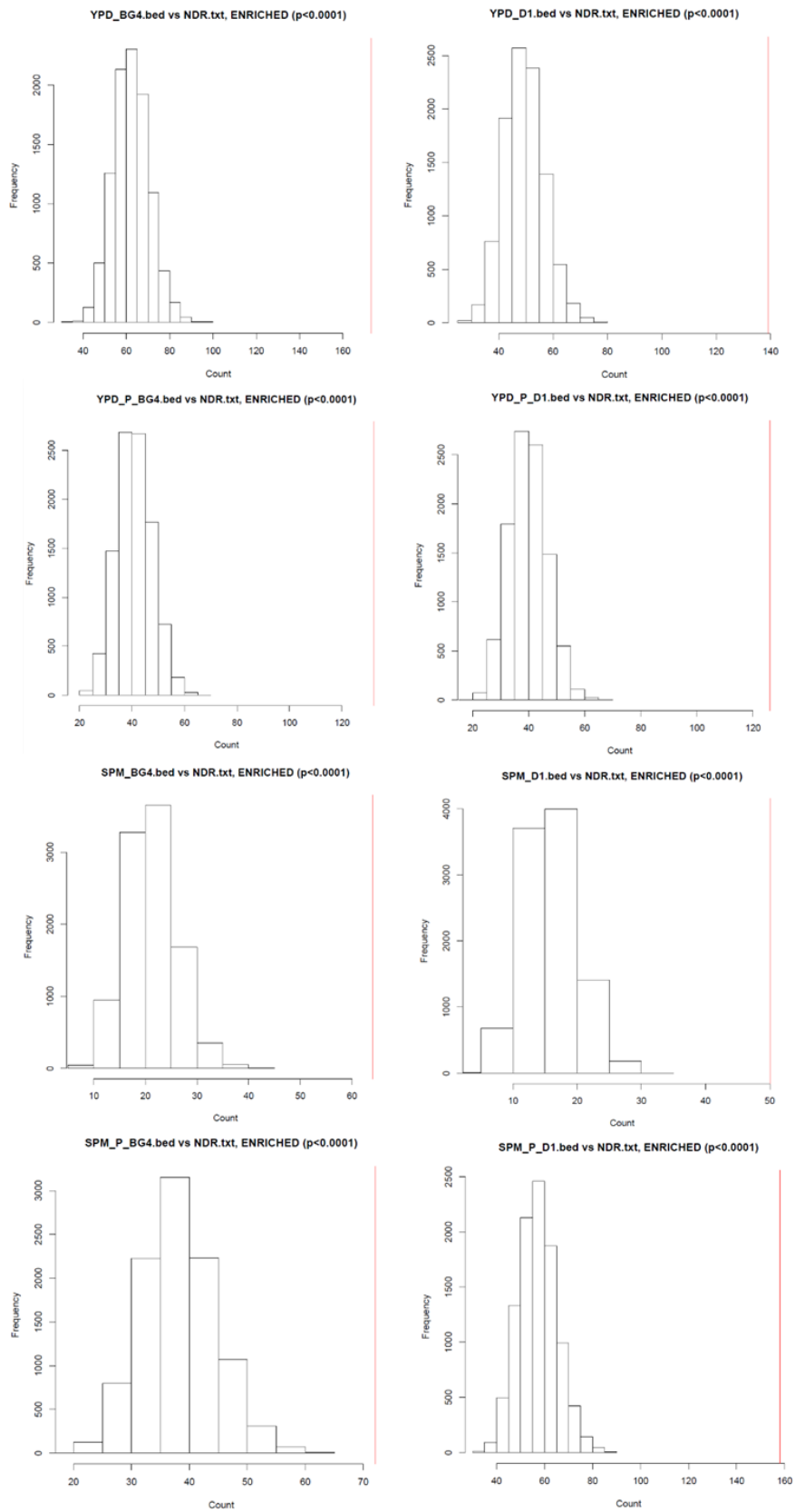
Appendix Figure 2: Overlap of BG4/D1 ChIP peaks with G4 motifs¹⁰. Vegetative cells (YPD), sporulating cells (SPM), Phen-DC₃ treated (P).



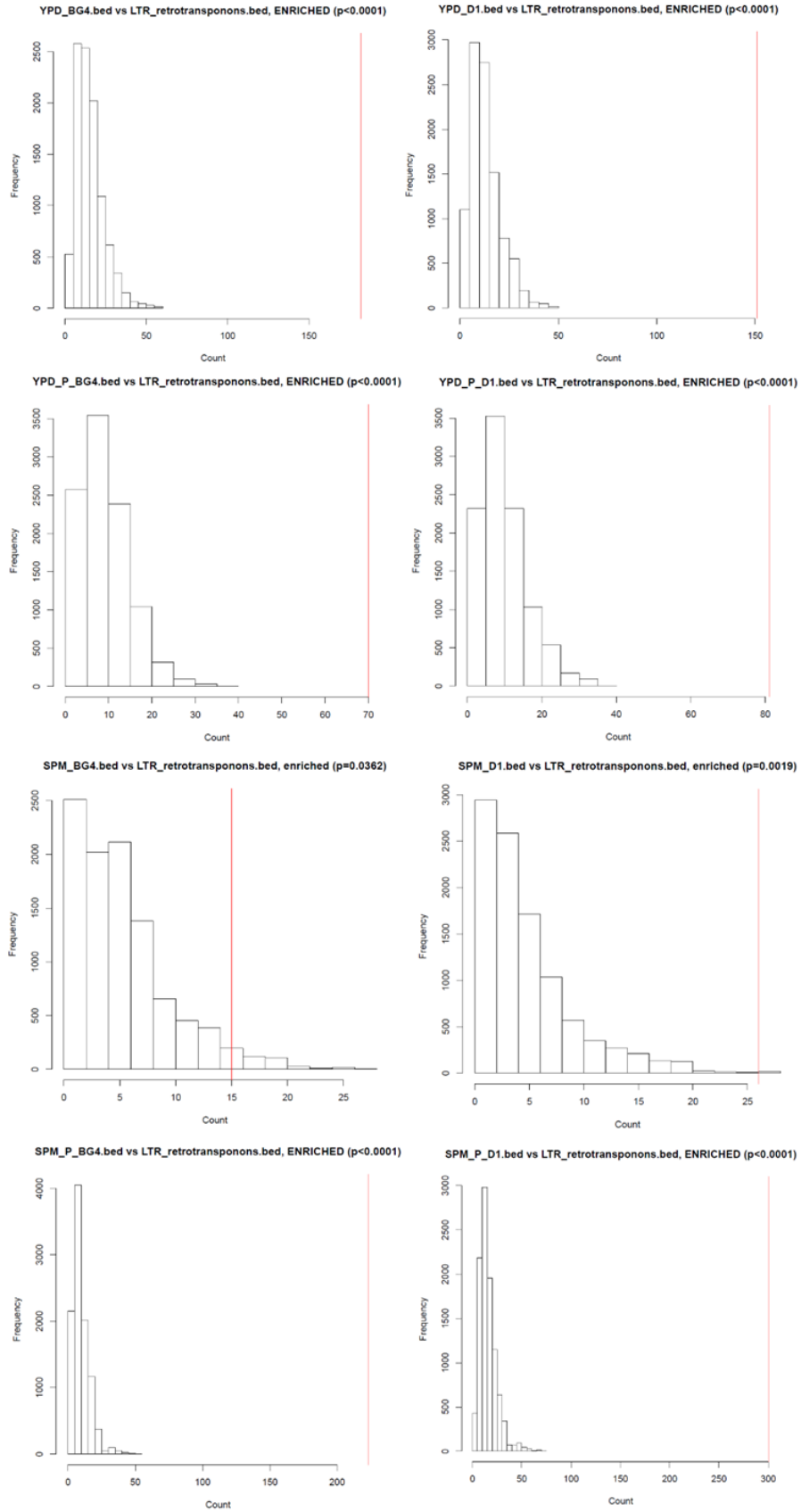
Appendix Figure 3: Overlap of BG4/D1 ChIP peaks with map from G4-sequencing²⁶⁵. Vegetative cells (YPD), sporulating cells (SPM), Phen-DC3 treated (P).



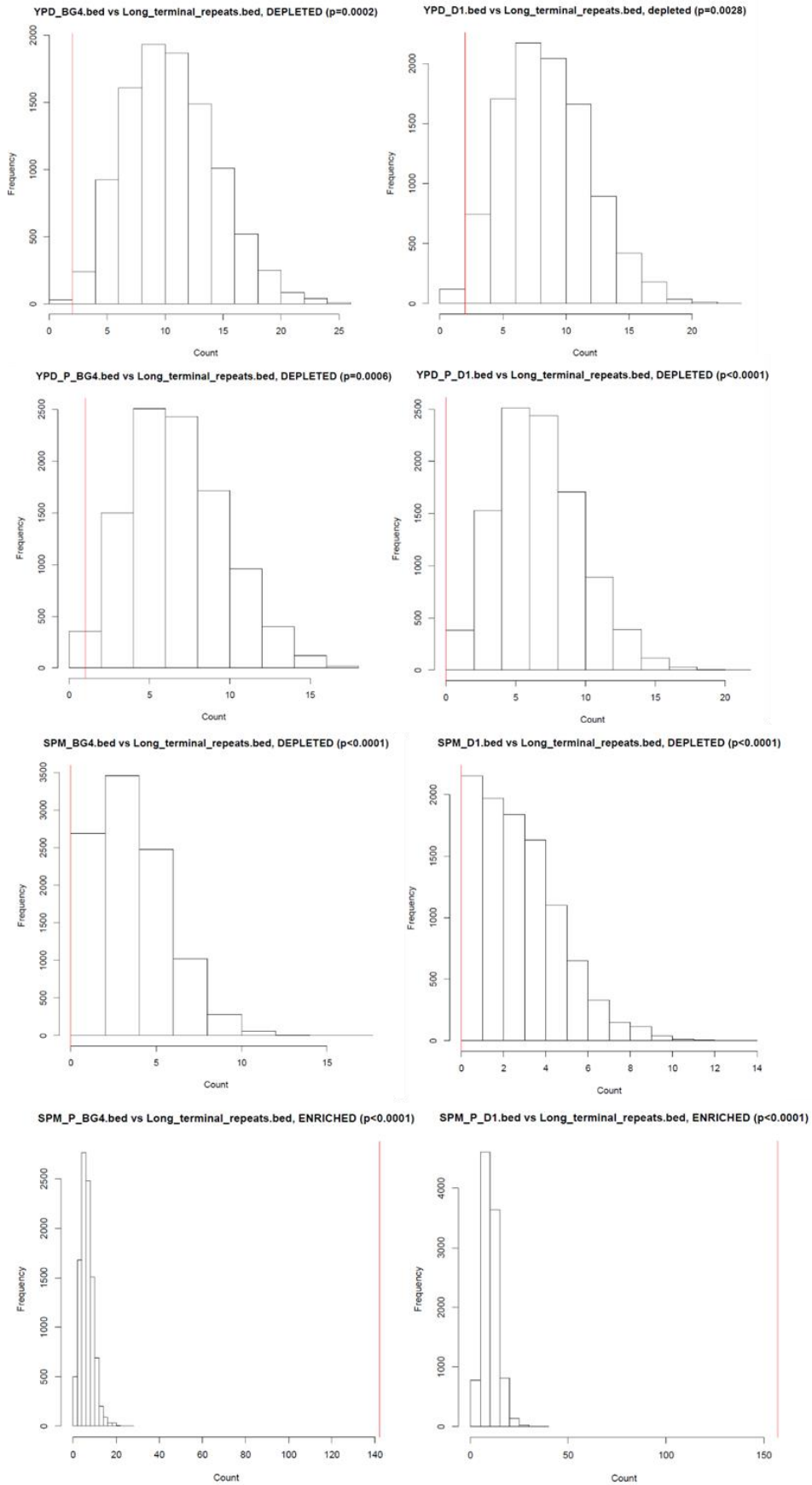
Appendix Figure 4: Overlap of BG4/D1 ChIP peaks with list from PDS treated G4-sequencing²⁶⁵. Vegetative cells (YPD), sporulating cells (SPM), Phen-DC3 treated (P).



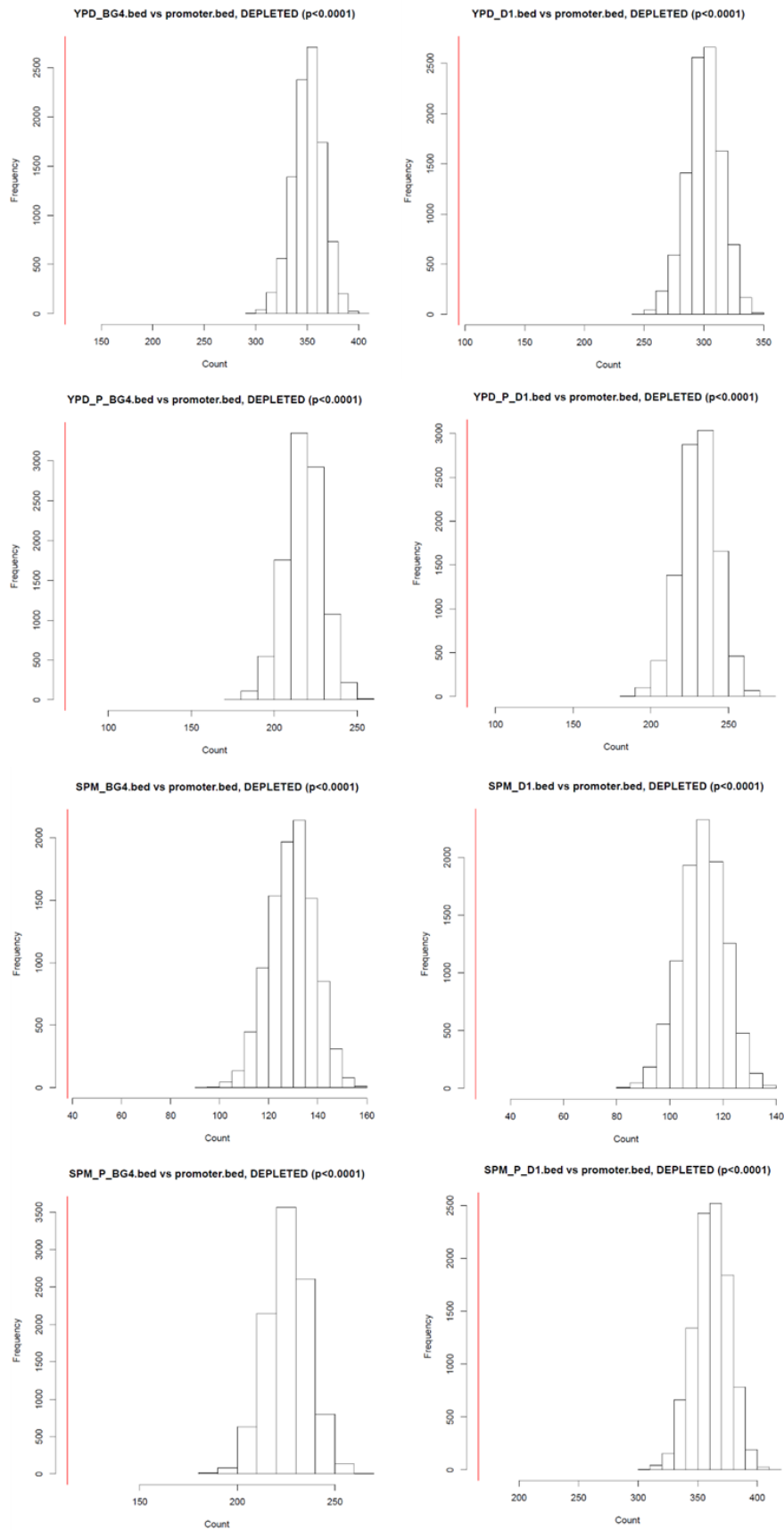
Appendix Figure 5: Overlap of BG4/D1 ChIP peaks with NDRs³⁴⁸. Vegetative cells (YPD), sporulating cells (SPM), Phn-DC3 treated (P).



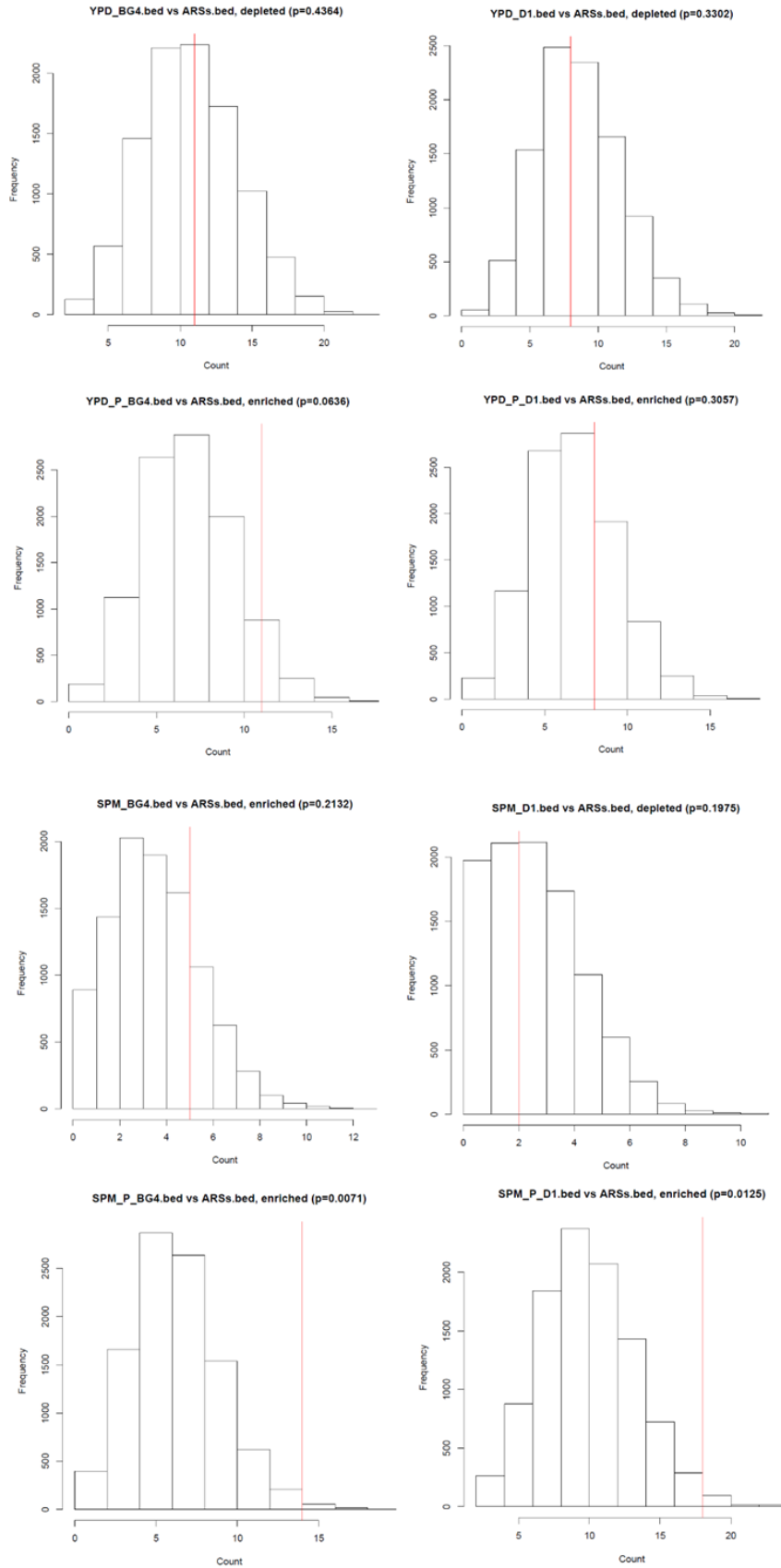
Appendix Figure 6: Overlap of BG4/D1 ChIP peaks with retrotransposons (on basis of genomic features at <https://www.yeastgenome.org>). Vegetative cells (YPD), sporulating cells (SPM), Phen-DC3 treated (P).



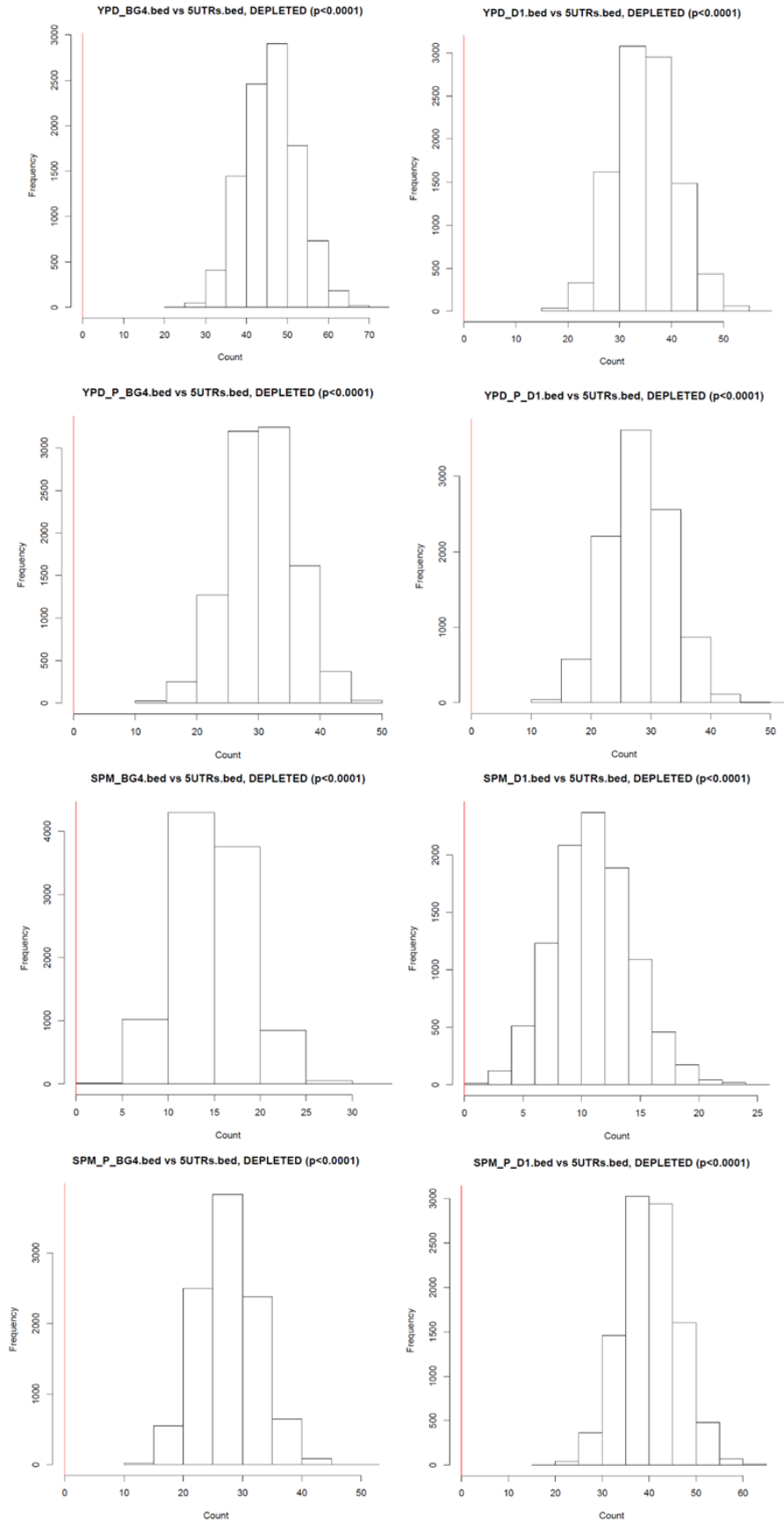
Appendix Figure 7: Overlap of BG4/D1 ChIP peaks with LTRs (on basis of genomic features at <https://www.yeastgenome.org>). Vegetative cells (YPD), sporulating cells (SPM), Phen-DC3 treated (P).



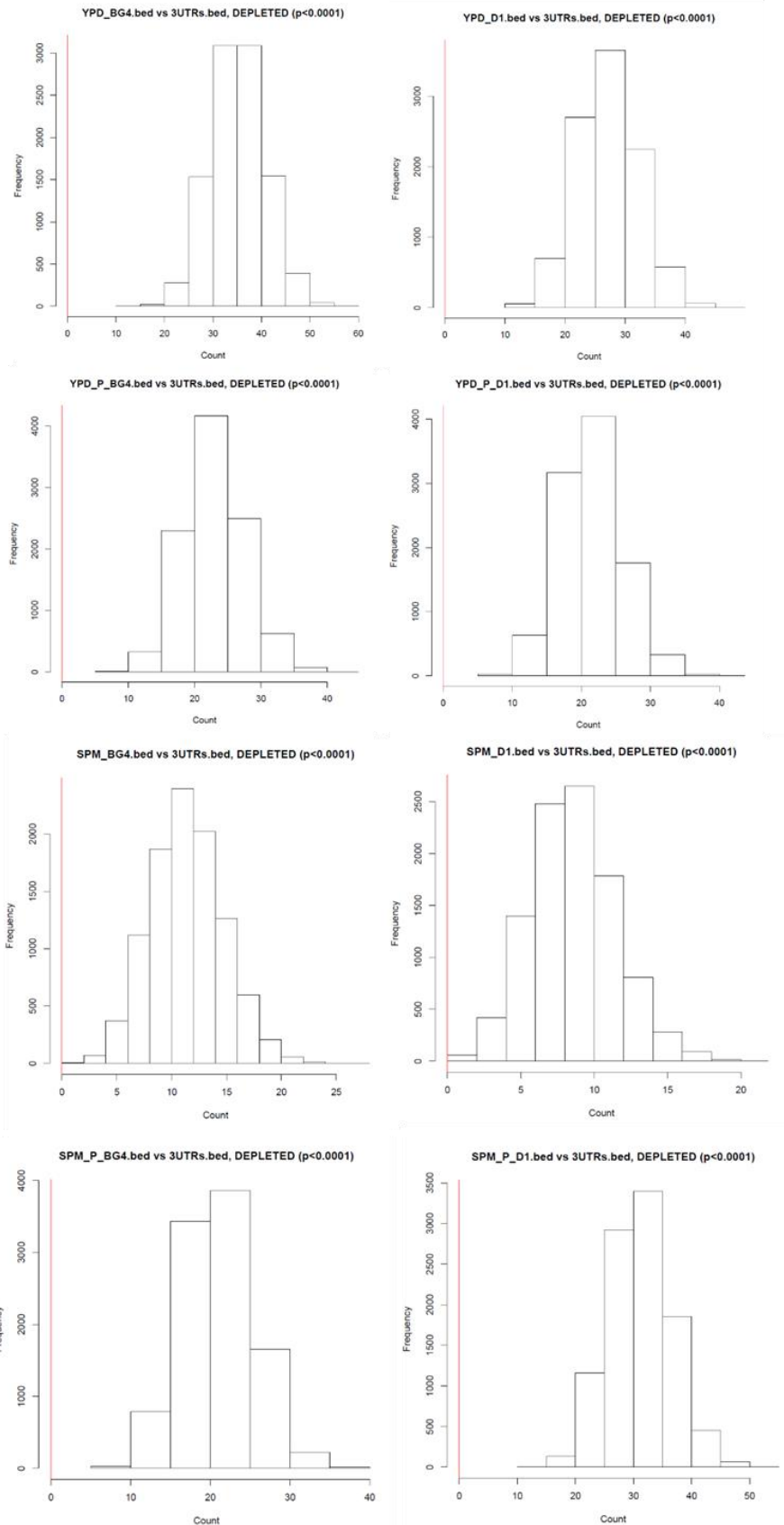
Appendix Figure 8: Overlap of BG4/D1 ChIP peaks with promoters¹⁰. Vegetative cells (YPD), sporulating cells (SPM), Phen-DC3 treated (P).



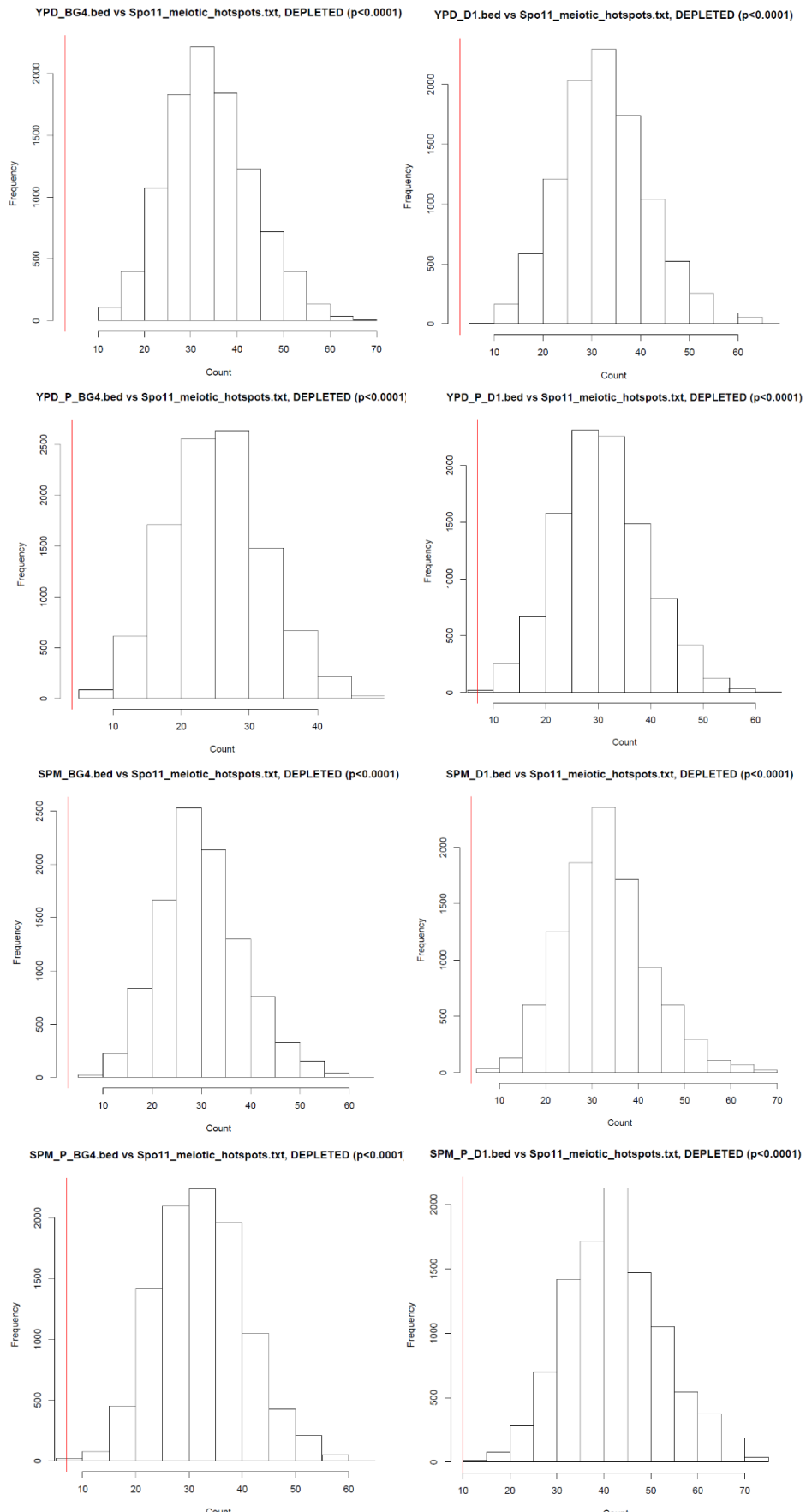
Appendix Figure 9: Overlap of BG4/D1 ChIP peaks with replication start sites (ARS) (on basis of genomic features at <https://www.yeastgenome.org>). Vegetative cells (YPD), sporulating cells (SPM), Phen-DC3 treated (P).



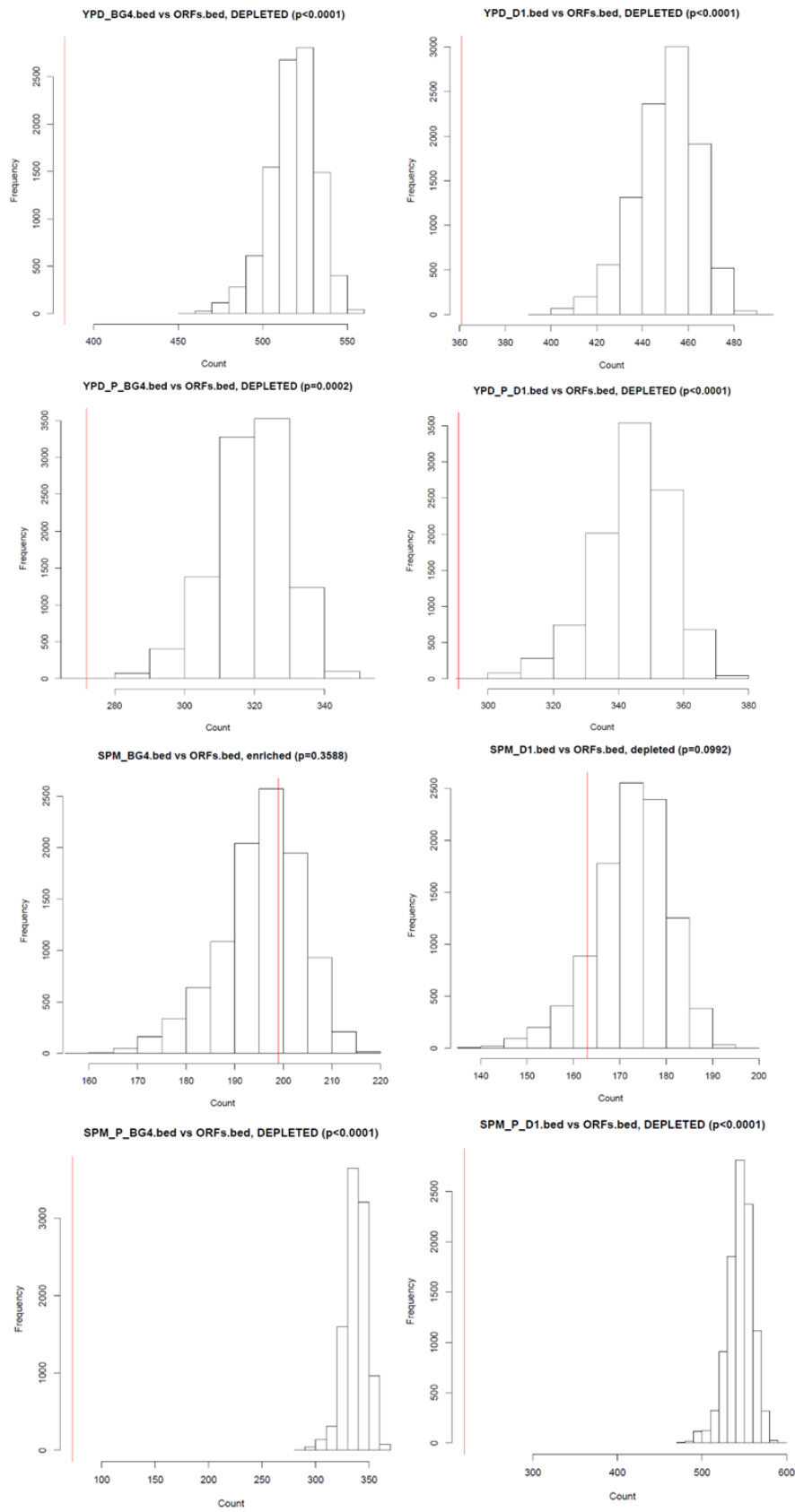
Appendix Figure 10: Overlap of BG4/D1 ChIP peaks with 5' UTRs (on basis of genomic features at <https://www.yeastgenome.org>). Vegetative cells (YPD), sporulating cells (SPM), Phen-DC₃ treated (P).



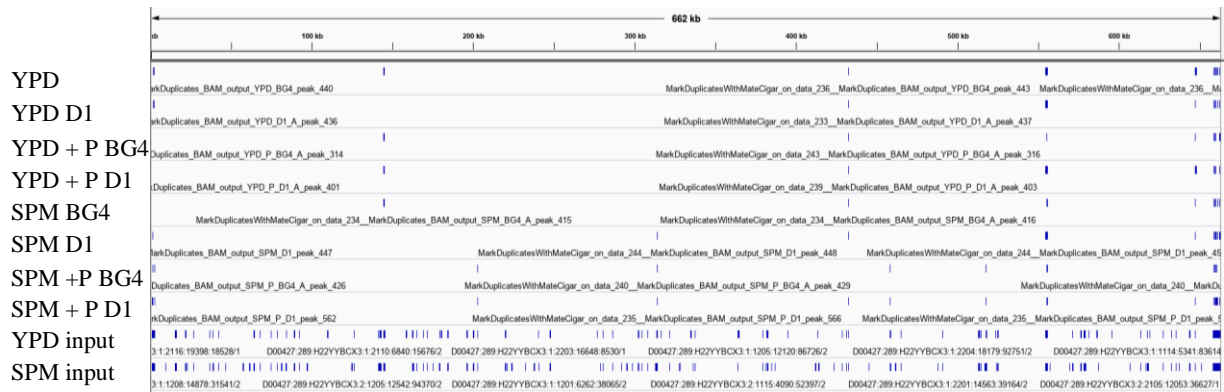
Appendix Figure 11: Overlap of BG4/D1 ChIP peaks with 3' UTRs (on basis of genomic features at <https://www.yeastgenome.org>). Vegetative cells (YPD), sporulating cells (SPM), Phen-DC₃ treated (P).



Appendix Figure 12: Overlap of BG4/D1 ChIP peaks with meiotic DSB hot spots³⁴⁹. Vegetative cells (YPD), sporulating cells (SPM), Phen-DC3 treated (P).



Appendix Figure 13: Overlap of BG4/D1 ChIP peaks with ORFs (on basis of genomic features at <https://www.yeastgenome.org>). Vegetative cells (YPD), sporulating cells (SPM), Phen-DC3 treated (P).



Appendix Figure 14: Genome browser screenshot of chromosome XI. Showing G4 ChIP peaks for BG4 and D1 of vegetative cells (YPD) and sporulating cells (SPM) with (+P) and without Phen-DC₃ treatment and input for vegetative cells (YPD) and sporulating cells (SPM).

Appearance in samples	Secondary-identifier	Symbol	Class	Organism short Name	Name
1	YLR430W	SEN1	ORF	S. cerevisiae	Splicing ENdonuclease
1	YDR172W	SUP35	ORF	S. cerevisiae	SUPpressor
1	YOR295W	UAF30	ORF	S. cerevisiae	Upstream Activation Factor subunit
1	YDR158W	HOM2	ORF	S. cerevisiae	HOMoserine requiring
1	YBR079C	RPG1	ORF	S. cerevisiae	
1	YHR119W	SET1	ORF	S. cerevisiae	SET domain-containing
1	YML009C	MRPL39	ORF	S. cerevisiae	Mitochondrial Ribosomal Protein, Large subunit
1	YGL036W		ORF	S. cerevisiae	
1	YKR046C	PLN1	ORF	S. cerevisiae	PeriLipiN
1	YMR049C	ERB1	ORF	S. cerevisiae	Eukaryotic Ribosome Biogenesis
1	YPR115W	RGC1	ORF	S. cerevisiae	Regulator of the Glycerol Channel
1	YDR507C	GIN4	ORF	S. cerevisiae	Growth Inhibitory
1	YMR064W	AEP1	ORF	S. cerevisiae	ATPase ExPression
1	YCL055W	KAR4	ORF	S. cerevisiae	KARyogamy
1	YBR103W	SIF2	ORF	S. cerevisiae	Sir4p-Interacting Factor
1	YGL148W	ARO2	ORF	S. cerevisiae	AROMatic amino acid requiring
1	YDR285W	ZIP1	ORF	S. cerevisiae	molecular ZIPper
1	YLR260W	LCB5	ORF	S. cerevisiae	Long-Chain Base
1	YDR513W	GRX2	ORF	S. cerevisiae	GlutaRedoXin
1	YFL045C	SEC53	ORF	S. cerevisiae	SECretory
1	YPR181C	SEC23	ORF	S. cerevisiae	SECretory
1	YML075C	HMG1	ORF	S. cerevisiae	3-Hydroxy-3-MethylGlutaryl-coenzyme a reductase
1	YJR016C	ILV3	ORF	S. cerevisiae	IsoLeucine-plus-Valine requiring
1	YOR234C	RPL33B	ORF	S. cerevisiae	Ribosomal Protein of the Large subunit

1	YMR110C	HFD1	ORF	S. cerevisiae	Homolog of Fatty aldehyde Dehydrogenase
1	YOR254C	SEC63	ORF	S. cerevisiae	SECretory
1	YDR091C	RLI1	ORF	S. cerevisiae	RNase L Inhibitor
1	YLR418C	CDC73	ORF	S. cerevisiae	Cell Division Cycle
1	YDR032C	PST2	ORF	S. cerevisiae	Protoplasts-SecreTed
1	YOR077W	RTS2	ORF	S. cerevisiae	
1	R0040C	REP2	ORF	S. cerevisiae	REPllication
1	YKR085C	MRPL20	ORF	S. cerevisiae	Mitochondrial Ribosomal Protein, Large subunit
1	YLR388W	RPS29A	ORF	S. cerevisiae	Ribosomal Protein of the Small subunit
1	YNL071W	LAT1	ORF	S. cerevisiae	
1	YBR218C	PYC2	ORF	S. cerevisiae	PYruvate Carboxylase
1	YOR020C	HSP10	ORF	S. cerevisiae	Heat Shock Protein
1	YLR372W	ELO3	ORF	S. cerevisiae	fatty acid ELongation
1	YMR256C	COX7	ORF	S. cerevisiae	Cytochrome c OXidase
1	YOR093C	CMR2	ORF	S. cerevisiae	Changed Mutation Rate
1	YGL006W	PMC1	ORF	S. cerevisiae	Plasma Membrane Calcium
1	YFR051C	RET2	ORF	S. cerevisiae	RETRetrieval from ER
1	YFL004W	VTC2	ORF	S. cerevisiae	Vacuolar Transporter Chaperone
1	YIL095W	PRK1	ORF	S. cerevisiae	p53 Regulatory Kinase
1	YGL001C	ERG26	ORF	S. cerevisiae	ERGosterol biosynthesis
1	YPR016C	TIF6	ORF	S. cerevisiae	Translation Initiation Factor
1	YNL027W	CRZ1	ORF	S. cerevisiae	Calcineurin-Responsive Zinc finger
1	YPL063W	TIM50	ORF	S. cerevisiae	Translocase of the Inner Mitochondrial membrane
1	YMR268C	PRP24	ORF	S. cerevisiae	Pre-mRNA Processing
1	YDL132W	CDC53	ORF	S. cerevisiae	Cell Division Cycle
1	YLL046C	RNP1	ORF	S. cerevisiae	RiboNucleoProtein
1	YMR270C	RRN9	ORF	S. cerevisiae	Regulation of RNA polymerase I

1	YPL215W	CBP3	ORF	S. cerevisiae	Cytochrome B mRNA Processing
1	YOR272W	YTM1	ORF	S. cerevisiae	
1	YMR183C	SSO2	ORF	S. cerevisiae	Supressor of Sec One
1	YFL037W	TUB2	ORF	S. cerevisiae	TUBulin
1	YHL024W	RIM4	ORF	S. cerevisiae	Regulator of IME2
1	YER122C	GLO3	ORF	S. cerevisiae	GLyOxalase
1	YMR231W	PEP5	ORF	S. cerevisiae	carboxyPEPTidase Y-deficient
1	YOL077W-A	ATP19	ORF	S. cerevisiae	ATP synthase
1	YGL110C	CUE3	ORF	S. cerevisiae	Coupling of Ubiquitin conjugation to ER degradation
1	YNL196C	SLZ1	ORF	S. cerevisiae	
1	YPL111W	CAR1	ORF	S. cerevisiae	Catabolism of ARGinine
1	YLL026W	HSP104	ORF	S. cerevisiae	Heat Shock Protein
1	YFR024C-A	LSB3	ORF	S. cerevisiae	Las Seventeen Binding protein
1	YGL216W	KIP3	ORF	S. cerevisiae	KInesin related Protein
1	YKR083C	DAD2	ORF	S. cerevisiae	Duo1 And Dam1 interacting
1	YHR158C	KEL1	ORF	S. cerevisiae	KELch repeat
1	YHR007C	ERG11	ORF	S. cerevisiae	ERGosterol biosynthesis
1	YIL010W	DOT5	ORF	S. cerevisiae	Disruptor Of Telomeric silencing
1	YNL138W	SRV2	ORF	S. cerevisiae	Suppressor of RasVal19
1	YMR307W	GAS1	ORF	S. cerevisiae	Glycophospholipid-Anchored Surface protein
1	YGL200C	EMP24	ORF	S. cerevisiae	EndoMembrane Protein
1	YOR201C	MRM1	ORF	S. cerevisiae	Mitochondrial rRNA Methyltransferase
1	YDL215C	GDH2	ORF	S. cerevisiae	Glutamate DeHydrogenase
1	YOR206W	NOC2	ORF	S. cerevisiae	NucleOlar Complex associated
1	YMR099C		ORF	S. cerevisiae	
1	YLR116W	MSL5	ORF	S. cerevisiae	Mud Synthetic-Lethal
1	YKL092C	BUD2	ORF	S. cerevisiae	BUD site selection

1	YNL022C	RCM1	ORF	S. cerevisiae	
1	YDL066W	IDP1	ORF	S. cerevisiae	Isocitrate Dehydrogenase, NADP-specific
1	YDR178W	SDH4	ORF	S. cerevisiae	Succinate DeHydrogenase
1	YNR010W	CSE2	ORF	S. cerevisiae	Chromosome SEgregation
1	YML030W	RCF1	ORF	S. cerevisiae	Respiratory superComplex Factor
1	YFR032C-A	RPL29	ORF	S. cerevisiae	Ribosomal Protein of the Large subunit
1	YDL005C	MED2	ORF	S. cerevisiae	MEDIator complex
1	YBR208C	DUR1,2	ORF	S. cerevisiae	Degradation of URea
1	YHR082C	KSP1	ORF	S. cerevisiae	Kinase Suppressing Prp20-10
1	YPR163C	TIF3	ORF	S. cerevisiae	Translation Initiation Factor
1	YIL043C	CBR1	ORF	S. cerevisiae	Cytochrome b Reductase
1	YPR091C	NVJ2	ORF	S. cerevisiae	Nucleus-Vacuole Junction
1	YDL085W	NDE2	ORF	S. cerevisiae	NADH Dehydrogenase, External
1	YDR452W	PPN1	ORF	S. cerevisiae	
1	YHR052W	CIC1	ORF	S. cerevisiae	Core Interacting Component
1	YDR322W	MRPL35	ORF	S. cerevisiae	Mitochondrial Ribosomal Protein, Large subunit
1	YNL096C	RPS7B	ORF	S. cerevisiae	Ribosomal Protein of the Small subunit
1	YLR406C	RPL31B	ORF	S. cerevisiae	Ribosomal Protein of the Large subunit
1	YML061C	PIF1	ORF	S. cerevisiae	Petite Integration Frequency
1	YPL180W	TCO89	ORF	S. cerevisiae	Tor Complex One
1	YBR149W	ARA1	ORF	S. cerevisiae	D-ARAbinose dehydrogenase
1	YNL115C		ORF	S. cerevisiae	
1	YLR096W	KIN2	ORF	S. cerevisiae	KINase
1	YJL010C	NOP9	ORF	S. cerevisiae	NucleOlar Protein
1	YNL064C	YDJ1	ORF	S. cerevisiae	Yeast dnaJ
1	YOR322C	LDB19	ORF	S. cerevisiae	Low Dye Binding

1	YLR071C	RGR1	ORF	S. cerevisiae	Resistant to Glucose Repression
1	YLR051C	FCF2	ORF	S. cerevisiae	Faf1p Copurifying Factor
1	YCR010C	ADY2	ORF	S. cerevisiae	Accumulation of DYads
1	YML048W	GSF2	ORF	S. cerevisiae	Glucose Signaling Factor
1	YHR199C-A	NBL1	ORF	S. cerevisiae	N-terminal-Borealin Like protein
1	YJR092W	BUD4	ORF	S. cerevisiae	BUD site selection
1	YOR069W	VPS5	ORF	S. cerevisiae	Vacuolar Protein Sorting
1	YNL271C	BNI1	ORF	S. cerevisiae	Bud Neck Involved
1	YPL024W	RMI1	ORF	S. cerevisiae	RecQ Mediated genome Instability
1	YPL237W	SUI3	ORF	S. cerevisiae	SUPpressor of Initiator codon
1	YBL038W	MRPL16	ORF	S. cerevisiae	Mitochondrial Ribosomal Protein, Large subunit
1	YMR189W	GCV2	ORF	S. cerevisiae	GlyCine cleaVage
1	Q0160	SCEI	ORF	S. cerevisiae	
1	YNL121C	TOM70	ORF	S. cerevisiae	Translocase of the Outer Mitochondrial membrane
1	YKL210W	UBA1	ORF	S. cerevisiae	UBiquitin Activating
1	YDL084W	SUB2	ORF	S. cerevisiae	SUPpressor of Brr1-1
1	YKL074C	MUD2	ORF	S. cerevisiae	Mutant U1 Die
1	YJL012C	VTC4	ORF	S. cerevisiae	Vacuolar Transporter Chaperone
1	YKL067W	YNK1	ORF	S. cerevisiae	Yeast Nucleoside diphosphate Kinase
1	YBR059C	AKL1	ORF	S. cerevisiae	Ark family Kinase-Like protein
1	YFL021W	GAT1	ORF	S. cerevisiae	
1	YLR371W	ROM2	ORF	S. cerevisiae	RhO1 Multicopy suppressor
1	YOL135C	MED7	ORF	S. cerevisiae	MEDIator complex
1	YPL240C	HSP82	ORF	S. cerevisiae	Heat Shock Protein
1	YPL271W	ATP15	ORF	S. cerevisiae	ATP synthase
2	YKL035W	UGP1	ORF	S. cerevisiae	UDP-glucose pyrophosphorylase
2	YLL011W	SOF1	ORF	S. cerevisiae	Suppressor Of Fibrillarlin

2	YDL067C	COX9	ORF	S. cerevisiae	Cytochrome c OXidase
2	YJL052W	TDH1	ORF	S. cerevisiae	Triose-phosphate DeHydrogenase
2	YLL027W	ISA1	ORF	S. cerevisiae	Iron Sulfur Assembly
2	YER082C	UTP7	ORF	S. cerevisiae	U Three Protein
2	YPR183W	DPM1	ORF	S. cerevisiae	Dolichol Phosphate Mannose synthase
2	YLR208W	SEC13	ORF	S. cerevisiae	SECretory
2	YBR057C	MUM2	ORF	S. cerevisiae	MUddled Meiosis
2	YHL007C	STE20	ORF	S. cerevisiae	STERile
2	YPL070W	MUK1	ORF	S. cerevisiae	coMpUtationally-linked to Kap95
2	YGR148C	RPL24B	ORF	S. cerevisiae	Ribosomal Protein of the Large subunit
2	YNL330C	RPD3	ORF	S. cerevisiae	Reduced Potassium Dependency
2	YOR174W	MED4	ORF	S. cerevisiae	MEDIator complex
2	YML117W	NAB6	ORF	S. cerevisiae	Nucleic Acid Binding protein
2	YDR148C	KGD2	ORF	S. cerevisiae	alpha-KetoGlutarate Dehydrogenase
2	YGL137W	SEC27	ORF	S. cerevisiae	SECretory
2	YDL087C	LUC7	ORF	S. cerevisiae	Lethal Unless Cap-binding complex is produced
2	YPL217C	BMS1	ORF	S. cerevisiae	BMh Sensitive
2	YHR086W	NAM8	ORF	S. cerevisiae	Nuclear Accommodation of Mitochondria
2	YJL005W	CYR1	ORF	S. cerevisiae	CYclic AMP Requirement
2	YDR138W	HPR1	ORF	S. cerevisiae	HyPerRecombination
2	YBL007C	SLA1	ORF	S. cerevisiae	Synthetic Lethal with ABP1
2	YER080W	AIM9	ORF	S. cerevisiae	Altered Inheritance rate of Mitochondria
2	YFL016C	MDJ1	ORF	S. cerevisiae	Mitochondrial DnaJ
2	YER148W	SPT15	ORF	S. cerevisiae	SuPpressor of Ty insertions
2	YER161C	SPT2	ORF	S. cerevisiae	SuPpressor of Ty's
2	YGL025C	PGD1	ORF	S. cerevisiae	PolyGlutamine Domain

2	YHL023C	NPR3	ORF	S. cerevisiae	Nitrogen Permease Regulator
2	YPL093W	NOG1	ORF	S. cerevisiae	Nucleolar G-protein
2	YIL036W	CST6	ORF	S. cerevisiae	Chromosome STability
2	YLR226W	BUR2	ORF	S. cerevisiae	Bypass UAS Requirement
2	YIL129C	TAO3	ORF	S. cerevisiae	Transcriptional Activator of OCH1
2	YHR072W-A	NOP10	ORF	S. cerevisiae	Nucleolar Protein
2	YBR029C	CDS1	ORF	S. cerevisiae	CDP-Diacylglycerol Synthase
2	YHR012W	VPS29	ORF	S. cerevisiae	Vacuolar Protein Sorting
2	YOL051W	GAL11	ORF	S. cerevisiae	GALactose metabolism
2	YKL065C	YET1	ORF	S. cerevisiae	Yeast Endoplasmic reticulum Transmembrane protein
2	YER125W	RSP5	ORF	S. cerevisiae	Reverses Spt- Phenotype
2	YHR041C	SRB2	ORF	S. cerevisiae	Suppressor of RNA polymerase B
2	YLR298C	YHC1	ORF	S. cerevisiae	Yeast Homolog of human U1C
2	YBR086C	IST2	ORF	S. cerevisiae	Increased Sodium Tolerance
2	YDR201W	SPC19	ORF	S. cerevisiae	Spindle Pole Component
2	YJL173C	RFA3	ORF	S. cerevisiae	Replication Factor A
2	YNL252C	MRPL17	ORF	S. cerevisiae	Mitochondrial Ribosomal Protein, Large subunit
2	YGL120C	PRP43	ORF	S. cerevisiae	Pre-mRNA Processing
2	YDL175C	AIR2	ORF	S. cerevisiae	Arginine methyltransferase-Interacting RING finger protein
2	YLR396C	VPS33	ORF	S. cerevisiae	Vacuolar Protein Sorting
2	YNL177C	MRPL22	ORF	S. cerevisiae	Mitochondrial Ribosomal Protein, Large subunit
2	YBR143C	SUP45	ORF	S. cerevisiae	SUPpressor
2	YML112W	CTK3	ORF	S. cerevisiae	Carboxy-Terminal domain Kinase
2	YBL104C	SEA4	ORF	S. cerevisiae	SEh1-Associated
2	YIL112W	HOS4	ORF	S. cerevisiae	Hda One Similar
2	YDR164C	SEC1	ORF	S. cerevisiae	SECretory

2	YOL115W	PAP2	ORF	S. cerevisiae	Poly(A) Polymerase
2	YMR176W	ECM5	ORF	S. cerevisiae	ExtraCellular Mutant
2	YKR029C	SET3	ORF	S. cerevisiae	SET domain-containing
2	YMR287C	DSS1	ORF	S. cerevisiae	Deletion of SUV3 Suppressor
2	YOR100C	CRC1	ORF	S. cerevisiae	CaRnitine Carrier
2	YDR239C		ORF	S. cerevisiae	
2	YGL078C	DBP3	ORF	S. cerevisiae	Dead Box Protein
2	YOL006C	TOP1	ORF	S. cerevisiae	TOPoisomerase
2	YBR123C	TFC1	ORF	S. cerevisiae	Transcription Factor class C
3	YKL129C	MYO3	ORF	S. cerevisiae	MYOsin
3	YER126C	NSA2	ORF	S. cerevisiae	Nop Seven Associated
3	YBR071W		ORF	S. cerevisiae	
3	YNL087W	TCB2	ORF	S. cerevisiae	Three Calcium and lipid Binding domains (TriCalBins)
3	YLR196W	PWP1	ORF	S. cerevisiae	Periodic tryptophan (W) Protein
3	YOR267C	HRK1	ORF	S. cerevisiae	Hygromycin Resistance Kinase
3	YPR112C	MRD1	ORF	S. cerevisiae	Multiple RNA-binding domain
3	YDR233C	RTN1	ORF	S. cerevisiae	ReTiculoN-like
3	YCR030C	SYP1	ORF	S. cerevisiae	Suppressor of Yeast Profilin deletion
3	YNL061W	NOP2	ORF	S. cerevisiae	NucleOlar Protein
3	YPL134C	ODC1	ORF	S. cerevisiae	OxoDicarboxylate Carrier
3	YJL076W	NET1	ORF	S. cerevisiae	Nucleolar silencing Establishing factor and Telophase regulator
3	YDL074C	BRE1	ORF	S. cerevisiae	BREfeldin A sensitivity
3	YDR240C	SNU56	ORF	S. cerevisiae	Small NUClear ribonucleoprotein associated
3	YPL119C	DBP1	ORF	S. cerevisiae	Dead Box Protein
3	YIL154C	IMP2'	ORF	S. cerevisiae	Independent of Mitochondrial Particle
3	YIL061C	SNP1	ORF	S. cerevisiae	

3	YPR104C	FHL1	ORF	S. cerevisiae	Fork Head-Like
3	YCR033W	SNT1	ORF	S. cerevisiae	SaNT domains
3	YDR436W	PPZ2	ORF	S. cerevisiae	Protein Phosphatase Z
3	YJL131C	AIM23	ORF	S. cerevisiae	Altered Inheritance rate of Mitochondria
3	YDL208W	NHP2	ORF	S. cerevisiae	Non-Histone Protein
3	YOL123W	HRP1	ORF	S. cerevisiae	Heterogenous nuclear RibonucleoProtein
3	YKL139W	CTK1	ORF	S. cerevisiae	Carboxy-Terminal domain Kinase
3	YNL047C	SLM2	ORF	S. cerevisiae	Synthetic Lethal with Mss4
3	YIR001C	SGN1	ORF	S. cerevisiae	Slower Growth on Non-fermentable carbon sources
3	YCL011C	GBP2	ORF	S. cerevisiae	G-strand Binding Protein
3	YGR013W	SNU71	ORF	S. cerevisiae	Small NUClear ribonucleoprotein associated
3	YGR231C	PHB2	ORF	S. cerevisiae	ProHiBitin
3	YGL131C	SNT2	ORF	S. cerevisiae	
3	YHR120W	MSH1	ORF	S. cerevisiae	MutS Homolog
3	YGR074W	SMD1	ORF	S. cerevisiae	snRNA Sm binding site protein D1
3	YMR098C	ATP25	ORF	S. cerevisiae	ATPase
3	YMR212C	EFR3	ORF	S. cerevisiae	PHO Eighty Five Requiring
4	YDR190C	RVB1	ORF	S. cerevisiae	RuVB-like
4	YGL013C	PDR1	ORF	S. cerevisiae	Pleiotropic Drug Resistance
4	YKL012W	PRP40	ORF	S. cerevisiae	Pre-mRNA Processing
4	YHL034C	SBP1	ORF	S. cerevisiae	
4	YER029C	SMB1	ORF	S. cerevisiae	SmB/B' homolog
4	YML010W	SPT5	ORF	S. cerevisiae	SuPpressor of Ty's
4	YDR389W	SAC7	ORF	S. cerevisiae	Suppressor of ACTin
4	YPL235W	RVB2	ORF	S. cerevisiae	RuVB-like
4	YHR089C	GAR1	ORF	S. cerevisiae	Glycine Arginine Rich
4	YGR237C		ORF	S. cerevisiae	

4	YJR019C	TES1	ORF	S. cerevisiae	ThioEsterase
4	YLL029W	FRA1	ORF	S. cerevisiae	Fe Repressor of Activation
4	YDR374C	PHO92	ORF	S. cerevisiae	PHOspate metabolism
4	YNL312W	RFA2	ORF	S. cerevisiae	Replication Factor A
4	YMR037C	MSN2	ORF	S. cerevisiae	Multicopy suppressor of SNF1 mutation
4	YNL218W	MGS1	ORF	S. cerevisiae	Maintenance of Genome Stability
4	YKR072C	SIS2	ORF	S. cerevisiae	Slit4 Suppressor
4	YGL049C	TIF4632	ORF	S. cerevisiae	Translation Initiation Factor

Appendix Table 1: Identified G4 binder. From lysate 3 and 7 hours after inducing sporulation. Analysis was performed in duplicates. Appearance in samples 4 means that the protein was present in all four samples without binding to mutated G4 motif.

Only in SPM	Only in Phen-DC ₃
FDH1	CAN
RIM4	RPA49
HIS8	TRP
ADY2	SYV
ARLY	RPAC1
DBP2	NPT1
VPS27	CEF1
DLD1	PFKA2
ARO9	YPT1
METE	SYFB
BCA1	SRP68
METC	MGLL
LEU1	IDH2
MTR4	TUP1
AGX1	FET5
CACP	FUMH
DHE5	DUG1
ARGJ	SSBP1
ARGI	MMF1
ARO8	ATPG
METK2	FHP
TRXB2	YEF3
DHOM	PYRC
PURA	RSSA2
KES1	SYYC
TBA1	HSP31
FIP1	PP2C3
PEX19	RL20A
GLYM	SNF7

CYSD	RIR4
PSA6	YP148
METK1	COPD
GET3	SFM1
C1TC	IGD1
MCFS2	PYRD
KAR	YHM2
RAS2	NET1
THIL	RM10
PDC1	ARGD
DLD2	XPO1
HSP78	SIC1
BLH1	RHO1
AMPL	AROF
GCST	PLR1
HMCS	NNRE
RT04	MPCP
F16P	RS11B
YM94	ADH2
RT23	SEC16
TPS1	TOM40
AIM17	APE3
EMI2	IDHP
HS104	RM24
RTS3	GBLP
PHB2	LGUL
IMDH3	VDAC1
DAK1	SYP1
SIS2	ATPA
ILV5	FAT2
SYLC	IDHC
DED1	COX1
RUVB1	NUP53
G6PI	AAKG
KYNU	NOP2
LEU9	RS13
ACT	ILV6
CDC42	TBB
AATC	ARG56
PDC5	SYFA
SUCB	HXKB
ACS1	ACAC
PWP1	NCPR
SYIC	HSP60
RL2B	SEC14
PYRE	GCY1
VATB	EIS1

RL11B	PMM
MIC60	SCP1
SYTC	RLA0
YPR1	RIR2
YAT2	VPS4
SUB2	SAM4
SUCA	YN8H
PUR6	HMX1
RL1B	RTN1
NUP42	ARA1
SYDM	ERG2
PMA1	CBS
GGA2	TAL1
CRP1	ENT2
NDI1	NOP3
EXG1	SOL2
SYRC	SDS22
GUAA	UAP1
GGA1	PSA3
YG3A	VA0D
HSP74	RNQ1
DPM1	CDC37
RL28	EF1B
SC160	CTR3
CHMU	ACBP
PUR91	PAN1
TCPB	IAH1
RS14A	
KC12	
RL15B	
FAS2	
KAPR	
QCR10	
HEM2	
NSP1	
PDX3	
ODPB	
SYSC	
RL8B	
MVD1	
CISY1	
EF3A	
MPI	
GDI1	
OM45	
PSP2	
VATH	

UBA1	
OLA1	
PP2C2	
BMH2	
BBC1	
ATG27	
TCPE	
ASPG1	
GPD1	
SEC23	
RPN1	
RL6B	
YNU8	
ODO2	
PPB	
RS22A	
CAJ1	
RM35	
INV2	
XKS1	
PSA7	
ARPC3	
RPN6	
AIM2	
YBD6	
UCRI	
PCNA	
CAPZB	
PABP	
RL24B	
FDFT	
RS4A	
RT35	
CYS3	
FKBP3	
CARP	
YLF2	
FPPS	
SERC	
COX5A	
YPT7	
RNA1	
SEG1	
RL23B	
HRP1	
RT28	
RL17A	

NUG1	
NAP1	
EAP1	
KTHY	
PMG1	
IXR1	
SAR1	
MDG1	
RS25B	
IDI1	
GCS1	
AIM3	
IMB1	
VTI1	
MSC6	
EDE1	
RL16A	
H4	
YKD3A	
MAP2	
RL16B	
MDM38	
FABD	
RM40	
GSF2	
HSP42	
YNB0	
NOP56	
ERF1	
YOP1	
RL9B	
RIB4	
RM37	
GAS3	
PAF1	
CYAA	
ZUO1	
RM04	
ODPX	
RCN2	
RS29A	
FMP46	
REP2	
YP199	
GRP78	
ATP19	
COFI	

RV161	
PAA1	
YP036	
SOL3	
YFI6	
RAD23	
EMP24	
YPT52	
APD1	
RL36A	
STB3	
RT07	
HRB1	
RS6B	
SIL1	
RT24	
RS15	
RM25	
CDC3	
CUE5	
NUP60	
IF1A	
YGP1	
YK03	
IF4E	
RL12A	
ISD11	
RM41	
MTC1	
STE50	
RS24A	
ETFB	
YLH47	
RT25	
BSP1	
YJF5	
LHP1	
MSP1	
SRO9	
ACA2	
SEC17	
RDL2	
HMF1	
UBC1	
COQ1	
ATP11	
RPN12	

SLF1	
KC11	
COQ7	
APT1	
HSP26	
IMB4	
PRM4	
MPM1	
YOR31	
KAD3	
RM16	
RL25	
ENG2	
CYT2	
CCS1	
UTH1	
TIM23	
RL4P	
RPN5	
TRX2	
YMH9	
HAA1	
UBC13	
PIN3	
JSN1	
CYC1	
TOM20	
RM49	
MMS2	
LSM5	
CYB5	
TOM22	
FSH2	
RPN10	
NACA	
KCC1	
LSB3	
UBC4	
FMC1	
YL179	
MDY2	
LSB1	
CANB	
PST1	
NU100	
SODC	
TRX3	

GPP2	
RIM1	
LSM6	
NTF2	
YL257	
CAF20	
SUB1	
TOM7	
RS28A	
GCSH	
MIC19	
YNT5	
RT10	
RGI1	
SDS23	
TPM1	
RLA3	
RM19	
TRX1	
YP010	
LCL2	
RRF1	
GLRX8	
SKP1	
RS21A	
DAP1	
VATF	
SLA1	
RT19	
RLA1	
YAP3	
ITPA	
CTR1	
RM50	
RRS1	
FKBP2	
YM8V	
TIM13	
RPAC2	

Appendix Table 2: Proteome analytical identified proteins, which were only present in sporulating cells (SPM) or cells treated with 5 μ M Phen-DC₃ (Phen-DC₃).

SPM \geq 2-fold increase	SPM \geq 2-fold decrease	Phhen-DC ₃ \geq 2-fold increase	Phhen-DC ₃ \geq 2-fold decrease
FDH1	ARC1	YHM2	RL20A
RIM4	RL9B	NET1	RIB3
HIS8	RIB4	RM10	ATP5E
ADY2	RM37	DHAS	PSD10

CISY3	GAS3	CAN	ADPP
ARLY	PHSG	ARGD	SDS22
INO1	PUR7	INO1	RT51
LYS1	RS26B	CISY3	RS10A
DBP2	PAF1	PHB1	ATPJ
THIK	PLB1	RPA49	FKBP
VPS27	CYAA	ILV3	CKS1
PRPD	CYPH	TRP	MTND
DLD1	ZUO1	XPO1	SNF7
YBQ6	RM04	SYV	UAP1
OAT	ODPX	RPAC1	PSA3
EF1G2	RCN2	NPT1	RIR4
ARO9	TAF14	RPE	RS12
METE	RS29A	SIC1	PUR7
BCA1	FMP46	LIP1	GLRX5
PGM2	REP2	CEF1	RL31B
DHAS	YP199	PFKA2	TIM9
METC	CAPZA	EF1G2	H2B1
CDK1	GRP78	MAOM	HNT1
LEU1	ATP19	RHO1	VA0D
MTR4	COFI	TKT1	SDHF2
AGX1	RV161	OAT	COX12
UGPA1	PAA1	YPT1	NHP6B
CACP	YP036		RNQ1
DHE5	CWP1		RS27A
ARGJ	SOL3		CDK1
ARGI	YFI6		YP148
HIS2	YRA1		CDC37
ARO8	RAD23		FCY1
METK2	EMP24		COPD
GLNA	DSK2		DDR48
TRXB2	YPT52		MNP1
DHOM	IF2B		TCTP
PURA	APD1		PROF
KES1	SIS1		PRS6A
TBA1	RL36A		IGO2
FIP1	STB3		RS21B
PEX19	RT07		TMA17
TMEDA	LSP1		EF1B
GLYM	HRB1		RT26
ARB1	RS6B		SGT2
CYSD	SIL1		MIX17
PSA6	RT24		SYC
HRI1	RS27A		CTR3
METK1	UBX1		SFM1
FRDS	RS15		RL38
GET3	RM25		ACBP

C1TC	RS3		YP260
MCFS2	CDC3		TMA10
KAR	GPP1		GLRX2
RL4A	CUE5		SUI1
RAS2	NUP60		BMH1
ODO1	IF1A		SEC4
THIL	YGP1		SBA1
PDC1	YK03		RSP5
ILV3	IF4E		COX6
ERG6	RL12A		PAN1
DLD2	ISD11		DOHH
HSP78	RM41		ATP14
BLH1	MTC1		YN034
AMPL	STE50		IGD1
GCST	RS24A		STF2
PRS7	GVP36		IAH1
HMCS	ETFB		PRS6B
RT04	YLH47		ZEO1
F16P	SCD6		PYRD
YM94	SGT2		HSP12
	RSM28		GLRX1
	RT25		PRS10
	IWS1		IPB2
	BSP1		SDO1L
	YJF5		YP225
	HPRT		
	LHP1		
	MSP1		
	BMH1		
	SRO9		
	ACA2		
	PDXH		
	SEC17		
	RDL2		
	HMF1		
	UBC1		
	COQ1		
	RL31B		
	RS5		
	ATPO		
	VATE		
	ATP11		
	THO1		
	RPN12		
	HMO1		
	SLF1		
	KC11		

	COQ7		
	APT1		
	HSP26		
	IMB4		
	PRM4		
	IF5A1		
	PRX1		
	MPM1		
	YOR31		
	RL35A		
	KAD3		
	VHS2		
	ADPP		
	RM16		
	KGUA		
	RL25		
	ENG2		
	RM01		
	GPX3		
	CYT2		
	CCS1		
	UTH1		
	TIM23		
	RL4P		
	HBT1		
	RPN5		
	TRX2		
	YMH9		
	HAA1		
	UBC13		
	PIN3		
	RL14A		
	YP260		
	SEC4		
	RT51		
	JSN1		
	CYC1		
	TOM20		
	BFR1		
	RM49		
	YP225		
	MMS2		
	RL38		
	LSM5		
	ENT3		
	CYB5		
	FSH1		

	DHE2		
	TOM22		
	FSH2		
	DCS2		
	ATP18		
	RPN10		
	NACA		
	KCC1		
	H2B1		
	FKBP		
	ESS1		
	HSP12		
	LSB3		
	UBC4		
	FMC1		
	SNU13		
	YL179		
	MDY2		
	ATP5E		
	MSRA		
	RS19B		
	DOHH		
	RM13		
	TCTP		
	LSB1		
	YN034		
	CANB		
	ATPJ		
	EIF3J		
	CYPC		
	PST1		
	NU100		
	SODC		
	MRP8		
	HBN1		
	TRX3		
	GPP2		
	HSC82		
	RIM1		
	RS12		
	RLA4		
	LSM6		
	SUI1		
	HNT1		
	H2A2		
	NTF2		
	YL257		

	IPB2		
	TMA17		
	ATPD		
	SBA1		
	CAF20		
	SUB1		
	TOM7		
	NHP6B		
	RS28A		
	CYPD		
	MAM33		
	GCSH		
	NOP6		
	HCH1		
	RT26		
	MIC19		
	YNT5		
	RT10		
	ATP7		
	CH10		
	RGI1		
	NHP6A		
	RS10A		
	MBF1		
	SDS23		
	IGO2		
	QCR7		
	RSP5		
	STM1		
	TPM1		
	ABF2		
	FCY1		
	GLRX2		
	RLA3		
	TIM10		
	RM19		
	SDHF4		
	GLRX1		
	NACB1		
	TRX1		
	SDO1L		
	MNP1		
	YP010		
	ZEO1		
	LCL2		
	PBP4		
	RLA2		

	COX6		
	RRF1		
	GLRX8		
	GRPE		
	SKP1		
	TMA10		
	PAL1		
	CKS1		
	RS21B		
	COX12		
	STF2		
	RS21A		
	VPS60		
	DDR48		
	DAP1		
	SDHF2		
	TIM9		
	SSU72		
	VATF		
	SLA1		
	GLRX5		
	ARPC5		
	RT19		
	ATP14		
	RLA1		
	YAP3		
	ITPA		
	CTR1		
	RM50		
	MTND		
	RRS1		
	FKBP2		
	YM8V		
	MIX17		
	TIM13		
	RPAC2		

Appendix Table 3: Proteome analytical identified proteins, which have an altered appearance between timepoint 0 and 7 hours after inducing sporulation. Protein concentration from cells in SPM (SPM) and cells in SPM plus 5 μ M Phen-DC₃ either 2-fold or more increased or 2-fold or more decreased.

Name	Sequence	Purpose
HIS4 probe for	CTTGTTGGTCAGGTACTTTTGGATGG	DNA probe HIS4
HIS4 probe rev	GATTCTAGCCCCACCAAACCATGCTT	DNA probe HIS4
YDR189w for	GCAGGAGATCATCTGGAAGGTG	DNA probe YDR189w
YDR189w rev	CAGGAGGTTTCTGGGCAGAG	DNA probe YDR189w
pUG6/loxP site insertion at HIS4 for	TGAATATAACGTTCCATATCTATTAT ATACACAGTATACTACTGTTTCATATT CGTACGCTGCAGGTTCGAC	Insert at HIS4
pUG6/loxP site insertion at HIS4 rev	ATACAGCAGAATGCCCCATCACAAT CCTGACAACCAGCAGTTCTTCTAGGC ATAGGCCACTAGTGGATCTG	Insert at HIS4
pCM51-Ime1 for	ggatccgatccATGCAAGCGGATATGCAT GG	pCM251-Ime1 construction
pCM51-Ime1 rev	gcggccgcggggccgcTTAAGAATAGGTTTT ACTAAACTTGTAGG	pCM251-Ime1 construction
Mec1 del for	TGAAGACAAAGTGAGGCTGGACAAC AAGAACGACATACACCGCGTAAAGG CCCACAAGACTGCcgtttcggtgatgac	Mec1 deletion via pRS303
Mec1 del rev	ACCTGCAGTGATGGTTAGATCAAGAG GAAGTTCGTCTGTTGCCGAAAATGGT GGAAAGTCGttcctgatcggtattttcct	Mec1 deletion via pRS303
Sml1 del for	ATCTGCTCCTTTGTGATCTTACGGTCT CACTAACCTCTCTTCAACTGCTCAAT AATTTCCCGCTcgtttcggtgatgac	Sml1 deletion via pRS306
Sml1 del rev	AAAAGAACAGAACTAGTGGGAAATG GAAAGAGAAAAGAAAAGAGTATGAA AGGAACTttcctgatcggtattttcct	Sml1 deletion via pRS306
Tel1 del for	CGGTAAGGAATGTGCCGATTTATGG	Tel1 deletion
Tel1 del rev	CCAACCCAACAAAACAACGAAGAGC	Tel1 deletion
Act1 for	CGCTCCTCGTGCTGTCTTCC	qPCR
Act1 for	CAGGGTGTCTTCTGGGGCAAC	qPCR
Atg8 for	GAAGGCGGAGTCGGAGAGG	qPCR
Atg8 for	ATCAACGCCGCAGTAGGTGG	qPCR
Rnr3 for	GAACAGAGTTATCGACCGTAAT	qPCR
Rnr3 rev	CTGGACACCAAGAGCAATAG	qPCR
Ape1 for	AGGACTCCATTGGCGAAGATGG	qPCR
Ape1 rev	TACCTCCATAGGGAGCAACAGC	qPCR
Cln3 for	TCAGCGCTGCCTCATGTCCT	qPCR
Cln3 rev	AGCGGCCTTTCTGTGTGGGA	qPCR
Ime1 for	CATCTACGTTCCACTCATCAT TCAATAACC	qPCR
Ime1 rev	GTATATGGGTAGAAGTCTTG TGTGTATGG	qPCR

Appendix Table 4: Primer used in this study

FX3 ¹⁹⁹	MATa, ho::LYS2, lys2, ura3, leu2::hisG, his3::hisG, trp1::hisG, his4-lopc, rad50s MATa, ho::LYS2, lys2, ura3, leu2::hisG, his3::hisG, trp1::hisG, HIS4, rad50s University of North Carolina, Department of Biology, Curriculum in Genetics and Molecular Biology
FX4 ¹⁹⁹	MATa, ho::LYS2, lys2, ura3, leu2::hisG, his3::hisG, trp1::hisG, his4-202 his4-lopc, rad50s

	MAT α , ho::LYS2, lys2, ura3, leu2::hisG, his3::hisG, trp1::hisG, his4-202 HIS4, rad50s University of North Carolina, Department of Biology, Curriculum in Genetics and Molecular Biology
DNY107	MAT α , ho::LYS2, lys2, ura3, leu2::hisG, his3::hisG, trp1::hisG, HIS4, rad50s University of North Carolina, Department of Biology, Curriculum in Genetics and Molecular Biology
HF4	MAT α , ho::LYS2, lys2, ura3, leu2::hisG, his3::hisG, trp1::hisG, his4-lopc, rad50s University of North Carolina, Department of Biology, Curriculum in Genetics and Molecular Biology
Telomere sequence	MAT α , ho::LYS2, lys2, ura3, leu2::hisG, his3::hisG, trp1::hisG, Telomere seq HIS4, rad50s MAT α , ho::LYS2, lys2, ura3, leu2::hisG, his3::hisG, trp1::hisG, Telomere seq HIS4, rad50s
Mutated sequence	MAT α , ho::LYS2, lys2, ura3, leu2::hisG, his3::hisG, trp1::hisG, Mut seq HIS4, rad50s MAT α , ho::LYS2, lys2, ura3, leu2::hisG, his3::hisG, trp1::hisG, Mut seq HIS4, rad50s
Alternative Loop sequence	MAT α , ho::LYS2, lys2, ura3, leu2::hisG, his3::hisG, trp1::hisG, Alt loop seq HIS4, rad50s MAT α , ho::LYS2, lys2, ura3, leu2::hisG, his3::hisG, trp1::hisG, Alt loop seq HIS4, rad50s
Short Loop sequence	MAT α , ho::LYS2, lys2, ura3, leu2::hisG, his3::hisG, trp1::hisG, Short loop seq HIS4, rad50s MAT α , ho::LYS2, lys2, ura3, leu2::hisG, his3::hisG, trp1::hisG, Short loop seq HIS4, rad50s
Extended loop sequence	MAT α , ho::LYS2, lys2, ura3, leu2::hisG, his3::hisG, trp1::hisG, Ext loop seq HIS4, rad50s MAT α , ho::LYS2, lys2, ura3, leu2::hisG, his3::hisG, trp1::hisG, Ext loop seq HIS4, rad50s
ES100	MAT α , ho::LYS2, lys2, ura3, leu2::hisG, his3::hisG, trp1::hisG, tel1::KANMX, sml1::URA3, mec1::HIS3 MAT α , ho::LYS2, lys2, ura3, leu2::hisG, his3::hisG, trp1::hisG, tel1::KANMX, sml1::URA3, mec1::HIS3
A32041 ¹⁵⁵	MAT α , ho::LYS2, lys2, ura3, leu2::hisG, his3::hisG, trp1::hisG, set2::His3MX6, set3::His3MX6 MAT α , ho::LYS2, lys2, ura3, leu2::hisG, his3::hisG, trp1::hisG, set2::His3MX6, set3::His3MX6 Amon Lab, Massachusetts Institute of Technology, 77 Massachusetts Avenue 76-561, Cambridge, MA 02139
FW2444 ²⁰⁴	MAT α , ho::LYS2, lys2, ura3, leu2::hisG, his3::hisG, trp1::hisG, irt1::pCUP3HA-IME1::KANMX MAT α , ho::LYS2, lys2, ura3, leu2::hisG, his3::hisG, trp1::hisG, irt1::pCUP3HA-IME1::KANMX van Werven lab, The Francis Crick Institute, 1 Midland Road, London NW1 1AT
pCM251 ²⁰² -IME1	centromeric vector, <i>TRP1</i> as genetic marker, <i>IME1</i> ORF under the control of tetO2 promoter
psH65	Cre-expressing (pGAL1-cre) CEN/ARS plasmid, marker gene: pAgTEF1-ble-tScCYC1, selectable phenotype: Phleo resistance

Appendix Table 5: Strains and plasmids used in this study

7 Acknowledgments

At the end of my thesis I would like to express my deepest gratitude to all people who helped me during the time of my PhD studies.

First and foremost, I would like to thank my primary supervisor Prof. Dr. Katrin Paeschke for giving me the opportunity to work in her lab, for always having an open door and willing to share her knowledge with me, without her support and guidance this journey would have not been possible.

I am grateful to the members of my thesis committee, my second supervisor Prof. Dr. Oliver Gruss, Dr. Michael Chang and Prof. Dr. Eva Kiermaier for spending time and effort to assess this thesis.

I want to thank Dr. Stefan Juranek for countless answers on questions about bioinformatics as well as many discussions about everything and anything.

I want to thank all the Paeschke and Juranek lab members, past and present for the good times. My colleagues, especially Sanjay Gupta, Thomas Ziegenhals, Markus Sauer, Daniel Hilbig, Mona Hajikazemi, Theresa Schmitz, Alessio De Magis, Michaela Limmer, Melanie Kastl, Philipp Schult, Marco Caterino and Satyaprakash Pandey for help, the harmonic working atmosphere, and every scientific or non-scientific discussion. Also, I want to thank all people at the Department of Biochemistry at the University of Würzburg for their support and help during my time in Würzburg.

Many thanks to the people at the European Research Institute for the Biology of Ageing (ERIBA) in the Netherlands for their help and fun times. The Team of the Yeast group, consisting of Chang and Veenhof lab for their helpful input and ideas in lab meetings and outside of work. Especially Sonia Stinuz and Fernando Rosas Bringas for their help during my time in Groningen and moreover for being my friends.

Additionally, I want to say thanks to the people of the Medical Clinic III at the Biomedical Center I at the University Hospital Bonn, especially Pia Sauerborn and Andre Gauchel.

Last but not least, I want to thank my friends and family for their encouragement and help during the whole time of my studies.